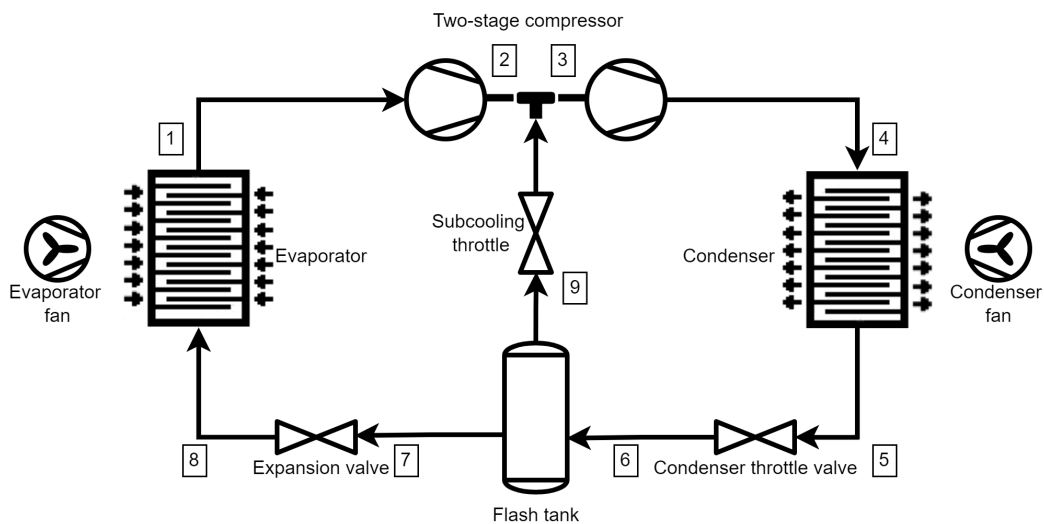

Modelling, Control and Optimisation of Electric Transport Refrigeration Unit



Project Report

Group: 931

Andreas Hertherington, Ryan Sebastian Abbas

Aalborg University
Electronics and IT



Electronics and IT
Aalborg University
<http://www.aau.dk>

AALBORG UNIVERSITY

STUDENT REPORT

Title:

Modelling, Control and Optimisation of Electric Transport Refrigeration Unit

Theme:

Control and optimisation of non-linear refrigeration system

Project Period:

01/09/22 - 02/06/23

Project Group:

931

Participant(s):

Andreas Hetherington
Ryan Sebastian Abbas

Supervisor(s):

Jan Dimon Bendtsen
John-Josef Leth

Copies: 0

Page Numbers: 141

Date of Completion:

June 2, 2023

The content of this report is freely available, but publication (with reference) may only be pursued due to agreement with the author.

Abstract:

With the transportation of foods, medicine and other commodities across the world, refrigeration has become a subject of great importance. With the wide usage of conventional refrigeration systems, the energy demand has increased steadily. As the pressing issues of global-warming in great degree is caused by burning of fossil-fuels, an increased demand for electrified solutions have followed. By fully or partly relying on battery powered refrigeration systems in transportation, this necessitates lower energy consumption and higher cooling efficiencies, to reduce the downtime caused by charging stops. In order to tackle this issue, BITZER has pursued the possibility of adding a flash-tank between the refrigeration system's evaporator and condenser. The addition of the flash-tank presents the issue of finding the optimal flash-tank intermediate pressure. By applying the genetic algorithm to a high-fidelity system-model, this appears to be feasible, given stable refrigerant pressure dynamics. Although, the limited optimisable states of the model at hand, does not justify the use of gradient free optimisation, the results suggest potential given a wider selection of optimisable set-points.

Contents

Preface	1
1 Introduction	3
2 System Description	7
2.1 Refrigeration Cycle	7
2.1.1 Vapour Compression	7
2.1.2 Refrigerant Expansion	8
2.1.3 Basic Vapour-compression	9
2.1.4 Flash-tank Vapour-compression	11
2.2 System Actuators and Sensors	13
2.3 Component Description	14
2.3.1 Compressor	14
2.3.2 Condenser	14
2.3.3 Expansion Valve	14
2.3.4 Flash-tank	15
2.3.5 Evaporator	15
2.3.6 Circulation Fan	16
2.3.7 Refrigerant R410A	16
2.4 System Description Summary	17
3 Modelling	19
3.1 Look-up Table	19
3.2 Expansion Valve	20
3.3 Scroll Compressor	23
3.4 Condenser	27
3.4.1 Condenser Mass Dynamics	27
3.4.2 Fan Dynamics	29
3.4.3 Heat Energy Flow to Condenser Metal	29
3.4.4 Condenser Output Enthalpy Dynamics	30
3.4.5 Pressure Dynamics	31
3.5 Flash-tank	36
3.5.1 Pressure Dynamics in Flash-tank	38
3.5.2 Enthalpy in Flash-tank	39
3.6 Evaporator	39
3.6.1 Evaporator Boundary and Regions	39

3.6.2	Fan Air Flow and Temperature	40
3.6.3	Dynamics of Evaporator Metal	41
3.6.4	Mass Balances	43
3.6.5	Output Enthalpy Dynamics	44
3.6.6	Pressure Dynamics	44
3.7	Reefer	45
3.7.1	Energy Flows	46
3.7.2	Temperature Dynamics	47
3.8	Model Efficiency	48
3.9	eTRU State-space Model	49
3.9.1	States and Inputs	50
3.9.2	State-space Model for Condenser Liquid Output	53
3.10	Module Test	53
3.10.1	Evaporator	54
3.10.2	Condenser	56
3.10.3	Flash-tank	59
3.10.4	Steady-state Test	62
3.11	Modelling Summary	65
4	Refrigeration Control	67
4.1	Control Method	67
4.1.1	Super-heat Control using Evaporator Input Flow	68
4.1.2	Sub-cool Control using Fans	68
4.1.3	Reefer Air Temperature Control using Compressor	69
4.1.4	Flash-tank Pressure Control using Condenser Output Flow	70
4.1.5	Flash-tank Mass Accumulation	70
4.2	Refrigeration Control Summary	71
5	Simulation of model	73
5.1	General Considerations	73
5.1.1	ODE solving	73
5.1.2	Look-up Table	74
5.1.3	Architecture	74
5.2	Simplifications of Model and Numerical Issues	74
5.2.1	Compressor Simplification	75
5.2.2	Valve Simplification	75
5.2.3	Evaporator Condenser Volume Boundary	75
5.2.4	Evaporator Mass Conservation	76
5.3	Simulation Test	76
5.3.1	Model Initiation	77
5.3.2	Initial Simulation of Model	78
5.3.3	Volume Scaling Ratios	83

5.3.4	Enthalpy Changes	84
5.4	Comparison with BITZER Test	84
5.4.1	Compressor Discharge Mass-flow Comparison	85
5.4.2	Reefer Temperature	86
5.4.3	Super-heat and Sub-cool	87
5.4.4	Pressure	87
5.4.5	Enthalpy Change	89
5.5	System States and COP	90
5.6	Simulation Summary	92
6	Set Point Optimisation	93
6.1	Optimisation Methods	93
6.1.1	Cost-function	93
6.1.2	Algorithm Choice	94
6.1.3	Genetic Algorithm	94
6.1.4	Swarm Algorithm	97
6.2	Optimisation Implementation	98
6.2.1	Results	98
6.3	Optimisation Summary	101
7	Discussion	103
7.1	Compressor Dynamics	103
7.2	Zero-boundary Condenser Model	103
7.3	Valve Simplification	104
7.4	Vapour Injection Mass-flow	104
7.5	Flash-tank Volume Drift	104
7.6	Pressure and Mass Dynamics	105
7.7	Model Realism	106
7.8	Optimisation	107
8	Conclusion	109
	Bibliography	111
A	Bitzer Data for Simulation Initials	115
B	Coefficients and System Constants	117
C	Model MATLAB Files	119
D	Flow-plot for Initial Simulation	121
E	Model Comparison with Valve Models Implemented	123

E.1	Reefer Temperature	123
E.2	Pressure	124
E.3	Super-heat and Sub-cool	125
E.4	Enthalpy	126
F	COP Simulation Test	127
F.0.1	Variable Super-heat	127
F.0.2	Variable Flash-tank Pressure Ratio	128
F.0.3	Variable Evaporator and Condenser Fans	128
G	Vapour Injection Characteristic	131
H	Optimization Appendix	133
H.0.1	Swarm Algorithm	133
I	Cascade Control for Valves	139
J	Controller Gains and variables	141

Preface

In-order to conclude the 120 ECTS "Control and Automation" Master's program in AAU (Aalborg University) and gain the titles of Master of Science (MSc) in Engineering (Control and Automation), Andreas Hetherington and Ryan Sebastian Abbas, have written this 50 ECTS extended thesis on the subject of optimisation and modelling of a flash-tank vapour compression refrigeration cycle. By extension of this project, a great understanding and insight into the challenges of highly coupled thermodynamic systems and modelling in general has been achieved. We believe this will benefit us greatly in our future endeavours as control engineers. We hope that this report will be of some value to the reader, who is interested in the subject.

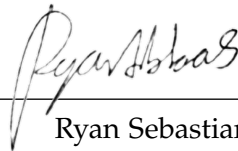
This project has been written in cooperation with project supervisors John Josef Leth and Jan Dimon Bendtsen and Kresten Sørensen of BITZER electronics, which we would like to thank for support and sparring. In addition system parameters and measurements made by Kresten Sørensen has been of great value and are much appreciated.

This project will be defended the 29th of June 2023.

Aalborg University, June 2, 2023



Andreas Hetherington
<ahethe18@student.aau.dk,
andreashetherington@gmail.com>



Ryan Sebastian Abbas
<rabbas21@student.aau.dk,
ryan.abbas@hotmail.com>

Chapter 1

Introduction

An eTRU is an electric Transport Refrigeration Unit. TRUs are insulated and refrigerated trailers that are used for transporting an array of commodities that require specific temperatures, this includes but is not limited to food, plants, bio-samples, pharmaceuticals, art and so on. The TRUs are for transport purposes placed on trucks, carrying the products over vast distances between suppliers and consumers. There are also examples using other land transport methods such as trains. While conventional TRUs such as Diesel TRUs are powered by a diesel-generator, eTRUs run entirely or partly on batteries. While the hybrid variant is diesel-powered on the road/rails, it is plugged into a power grid when the diesel motor is turned off. The all-electric TRU is on the other-hand fully powered by electricity, this means that during transit it must be connected to batteries [30].

The motivations behind a transition from the conventional TRU to an eTRU are plenty. Studies show that the transportation sector is responsible for 14% of greenhouse gas emissions [1], this is because 95% of transportation is petroleum-based. While green alternatives to fuels such as B100 bio-diesel exist, the energy density is considerably lower compared to low-level blends and fossil-alternatives [8]. Another factor is the economic incentive. In the United States, one of the largest grocery store chains Albertsons claim that not only have the use of eTRUs reduced air pollutants during transport, but they have projected a \$62,000 savings by transitioning 280/740 of their TRUs to hybrid-eTRUs [25].

eTRUs can be fitted with solar panels and wheel generators to ensure sufficient power to the reefer container, however solar panels are highly dependent on the weather and sun exposure. According to Thermo King, a producer of controllers for TRUs, solar panels on eTRUs in southern California may produce power for up to 2 hours of run time whereas solar panels in cloudier places may only result in 30-45 minutes of run time. In addition to this, solar panels fitted on eTRUs can add up to 500 lbs. to the weight of the trailer while product and installation costs can be \$15K-\$20K [31]. Clearly these systems cannot sustain a reefer trailer for longer journeys alone and therefore rechargeable batteries are needed. This poses a challenge since the batteries require charging at stations which can be difficult in places with inadequate charging station infrastructure. Charging times can also introduce

a significant delay to the transportation which in turn introduces additional costs. Part of the solution needed to make eTRUs viable therefore includes optimising the implemented control-method, such that the highest cooling efficiency is achieved. In-order to optimise the energy consumption of the eTRU system, the basic system components must be understood.

The eTRU system is similar to other refrigeration systems, but is driven by an electric compressor-motor.

This project is suggested by BITZER Electronics and the circuit initially provided by BITZER in Fig. 1.1 shows the components of the refrigeration system dealt with in this project.

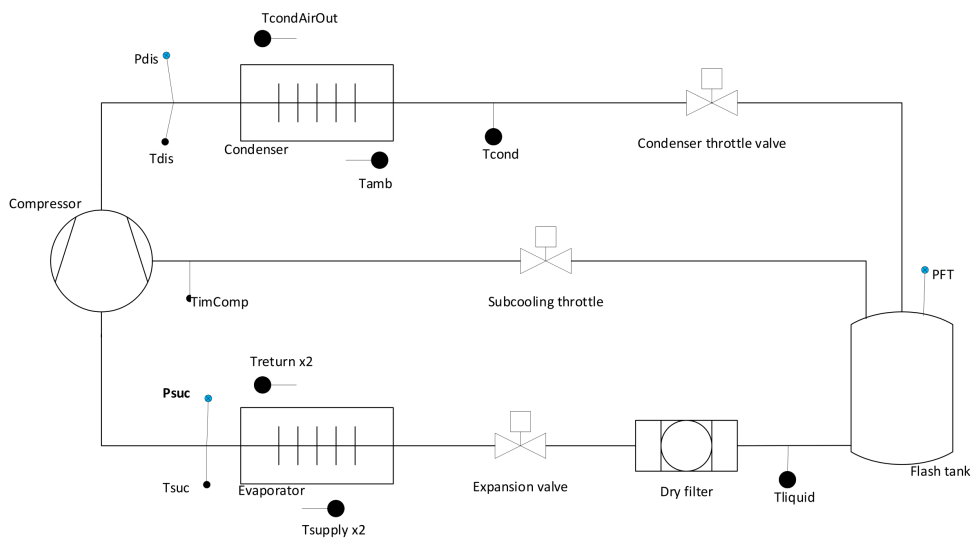


Figure 1.1: System model by BITZER

The system at hand is referred to as a *Vapour-compression Refrigeration system*. The main thermodynamic processes that take place are:

- Compression
- Condensation
- Expansion
- Evaporation

For now it is sufficient to understand that the *compressor* compresses low temperature refrigerant, heating it in the process. The heated vapour transfers its heat through the *Condenser* to the ambient environment, ideally shifting all vaporised refrigerant to a liquid state. Disregarding the flash-tank (for the moment) the liquid

refrigerant is then propelled by the pressure difference through a variable expansion valve to the *Evaporator*. Here it absorbs heat from the reefer container air, then boils, and once more becomes a vapour which is then recycled in the compressor as the cycle repeats [29]. As the refrigerant passes through the expansion valve at the condenser output, the pressure of the refrigerant is reduced. The result of this is either 1. A reduction in sub-cooling (sub-cooling is the amount of cooling below the bubble-point), or 2. A complete removal of sub-cooling, resulting in mixed phase refrigerant. If the latter happens, a part of the refrigerant flashes into vapour during a process called flashing. A method for reducing the amount of flashing in the evaporator is implementing a flash-tank, such that there is an intermediate pressure drop between the evaporator and condenser. From the flash-tank the flash-vapour is directed to the compressor, while the liquid refrigerant is passed to the evaporator, through an expansion valve. Through the expansion valve the refrigerant flashes with respect to the pressure difference between the flash-tank and evaporator.

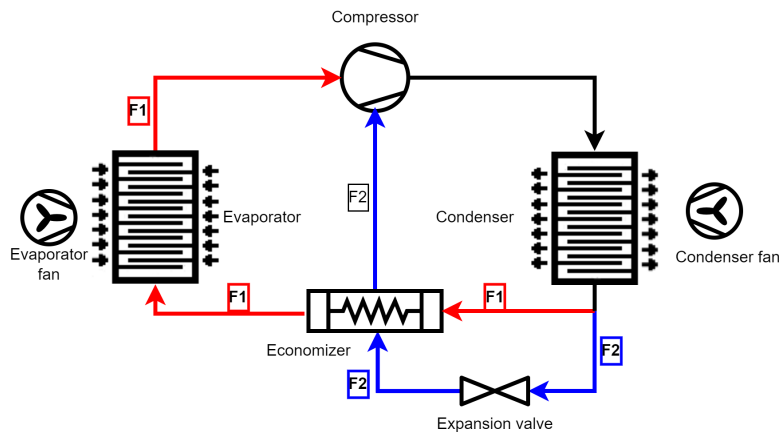


Figure 1.2: Diagram of sub-cooler system

In this report a flash-tank is used to reduce flashing in the evaporator, an alternative approach is the use of sub-coolers. The sub-cooler separates the condenser output into two parts, as seen in Fig. 1.2 one part (F1) flows directly into the sub-cooler economiser while the other (F2) flows through an expansion valve, reducing the pressure. The refrigerant (F2) then flows into the sub-cooler where it absorbs heat from the aforementioned refrigerant (F1) that also coincides in the sub-cooler. The refrigerant (F2) is then vaporised by the heat and sucked into the compressor, while the now sub-cooled (F1) refrigerant flows to the evaporator.

Research shows that the flash-tank approach is more efficient for heating under low ambient temperatures, with a 4.3% greater COP (coefficient of performance)

[17]. Combinations of the flash-tank and sub-cooler have also been implemented with success, with even greater efficiency [27].

The overall purpose of the economiser is to increase the efficiency of the system, as the liquid refrigerant has a higher heat capacity than the vapour and transfers more heat from the reefer air to the refrigerant [29].

Flash-tanks are in literature referred to as *flash-tank*, *flash-economiser*, *flash-chamber*, the terms seem to be used interchangeably, while in some instances a flash-chamber often describes a smaller variant of the flash-tank.

Controlling of the flash-tank for optimal refrigeration efficiency has proved to be a challenge for control engineers. The challenges stem from the difficulty of modelling the drastically changing conditions of the liquid-vapour phase [6]. A key challenge in controlling refrigeration systems is to determine the Economiser Optimum Pressure (EOP). An economiser in this sense refers to a flash-tank with a throttle and expansion valve. In [28] it was found, through thermodynamic analysis of a heat pump with an economiser, that the efficiency could be optimised by identifying the minimum entropy generation. In the aforementioned paper the EOP was found to be at the flash-tank pressure ratio $\alpha = [0.25; 0.30]$, and specifically $\alpha = 0.29$ for the refrigerant R410a.

Given the complexity and non-linearity of the refrigeration system, the use of gradient free optimisation methods have been suggested by BITZER. The optimisation algorithm that will be implemented for the flash tank pressure optimisation is genetic optimisation. The genetic optimisation algorithm generates the optimal set-points based on previous evaluated parent points, which in theory converges towards an optimal set of set-points.

Other alternatives in gradient free optimisation includes the swarm optimisation algorithm which was also suggested by BITZER, however it was found in [24] that computational times are generally higher when using swarm optimisation compared to genetic optimisation, although swarm optimisation is expected to yield slightly better results. Because of the long computational time of the resulting model, the genetic algorithm was deemed to be best fitting for the problem at hand. Common for both optimisation methods, is the need for a sufficiently accurate model of the refrigeration system.

Chapter 2

System Description

2.1 Refrigeration Cycle

As mentioned in the introduction in Chapter 1, the eTRU refrigeration system is of the vapour-compression type. German scientist Clausius once stated in the renowned *Clausius statement* regarding the second law of thermodynamics "Heat can never pass from a colder to a warmer body without some other change, connected therewith, occurring at the same time." [37]. In other words, heat by its nature can only pass from a hot region to a cold region, without some "other change" happening. In the case of refrigeration where a refrigeration chamber needs to be cooled down, we must introduce such a "change" in form of a compressor exposing the refrigerant to external mechanical work.

Furthermore the vapour is also subject to expansion in order to lower the temperature and absorb heat energy. The compression and expansion processes will now be elaborated

2.1.1 Vapour Compression

Ideally refrigerant vapour compression happens isentropically, meaning that the entropy remains constant throughout the process. The enthalpy however changes as it is subject to Pressure-Vapour work (P-V work). The enthalpy in a substance is symbolically described:

$$H = U + pV \quad (2.1)$$

H	Refrigerant enthalpy	$[J]$
U	Internal thermal energy	$[J]$
p	Pressure	$[Pa]$
V	Volume	$[m^3]$

The Enthalpy is conceptualised as the internal energy U and pressure energy pV .

A change in enthalpy over time through isentropic compression is derived:

$$\frac{dH(t)}{dt} = \frac{dU(t)}{dt} + \frac{d(p(t) \cdot V(t))}{dt} \quad (2.2)$$

Using the product rule the term is expanded:

$$\frac{dH(t)}{dt} = \frac{dU(t)}{dt} + V(t) \frac{dp(t)}{dt} + p(t) \frac{dV(t)}{dt} \quad (2.3)$$

The change in internal energy is the sum of the added thermal energy dq and the V-P work, where p_{ext} is the external pressure:

$$\frac{dU(t)}{dt} = \frac{dq(t)}{dt} - p_{ext}(t) \frac{dV(t)}{dt} \quad (2.4)$$

In terms of entropy, the added thermal energy is the change in entropy dS multiplied with temperature T :

$$\frac{dU(t)}{dt} = T \frac{dS(t)}{dt} - p_{ext}(t) \frac{dV(t)}{dt} \quad (2.5)$$

The complete term is then:

$$\frac{dH(t)}{dt} = T \frac{dS(t)}{dt} - p_{ext}(t) \frac{dV(t)}{dt} + V(t) \frac{dp(t)}{dt} + p(t) \frac{dV(t)}{dt} \quad (2.6)$$

The term is reduced by noting that the process discussed is isentropic and adiabatically reversible such that $dS = 0$ and $p = p_{ext}$:

$$\frac{dH(t)}{dt} = V(t) \frac{dp(t)}{dt} \quad (2.7)$$

In the case of real mechanical compression, the change in enthalpy will be greater than this, as friction heat in addition to compressor leakage results in an entropy change that is non-zero. The degree of this change is known as isentropic efficiency which describes the ratio of actual compressor work to the ideal adiabatic isentropic work. Isentropic efficiency η , can be calculated using the enthalpy at the inlet of the compressor h_{in} , the ideal output enthalpy of the adiabatic reversible compression process $h_{isentropic}$, and the actual output enthalpy of the compressor h_{out} :

$$\eta = \frac{h_{isentropic} - h_{in}}{h_{out} - h_{in}} \quad (2.8)$$

2.1.2 Refrigerant Expansion

The expansion valve throttling process exploits the first law of thermodynamics that stresses conservation of energy. This means that through an ideal loss-less expansion process, the *refrigerant enthalpy* remains constant or *isenthalpic*.

While the expansion occurs and enthalpy remains constant, a number of notable nonlinear interdependent changes happen:

- Volume increases
- Pressure decreases
- Temperature decreases
- Dew- and bubble- point changes

The enthalpy remains constant as pressure decreases, this results in a lower energy concentration within the refrigerant, translating to a decrease in the refrigerant temperature. For an ideal gas this can be shown by the ideal-gas law for pressure p and Volume V :

$$pV = nRT \quad (2.9)$$

n	Amount of substance	$[mol]$
R	Gas constant	$[J \cdot K^{-1} \cdot mol^{-1}]$
T	Refrigerant temperature	$[K]$

However, most refrigerants are not ideal and can therefore not be described by the ideal-gas law. Instead, refrigerant specific look-up tables are used to find the relationship between the different nonlinear refrigerant properties.

As is the case with the compression, the expansion through the expansion valve is not truly isenthalpic, as friction and heat leakage has some effect.

2.1.3 Basic Vapour-compression

Refrigerant Properties

This section is meant to give short explanations of various terms that are used throughout the project.

The pH -diagram in Fig. 2.1 shows the pressure-enthalpy relationship and liquid-vapour characteristics for a refrigerant and will be used for elaboration of the different terms.

Bubble- and Dew-point

The bubble-point of a refrigerant is the point in a pressure-enthalpy diagram where the refrigerant first begins to evaporate. The dew-point is the point where the refrigerant begins to condense. In a non-gliding refrigerant all the refrigerant starts boiling at the same time, while a gliding refrigerant has different boiling points. In Fig. 2.1 The bubble point can be seen on the left hand side of the saturation curve, while the dew-point is on the right hand side.

Vapour Quality

The vapour quality χ , refers to the percentage of the refrigerant which is in vapour form. This is useful when the refrigerant is in the mixed-phase region, which is the region between the bubble- and dew-point. Quality is found via the mass of the vapour M_v , and the total mass of the refrigerant M_T :

$$\chi = \frac{M_v}{M_T} \quad (2.10)$$

As seen in Fig. 2.1 the mixed-phase region is under the saturation curve between the sub-cooled and super-heated regions.

Sub-cool and Super-heat

When the refrigerant is completely in liquid or vapour form it is referred to as being sub-cooled and super-heated respectively. The refrigerant can have different degrees of sub-cool and super-heat, which in this project will be described as the temperature difference between the dew-point and actual vapour temperature for the super-heat and the difference between the bubble-point and the actual liquid temperature for sub-cool.

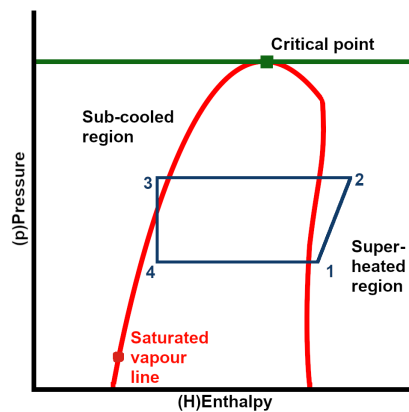


Figure 2.1: pH-diagram of simple vapour-compression cycle

Refrigeration Cycle

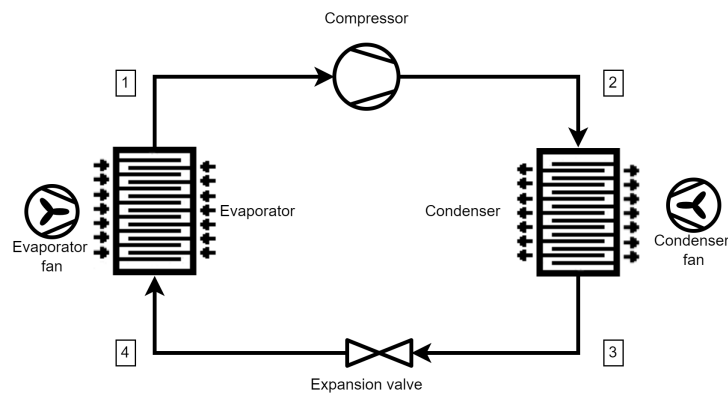


Figure 2.2: Refrigeration cycle model

Following the refrigeration cycle shown in Fig. 2.2 and illustrated in the pH-diagram in Fig. 2.1:

- (1-2) The compressor increases the pressure of the vapour refrigerant.
- (2-3) The refrigerant having higher temperature than the ambient air, emits heat energy, resulting in the lowering of refrigerant enthalpy, condensing and sub-cooling.
- (3-4) The refrigerant is passed through the condenser expansion valve, decreasing pressure through throttling, without significant enthalpy change. The mass-flow is dependent on the pressure difference and opening degree of the valve.
- (4-1) The refrigerant passes through the evaporator, where heat energy is absorbed from the refrigeration chamber. This results in an increase of enthalpy leading to evaporation and super-heating.

2.1.4 Flash-tank Vapour-compression

The basic vapour-compression system elaborated thus far is sufficient for general refrigeration, but as depicted in the pH-diagram in Fig. 2.1, the expanded refrigerant (3-4) ends within the mixed-phase region. This means that flash-vapour appears in the evaporator lowering its heat absorption efficiency. Adding a flash-tank to the system as shown in Fig. 2.3 decreases this inefficiency.

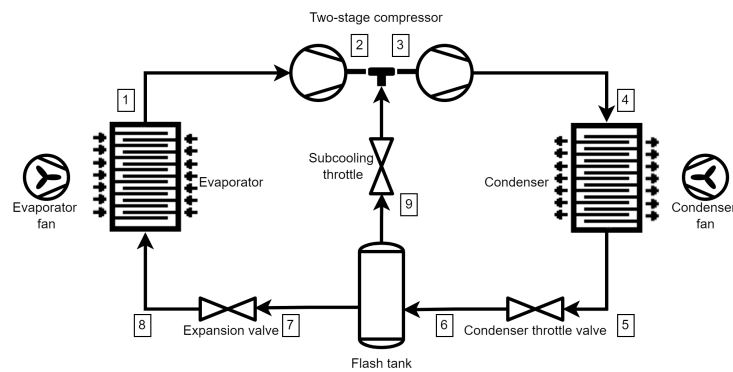


Figure 2.3: Refrigeration cycle model with flash tank

In addition to adding the flash-tank a throttle valve is added between the flash-tank and a two-stage compressor. This compressor variant has an intermediate stage, where the vapour is passed from the flash-tank.

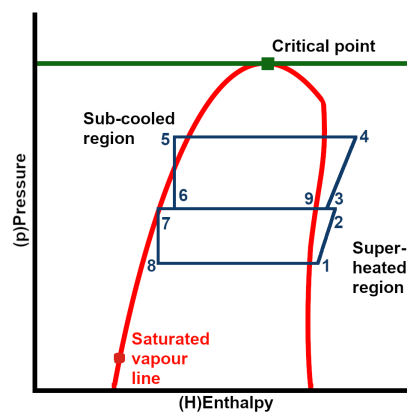


Figure 2.4: pH-diagram of refrigeration cycle with a flash-tank

Flash-tank Refrigeration Cycle

The refrigeration cycle for the flash-tank variant goes as following, with the associated pH-diagram in Fig. 2.4 and refrigeration cycle diagram in Fig. 2.3:

- (1-2) The compressor increases the pressure of the refrigerant vapour with an associated increase of enthalpy.
- (2-3)/(9-3) The flash-tank vapour is directed through the throttle to the second compression state, resulting in an intermediate drop in refrigerant enthalpy. The flow of flash-vapour through the vapour-injection port is dependent on

compressor speed and the pressure difference between the flash-tank and the compressor vapour injection port.

- (3-4) The second stage of compression is completed, increasing enthalpy and pressure.
- (4-5) The refrigerant having higher temperature than the ambient air, emits heat energy resulting in the lowering of refrigerant enthalpy, condensation and sub-cooling.
- (5-6) The refrigerant is expanded by passing through the condenser throttle valve, decreasing pressure, with insignificant change in enthalpy. The flow of the refrigerant into the flash-tank is dependent on the pressure in the condenser, pressure in the flash-tank and valve opening degree.
- (6-9)/(6-7) Flashing takes place inside the flash-tank, separating the liquid and vapour components of the refrigerant.
- (7-8) The refrigerant is passed through the expansion valve, decreasing pressure, with insignificant change in enthalpy. The flow of the refrigerant to the evaporator is dependent on the pressure in the evaporator, the pressure in the flash-tank and valve opening degree.
- (8-1) The refrigerant passes through the evaporator where heat energy is absorbed from the refrigeration chamber, resulting in an increase of enthalpy, evaporation and super-heating.

2.2 System Actuators and Sensors

In order to control the system, it is necessary to measure system states, such as: pressure p_x and temperature T_x . Because of the algebraic relationships between pressure, temperature, enthalpy h_x and mass-flow through valves \dot{m}_x , enthalpy and mass-flow can be estimated, as the characteristic of the refrigerant is documented by the manufacturer.

The actuators available in the system are shown in Fig. 2.3. Mass-flow and pressure between system components are controlled with the three valves: The condenser output valve, vapour injection valve and the evaporator valve. The two stage vapour injection scroll compressor which has a variable rotor speed Ω which controls the compressor suction flow from the evaporator. And the condenser and evaporator fans, which increase the heat-transfer of the heat exchangers.

2.3 Component Description

In this section the different components involved in the refrigeration cycle are described and specifications are given where possible. The interconnection of components is shown in Fig. 1.1.

2.3.1 Compressor

Compressors are vital in the vapour-compression cycle as they compress the refrigerant coming from the evaporator and propels the refrigerant throughout the system. The compressor type used in this project is a two-stage rotary scroll compressor with vapour injection. A scroll compressor consists of two interleaving scrolls, one stationary and one orbiting within the other. This motion causes the refrigerant to be compressed towards the centre of the two scrolls where the compressor outlet is placed. The implemented compressor is a Hitachi AA50 series scroll compressor [14], in Tab. 2.1 some specifications are provided.

Series	AA50	Unit
Displacement	8.70	$[m^3 \cdot h^{-1}]$
Speed	15-140	$[Hz]$
Cooling capacity	16.48	$[kW]$
Power input	5.07	$[kW]$

Table 2.1: Specifications of AA50 compressor

2.3.2 Condenser

An air cooled condenser is used to transfer heat from the refrigerant to the ambient environment via a centrifugal fan circulating air over condenser-pipes containing the refrigerant. This process causes the super-heated compressed refrigerant to change phase as it condenses. The documentation for the implemented condenser is sparse, but below in Tab. 2.2 are some specifications supplied by BITZER:

Unit	Internal Volume $[m^3]$	Casing material	Casing weight $[kg]$
Condenser	$2 \cdot 10^{-3}$	Copper	3.027

Table 2.2: Some technical specifications for the condenser.

2.3.3 Expansion Valve

Expansion valves are used to control pressure in refrigeration components by restricting the inter-component mass-flow to reach a pressure set-point.

The valves in the system are CAREL E2V [4] expansion valves and the flow gain characteristic of the valve is of the equal percentage variety, this is elaborated in the modelling Section 3.2.

step min [step]	step max [step]	step speed [step · s ⁻¹]	step close [step]
50	480	50	500

Table 2.3: Some technical specifications for the CAREL E2V expansion valves.

2.3.4 Flash-tank

The flash-tank is used to separate liquid refrigerant from vapour refrigerant as it is desired to only pass liquid to the evaporator. When the liquid-vapour mixture enters the flash-tank, gravity is utilised in order to separate the liquid and vapour. See Fig. 2.5 for a simplified illustration of this process.

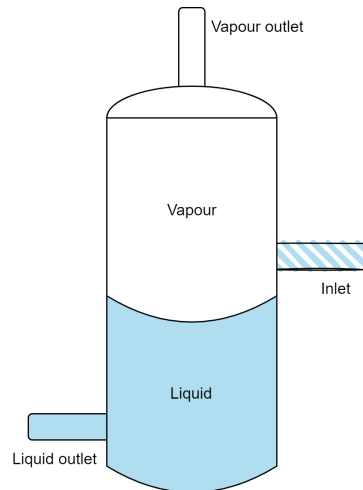


Figure 2.5: Simplified drawing of a flash-tank.

The implemented flash-tank model is the OCS COLD BIZRV1390440A

internal Volume [m ³]	Casing weight [kg]
$5.7 \cdot 10^{-3}$	9

Table 2.4: Some technical specifications for OCS COLD BIZRV1390440A

2.3.5 Evaporator

The evaporator cools the air in the refrigeration chamber. This is achieved in a similar manner to the condenser, namely a centrifugal fan circulates air over the

evaporator-pipes containing the refrigerant. In the evaporator the refrigerant is colder than the air in the refrigeration chamber, therefore heat-energy is transferred from the container to the refrigerant. This causes a phase change in the refrigerant from mixed-phase to vapour.

Unit	Internal Volume [m^3]	Casing material	Casing weight [kg]
Evaporator	$15.18 \cdot 10^{-3}$	Copper	22.976

Table 2.5: Some technical specifications for the evaporator.

2.3.6 Circulation Fan

Centrifugal fans in the system circulate air around the condenser and evaporator which ensures a more efficient heat transfer between refrigerant and air. The fan variant is the GTM031PHJ22M from Delta which is an electronically commutated (EC) fan [7]. Below in Tab. 2.6, the maximum displacement, speed and pressure are specified.

Model	Max Displacement [$m^3 \cdot h^{-1}$]	Max Speed [Hz]	Max Pressure [Pa]
GTM031PHJ22M	3704	51	1035

Table 2.6: Some technical specifications of the GTM031PHJ22M fan, tested at room temperature.

2.3.7 Refrigerant R410A

R410A [34] is a low-glide mixture of 50% difluoromethane (R32) and 50% pentafluoroethane (R125). Below in Tab. 2.7 specifications of the refrigerant can be seen. Critical pressure, temperature and density are states of R410A at the critical point of its pH-diagram.

Refrigerant	R410A
Boiling Point at 1 bar [$^{\circ}C$]	-51.5
Critical Pressure [MPa]	4.93
Critical Temperature [$^{\circ}C$]	72.1
Critical Density [$kg \cdot m^{-3}$]	489
Glide [K]	~ 0.3

Table 2.7: Specification for R410A [34].

In Fig. 2.6 below, the pH-diagram of R410A can be seen.

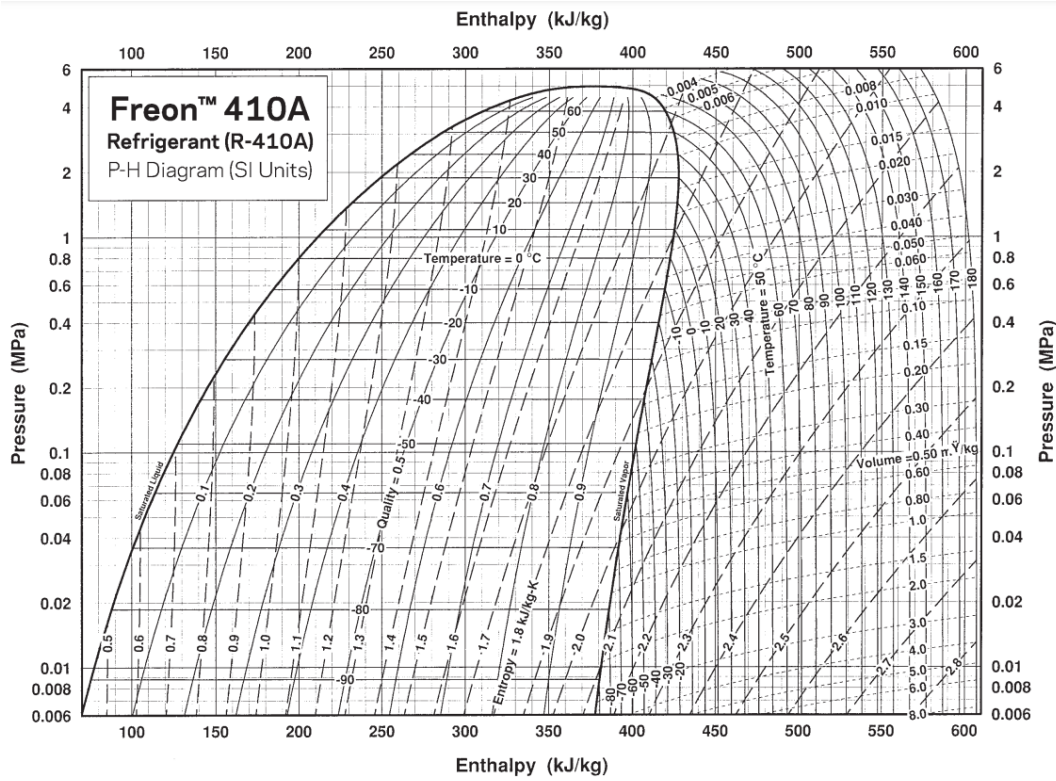


Figure 2.6: pH-diagram of R410A [10].

2.4 System Description Summary

It has in this section been explained how a vapour-compression cycle cools a refrigeration chamber, using a mechanical compressor and a refrigerant. Furthermore it is clear that the implementation of a flash-tank economiser, reduces the flashing of refrigerant in the evaporator resulting in a higher cooling capacity. With this concept in mind, it is now possible to create a dynamic model of the entire refrigeration cycle, such that a stabilising controller can be implemented and tested.

Chapter 3

Modelling

In this chapter the refrigeration system components described in Chapter 2 are modelled in order to obtain a combined state-space model for the system.

The first thing to be modelled are the three valves. The rest of the modelling is done sequentially starting from the compressor, then the condenser, flash-tank and finally the evaporator.

The objective is to model the overall dynamics of the system states through the first-principal-method. The states in the system include enthalpy, temperature, mass and pressure. For fan dynamics, exceptions are made, and fitted polynomial equations supplied by BITZER are used.

The differential equations that appear in the state-space diagram in section 3.9, are encapsulated in grey boxes, in the format of Eq. 3.1, where \dot{A} is the time derivative of A , with some constant c and b :

$$\dot{A} = bA - cA \quad (3.1)$$

While the compressor is modelled such that it can be turned off completely, the condenser model assumes some finite flow from the compressor to the condenser at all times. This issue will be dealt with briefly in Section 5.2, by setting a minimum allowed mass-flow through the compressor.

3.1 Look-up Table

Because of the high non-linearity between refrigerant properties, such as enthalpy and temperature, or dew-point and pressure, the use of look-up tables is necessary. Generally the interdependence of three properties, is such that given two quantities, a third one can be found. To denote this, the following function will be used throughout the report:

$$a = \Psi(x, y) \quad (3.2)$$

a , is the unknown output quantity, while x and y are the known input quantities, that are used in the look-up table.

As an example: The dew point enthalpy h_{dew} at pressure p with the associated quality $\chi = 1$ can be found as:

$$h_{dew} = \Psi(p, \chi) \quad (3.3)$$

The symbol Ψ , will be used to denote all look-up table functions. In Tab. 3.1 all the variables that are used in look-up tables throughout the report can be seen.

h	Enthalpy	$[J \cdot kg^{-1}]$
χ	Refrigerant quality	$[\%]$
p	Pressure	$[Pa]$
T	Temperature	$[K]$
D	Density	$[kg \cdot m^{-3}]$
S	Entropy	$[J \cdot K^{-1} \cdot kg^{-1}]$

Table 3.1: Look-up table symbols

3.2 Expansion Valve

Below in Fig. 3.1 a model of the expansion valve with states of the refrigerant at the input and output of the valve can be seen.

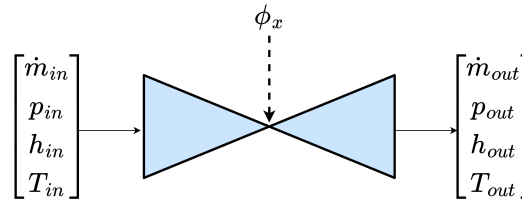


Figure 3.1: Expansion valve model

It is assumed that the expansion process is adiabatic due to the small surface area of the valve.

Because of the adiabatic assumption, the energy balance is:

$$h_{in} = h_{out} \quad (3.4)$$

The mass-flow balance is:

$$\dot{m}_{in} = \dot{m}_{out} \quad (3.5)$$

The expansion valve is modelled as done in [12], [22]. The mass flow can be expressed as a function of orifice area A_v , a function of the upstream and downstream pressure $\Delta p(p_{in}, p_{out})$, some experimentally found valve coefficient C_v , and

the upstream density of the refrigerant $D_{in} = \Psi(h_{in}, p_{in})$. Generally for liquids the density is constant, but for R410a, there is a small variability in density since it is compressible to some degree [10]. The mass-flow through the valve can then be expressed as:

$$\dot{m}_{out} = C_v A_v \sqrt{D_{in} \Delta p(p_{in}, p_{out})} \quad (3.6)$$

Furthermore the constants $C_v A_v$ can be collected into a term K_v such that $C_v A_v = K_v$.

$$\dot{m}_{out} = K_v \sqrt{D_{in} \Delta p(p_{in}, p_{out})} \quad (3.7)$$

\dot{m}_{out}	Mass flow through the valve	$[kg \cdot s^{-1}]$
C_v	Discharge coefficient of the valve	$[\cdot]$
A_v	Cross-sectional area of the valve orifice	$[m^2]$
D_{in}	Density of the refrigerant at valve input	$[kg \cdot m^{-3}]$
p_{in}	Pressure at the input of the valve (upstream)	$[Pa]$
p_{out}	Pressure at the output of the valve (downstream)	$[Pa]$

For generality, a function of the effective pressure difference is defined such that it is dependent on whether the flow is choked.

$$\Delta p(p_{in}, p_{out}) = \begin{cases} p_{in} - p_{out} & p_{in} - p_{out} < \Delta p_{choked} \\ \Delta p_{choked} & p_{in} - p_{out} \geq \Delta p_{choked} \end{cases} \quad (3.8)$$

A choked flow is when the mass-flow of the refrigerant through a valve becomes independent of downstream pressure, once a threshold Δp_{choked} is passed. Δp_{choked} is dependent on upstream pressure p_{in} , the valve model and the refrigerant type. Choking occurs at different pressure thresholds Δp_{choked} as seen in Eq. 3.9, this threshold is guaranteed to have been passed when the refrigerant flashes. Flashing happens at both the condenser and evaporator valve in the refrigeration cycle.

Δp_{choked} is also dependent on the liquid pressure recovery factor of the valve F_L , which is valve specific experimental estimated constant, the critical pressure ratio factor F_F and the vapour pressure of liquid p_V :

$$\Delta p_{choked} = F_L^2 (p_{in} - F_F \cdot p_V) \quad (3.9)$$

The critical pressure ratio factor F_F is found by using the critical pressure p_C , which is constant for the refrigerant, and the vapour pressure of the liquid refrigerant p_V :

$$F_F = 0.96 - 0.28 \sqrt{\frac{p_V}{p_C}} \quad (3.10)$$

p_V is a refrigerant specific fitted function of temperature, for R410a it can be found in [10].

Δp_{choked}	Maximum pressure across valve before choking	[Pa]
F_L	Valve recovery factor	[·]
F_F	Liquid critical pressure ratio factor	[·]
p_C	Critical pressure of refrigerant	[Pa]
p_V	Vapour pressure of liquid refrigerant	[Pa]

The actuation of the valve is done by a variable orifice area, this is modelled as a nonlinear function $f(\phi_x)$ added as a gain to the mass-flow valve Eq. 3.7 resulting in Eq. 3.12. The non-linearity stems from the equal-percentage characteristic of the valve as shown in Fig. 3.2.

The equal percentage equation is defined, such that $O_{\%}$ is valve specific and must be experimentally estimated:

$$f(\phi_x) = O_{\%}^{(\phi_x - 1)} \quad (3.11)$$

Using the equal percentage function Eq. 3.11 and the pressure difference function Eq. 3.8 in conjunction with the general valve function Eq. 3.7, the final valve function becomes:

$$\dot{m}_{out} = f(\phi_x) K_v \sqrt{D_{in} \Delta p(p_{in}, p_{out})} \quad (3.12)$$

ϕ_x	Opening degree of the valve	[%]
$O_{\%}$	Equal percentage constant	[·]

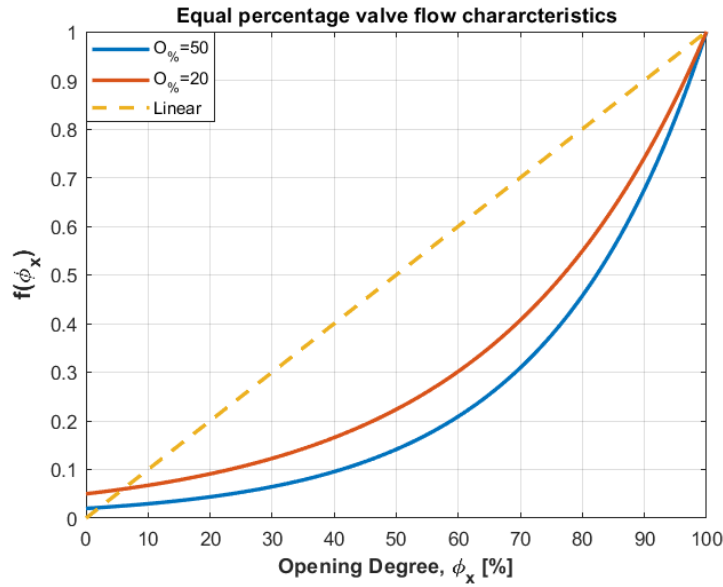


Figure 3.2: Flow characteristics of linear and equal percentage valve

The limitations on valve actuation resolution is described in Section 2.3.

3.3 Scroll Compressor

The compressor is an actuator controlled by a control signal U_ω ranging from $[0; 1]$. The compressor can be characterised as having two modes, Mode = 0, where the compressor is turned off, and Mode = 1 where the compressor is turned on. When on, the compressor speed $\Omega(U_\omega)$ and discharge mass-flow $\dot{m}_{dis}(\Omega)$ have an affine relationship to the control signal U_ω . The maximum compressor speed is $\Omega(1) = 8400rpm$, while the minimum running speed for a very small $U_\omega = \delta$ is $\Omega(\delta) = 900rpm$. It is however possible to turn off the compressor such that, $\Omega(0) = 0rpm$, therefore:

$$\Omega(U_\omega) = \begin{cases} 8400 & U_\omega \geq 1 \\ U_\omega \cdot 7500 + 900 & 1 > U_\omega > 0 \\ 0 & U_\omega = 0 \end{cases} \quad (3.13)$$

Given the compressor model so far, every mode-switching from 1 to 0 (on to off) or opposite, results in discontinuity. A simple model for removing this discontinuity is to add a first order transient to the newly defined dynamic compressor speed state $\Omega_{state}(t, U_\omega)$. The affine compressor speed function $\Omega(U_\omega)$ is used to find the reference error $\Omega(U_\omega) - \Omega_{state}(t, U_\omega)$

$$\dot{\Omega}_{state}(t, U_{\omega}) = \frac{\Omega(U_{\omega}) - \Omega_{state}(t, U_{\omega})}{\tau_{cpr}} \quad (3.14)$$

where

$\Omega(U_{\omega})$	Compressor speed reference in revolutions per minute	[rpm]
U_{ω}	Compressor control input	[%]
$\Omega_{state}(t, U_{\omega})$	Compressor speed state	[rpm]

As mentioned in Section 2.3, the implemented compressor with model name: Hitachi-AA50PHDG-D1K2 is a variable-speed scroll compressor with vapour injection [14]. This means that during rotation of the orbiting scroll, vapour is injected, mixing with the partly compressed refrigerant. This results in a mixing of refrigerant, a change of enthalpy and an increase in mass-flow. The mass-flow balance will therefore be:

$$\dot{m}_{suc} + \dot{m}_{inj} = \dot{m}_{dis} \quad (3.15)$$

\dot{m}_{suc}	Mass-flow from suction port into the compressor	[kg · s ⁻¹]
\dot{m}_{inj}	Mass-flow from flash tank into compressor vapour injection port	[kg · s ⁻¹]
\dot{m}_{dis}	Mass-flow out of the compressor discharge port	[kg · s ⁻¹]

Since the mass-flow of the injection vapour into the compressor is dependent on the pressure difference between the flash tank and the compressor, it is modelled as a fully open valve when the compressor is running. The model used is that of non-choked liquid flow, found at [22]. Typically for a vapour flow the formulation is slightly different when considering choked vapour flow, but by assuming a non-choked flow, the liquid model is a sufficient simplification [21]. When the compressor speed state $\Omega_{state}(t, U_{\omega}) = 0$, the mass-flow from flash-tank to compressor is blocked such that $\dot{m}_{inj} = 0$, this assertion follows from the compressor speed's influence on the vapour injection. This is modelled by multiplying a scaling factor $\frac{\Omega_{state}(t, U_{\omega})}{\Omega(1)}$ directly on the mass flow, where $\Omega(1)$ is the maximum compressor speed. An apparent flaw of this approach is the assumption that compressor speed has a direct influence on mass-intake, rather than volume-intake. Nevertheless, by doing this, the vapour injection will have a gradual characteristic as the compressor speed increases, instead of discontinuously switching on as soon as the compressor scroll starts spinning:

$$\dot{m}_{inj} = \begin{cases} \begin{cases} A_{vx} C_{vx} \sqrt{D_{v,FT}(p_{FT} - p_{vi})} \cdot \frac{\Omega_{state}(t, U_\omega)}{\Omega(1)} & p_{FT} - p_{vi} > 0 \\ 0 & p_{FT} - p_{vi} \leq 0 \end{cases} & \Omega_{state}(t, U_\omega) > 0 \\ 0 & \Omega_{state}(t, U_\omega) = 0 \end{cases} \quad (3.16)$$

The density at the flash-tank vapour section is found with the look-up table and vapour quality $\chi_{dew} = 1$:

$$D_{v,FT} = \Psi(\chi_{dew}, p_{FT}) \quad (3.17)$$

where

A_{vx}	Cross-sectional area of the vapour injection port	$[m^3]$
C_{vx}	Discharge coefficient	$[\cdot]$
$D_{v,FT}$	Density of the vapour coming from the flash tank	$[kg \cdot m^{-3}]$
p_{FT}	Pressure in flash tank	$[Pa]$
p_{vi}	Pressure in the vapour injection compartment of the compressor	$[Pa]$
χ_{dew}	Vapour quality at dew-point	$[\%]$

The pressure at the compressor vapour-injection port should ideally be found experimentally, as it is dependent on where the injection port is placed on the stationary scroll [9]. As an alternative to the experimental estimation, an algebraic solution Eq. 3.18 will be used, which can be found in several papers [2] [36].

$$p_{vi} = \sqrt{p_{suc} \cdot p_{dis}} \quad (3.18)$$

The pressure at the suction inlet p_{suc} is found in the evaporator model as p_{evap} while p_{dis} is found in the condenser model as p_{cond} . The suction mass-flow into the compressor \dot{m}_{suc} can be found using the volume intake V_{pr} given by the manufacturer:

$$\dot{m}_{suc} = D_{suc} \frac{\Omega_{state}(t, U_\omega)}{60} V_{pr} \cdot 10^{-6} \quad (3.19)$$

The density at the input of the compressor is found via look-up table:

$$D_{suc} = \Psi(T_{suc}, p_{suc}) \quad (3.20)$$

where

D_{suc}	Density of refrigerant at the suction input of the compressor	$[kg \cdot m^{-3}]$
T_{suc}	Temperature at the compressor suction input	$[K]$
p_{suc}	Pressure at the compressor input	$[Pa]$
V_{pr}	Volume of intake per revolution	$[cm^3 \cdot r^{-1}]$
U_{ω}	Compressor control input [0;1]	$[\%]$

As described in Section 2.1. The P-V work done on the refrigerant during compression increases the enthalpy of the refrigerant. In practice the mechanical compression is non-ideal, meaning that the process is not isentropic. Because of this the compressor's isentropic efficiencies must be taken into account.

First of, the mass specific entropy of the refrigerant at the compressor's suction inlet must be found:

$$s_{in_1} = \Psi(T_{suc}, p_{suc}) \quad (3.21)$$

Using the isentropic efficiency of the first compression stage η_1 , the entropy increase is calculated:

$$s_{out_1} = \frac{s_{in_1}}{\eta_1} \quad (3.22)$$

Finding the enthalpy after compression at injection pressure p_{vi} :

$$h_{out_1} = \Psi(s_{out_1}, p_{vi}) \quad (3.23)$$

Repeating the procedure to find flash tank vapour enthalpy, which is at dew-point (see Section 3.5):

$$h_{v,FT} = \Psi(p_{FT}, \chi = 1) \quad (3.24)$$

The two refrigerant flows are summed and normalised with the discharge mass-flow:

$$h_{in_2} = \frac{\dot{m}_{suc} \cdot h_{out_1} + \dot{m}_{inj} \cdot h_{v,FT}}{\dot{m}_{dis}} \quad (3.25)$$

The isentropic efficiency through the second compression stage η_2 is calculated:

$$s_{in_2} = \Psi(h_{in_2}, p_{vi}) \quad (3.26)$$

$$s_{out_2} = \frac{s_{in_2}}{\eta_2} \quad (3.27)$$

Finally the discharge enthalpy is found through the look-up table:

$$h_{dis} = \Psi(s_{out_2}, p_{dis}) \quad (3.28)$$

The symbols are described below:

s_{out_2}	Entropy at compressor discharge port	$[J \cdot K^{-1} \cdot kg^{-1}]$
s_{in_2}	Entropy after vapour injection	$[J \cdot K^{-1} \cdot kg^{-1}]$
s_{out_1}	Entropy before vapour injection	$[J \cdot K^{-1} \cdot kg^{-1}]$
s_{in_1}	Entropy at suction input of compressor	$[J \cdot K^{-1} \cdot kg^{-1}]$
h_{in_2}	Enthalpy after vapour injection	$[J \cdot kg^{-1}]$
h_{out_1}	Enthalpy before vapour injection	$[J \cdot kg^{-1}]$
$h_{v,FT}$	Enthalpy of vapour coming from flash tank	$[J \cdot kg^{-1}]$
η_1	Isentropic efficiency through compressor before vapour injection	[%]
η_2	Isentropic efficiency through compressor after vapour injection	[%]

The coefficients η_1, η_2 are given by collaborator Kresten Sørensen, author of [15].

3.4 Condenser

The purpose of the condenser is to transfer heat energy from the compressed refrigerant vapour to the ambient air, resulting in a drop in refrigerant enthalpy.

The condenser is the component following the compressor and the pressure across the condenser p_{cond} is therefore the same as the compressor discharge pressure. At the condenser outlet, an expansion-valve is placed, which feeds the cooled refrigerant to the flash-tank.

The available sensors in the condenser is a pressure and temperature sensor at the condenser inlet and a temperature sensor at the condenser output.

3.4.1 Condenser Mass Dynamics

The condenser is modelled as seen in Fig. 3.3, it consists of a single lumped region in which complete transition from super-heated vapour to sub-cooled liquid may take place.

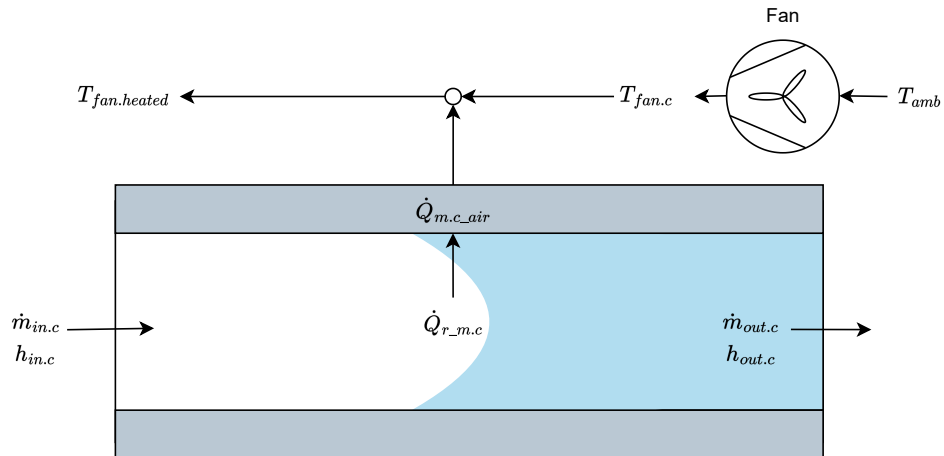


Figure 3.3: Model of condenser

The condenser is modelled as a zero-boundary, mixed region model. In practice a gradual change in enthalpy is expected across the condenser. Because the model enthalpy output may lay within either refrigerant phase (vapour, mixed or liquid) at a given pressure, it was chosen to implement a zero-boundary model.

Because of the gradual enthalpy drop across the condenser, where each point has a different heat-transfer coefficient to the condenser metal, some generalisation must be made in order to simulate the process. To model the heat exchange from the condenser to the ambient environment, and model the change in refrigerant enthalpy, some heat transfer coefficient UA_c must be assumed. The largest change in heat-transfer coefficient is assumed to be associated with phase change [11], this dynamic is however not modelled, as the heat transfer coefficient UA_c is held constant across the entire condenser independent of pressure and enthalpy change.

The condenser mass dynamics are derived from the mass flow into the condenser, $\dot{m}_{in,c}$, and the mass flow out of the condenser $\dot{m}_{out,c}$. For simplicity, it is assumed that some minimal input flow $\dot{m}_{in,c} > 0$ is present:

$$\dot{M}_c = \dot{m}_{in,c} - \dot{m}_{out,c} \quad (3.29)$$

$\dot{m}_{in.c}$	Mass flow into the condenser	$[kg \cdot s^{-1}]$
$\dot{m}_{out.c}$	Mass flow out of the condenser	$[kg \cdot s^{-1}]$
M_c	Refrigerant mass in condenser	$[kg]$
\dot{M}_c	Derivative of refrigerant mass in condenser	$[kg \cdot s^{-1}]$
V_{cond}	Total volume of condenser	$[m^3]$
$h_{in.c}$	Enthalpy of refrigerant at the input of the condenser	$[J \cdot kg^{-1}]$
$h_{out.c}$	Enthalpy of refrigerant at the output of the condenser	$[J \cdot kg^{-1}]$

3.4.2 Fan Dynamics

The condenser fan contributes to the overall enthalpy drop across the condenser. The fan is controlled by the input signal $U_{f.c}$. In order to later calculate the output enthalpy $h_{out.c}$, the air-flow velocity must be estimated. Airflow is calculated as following:

$$\dot{m}_{fan.c}(U_{f.c}) = \dot{V}_{air.c} \cdot D_{air.c} \quad (3.30)$$

The volume flow polynomial is supplied by BITZER

$$\dot{V}_{air.c} = 0.7273 + 0.1202 \cdot U_{m.c} - 0.0044 \cdot U_{m.c}^2 \quad (3.31)$$

U_m is the transformed fan speed given by:

$$U_{m.c} = (3060 \cdot U_{f.c} - 2270.4) \cdot 0.0017 \quad (3.32)$$

$D_{air.c}$	Density of air	$[kg \cdot m^{-3}]$
$U_{f.c}$	Control input of the condenser fan	$[\%]$
$U_{m.c}$	Transformed fan speed	$[s^{-1}]$
$\dot{V}_{air.c}$	Air volume flow through fan	$[m^3 \cdot s^{-1}]$

3.4.3 Heat Energy Flow to Condenser Metal

In order to model the condenser metal temperature dynamics, the heat transfer between the refrigerant, air and metal needs to be found for the entire condenser.

First the advection heat transfer from condenser refrigerant to metal is calculated with the heat transfer coefficient UA_c . The output temperature $T_{out.c}$ of the condenser is taken as the heat source.

$$\dot{Q}_{r_m.c} = UA_c(T_{out.c} - T_{m.c}) \quad (3.33)$$

The heat transfer to the air from the condenser metal $\dot{Q}_{m.c_air}$, is found with the temperature of the metal $T_{m.c}$, the temperature of the air coming from the fan, $T_{fan.c}$, the mass flow through the fan, $\dot{m}_{fan.c}$ and the heat capacity of the air, $C_{p,air}$:

$$\dot{Q}_{m.c_air} = (T_{m.c} - T_{fan.c})\dot{m}_{fan.c}C_{p,air} \quad (3.34)$$

By adding up the total heat-flow to and from the condenser metal and dividing with the constant $M_{m.c}C_{p,m}$, the metal temperature dynamic is modelled:

$$\dot{T}_{m.c} = \frac{\dot{Q}_{r.c.m.c} - \dot{Q}_{m.c.air}}{M_{m.c}C_{p,m}} \quad (3.35)$$

UA_c	Heat transfer coefficient between condenser metal and refrigerant	$[J \cdot K^{-1} \cdot s^{-1}]$
$T_{out.c}$	Refrigerant temperature at the output of the condenser	$[K]$
$T_{m.c}$	Metal temperature of the condenser	$[K]$
$\dot{Q}_{r.m.c}$	Heat energy flow from refrigerant to metal	$[W]$
$\dot{Q}_{m.c.air}$	Heat energy flow from condenser metal to air	$[W]$
$M_{m.c}$	Mass of condenser metal	$[kg]$
$C_{p,m}$	Heat capacity of the metal	$[J \cdot K^{-1}]$
$\dot{T}_{m.c}$	Time derivative of condenser metal temperature	$[K \cdot s^{-1}]$

3.4.4 Condenser Output Enthalpy Dynamics

In order to find the output enthalpy of the condenser, $h_{out.c}$ dynamics must be derived. To derive the $h_{out.c}$ dynamic $\dot{h}_{out.c}$, the energy-flow balance in the condenser is found by subtracting the mass related output energy flow from the input flow, furthermore the heat energy-flow to the metal is subtracted.

$$\frac{dM_c(t)h_{r.c}(t)}{dt} = \dot{m}_{in.c}h_{in.c} - \dot{m}_{out.c}h_{out.c} - \dot{Q}_{r.m.c} \quad (3.36)$$

The enthalpy in the condenser refrigerant, $h_{r.c}$, is modelled such that it is equal to the output, $h_{r.c} = h_{out.c}$:

$$\frac{dM_c(t)h_{out.c}(t)}{dt} = \dot{m}_{in.c}h_{in.c} - \dot{m}_{out.c}h_{out.c} - \dot{Q}_{r.m.c} \quad (3.37)$$

Using the product rule on the LHS. of 3.37:

$$\frac{dM_c(t)h_{out.c}(t)}{dt} = M_c\dot{h}_{out.c} + \dot{M}_c h_{out.c} \quad (3.38)$$

Equating equation 3.38 and 3.37:

$$M_c\dot{h}_{out.c} + \dot{M}_c h_{out.c} = \dot{m}_{in.c}h_{in.c} - \dot{m}_{out.c}h_{out.c} - \dot{Q}_{r.m.c} \quad (3.39)$$

Solving for $\dot{h}_{out.c}$:

$$\dot{h}_{out.c} = \frac{\dot{m}_{in.c}h_{in.c} - \dot{m}_{out.c}h_{out.c} - \dot{Q}_{r.m.c} - \dot{M}_c h_{out.c}}{M_c} \quad (3.40)$$

$h_{r.c}$	Enthalpy of entire condenser	$[J \cdot kg^{-1}]$
$h_{out.c}$	Output enthalpy of the condenser	$[J \cdot kg^{-1}]$
$\dot{m}_{out.c}$	Mass flow out of condenser	$[kg \cdot s^{-1}]$
$\dot{h}_{out.c}$	Time derivative of condenser output enthalpy $h_{out.c}$	$[J \cdot kg^{-1} \cdot s^{-1}]$

3.4.5 Pressure Dynamics

The pressure dynamics of the condenser is split into a sum of 2 different pressure contributions \dot{p}_{cond_1} and \dot{p}_{cond_2} . The first dynamic is the pressure change as a result of different input and output flows. The result is an increase in pressure when the input flow is bigger than the output flow and vice versa.

The other pressure dynamic considered is the pressure increase caused by an increase in enthalpy. As the enthalpy increases, so does the refrigerants willingness to expand and thus the pressure on the condenser metal tubing. A challenge presented by the zero-boundary condenser model, is the different characteristics of the three refrigerant phases. Because of this, different mass regions are estimated for calculating the pressure state. The regions are separated by the bubble and dew points as shown in Fig. 3.4.

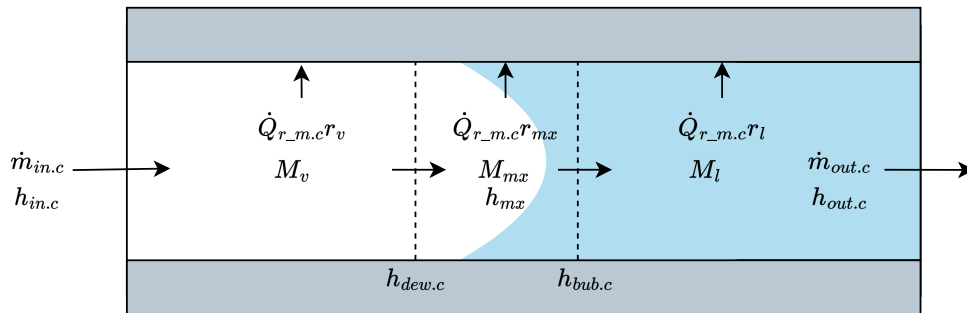


Figure 3.4: Model of condenser showing pressure region masses

It is apparent that the model shown in Fig. 3.4 is only valid when sub-cooling is present at the condenser output. The derivations below will assume this is the case, while the altered models for the mixed and vapour output will be shown after derivation.

Constant Enthalpy Pressure Dynamics

The pressure increase resulting from different mass flows is based on the condenser inlet and outlet mass-flow and the associated change of mass M_c . Because of the vastly different characteristics of the vapour, mixed and liquid parts, the model will be partitioned accordingly. It is for simplicity naively assumed that the mass

in each section corresponds to their relative enthalpy span, such that the mass ratio of the three sections are defined:

$$r_v = \frac{h_{in.c} - h_{dew}}{h_{in.c} - h_{out.c}} \quad (3.41)$$

$$r_{mx} = \frac{h_{dew.c} - h_{bub.c}}{h_{in.c} - h_{out.c}} \quad (3.42)$$

$$r_l = \frac{h_{bub.c} - h_{out.c}}{h_{in.c} - h_{out.c}} \quad (3.43)$$

Such that the masses are defined:

$$M_v = r_v \cdot M_c \quad (3.44)$$

$$M_{mx} = r_{mx} \cdot M_c \quad (3.45)$$

$$M_l = r_l \cdot M_c \quad (3.46)$$

Furthermore the respective mass dynamics for the three masses are found:

$$\dot{M}_v = \dot{m}_{in.c} - \frac{\dot{Q}_{r.m.c} \cdot r_v}{h_{in.c} - h_{dew}} \quad (3.47)$$

$$\dot{M}_{mx} = \frac{\dot{Q}_{r.m.c} \cdot r_v}{h_{in.c} - h_{dew}} - \frac{\dot{Q}_{r.m.c} \cdot r_{mx}}{h_{dew} - h_{bub}} \quad (3.48)$$

$$\dot{M}_l = \frac{\dot{Q}_{r.m.c} \cdot r_{mx}}{h_{dew} - h_{bub}} - \dot{m}_{out.c} \quad (3.49)$$

$h_{bub.c}$	Enthalpy at condenser bubble-point	$[J \cdot kg^{-1}]$
$h_{dew.c}$	Enthalpy at condenser dew-point	$[J \cdot kg^{-1}]$
M_v	Estimated mass of vapour region	$[kg]$
M_{mx}	Estimated mass of mixed phase region	$[kg]$
M_l	Estimated mass of liquid region	$[kg]$
\dot{M}_v	Estimated mass dynamic of vapour region	$[kg \cdot s^{-1}]$
\dot{M}_{mx}	Estimated mass dynamic of mixed phase region	$[kg \cdot s^{-1}]$
\dot{M}_l	Estimated mass dynamic of liquid region	$[kg \cdot s^{-1}]$

With this in mind, the following mass-flow balance is written

$$\frac{dM_l(t, p)}{dt} + \frac{dM_{mx}(t, p)}{dt} + \frac{dM_v(t, p)}{dt} = \dot{m}_{in.c} - \dot{m}_{out.c} \quad (3.50)$$

Substituting the masses with the equivalent pressure dependent density and volume terms:

$$\frac{d(D_l(t, p) \cdot V_l(t))}{dt} + \frac{d(D_v(t, p) \cdot V_v(t))}{dt} + \frac{d(D_{mx}(t, p) \cdot V_{mx}(t))}{dt} = \dot{m}_{in.c} - \dot{m}_{out.c} \quad (3.51)$$

Using the product rule on the LHS results in the following expression:

$$\begin{aligned} D_l(t, p)\dot{V}_l(t) + \dot{D}_l(t, p)V_l(t) + D_{mx}(t, p)\dot{V}_{mx}(t) \\ + \dot{D}_{mx}(t, p)V_{mx}(t) + D_v(t, p)\dot{V}_v(t) + \dot{D}_v(t, p)V_v(t) \end{aligned} = \dot{m}_{in.c} - \dot{m}_{out.c} \quad (3.52)$$

Expanding further with the chain-rule on \dot{D} to find the time derivative of pressure p_{cond} :

$$\begin{aligned} \frac{\partial D_l(t, p)}{\partial p} \dot{p}_{cond_1} V_l(t) + \frac{\partial D_{mx}(t, p)}{\partial p} \dot{p}_{cond_1} V_{mx}(t) + \frac{\partial D_v(p)}{\partial p} \dot{p}_{cond_1} V_v(t) \\ + D_l(t, p)\dot{V}_l(t) + D_{mx}(t, p)\dot{V}_{mx}(t) + D_v(t, p)\dot{V}_v(t) \end{aligned} = \dot{m}_{in.c} - \dot{m}_{out.c} \quad (3.53)$$

The pressure dynamic terms are collected:

$$\begin{aligned} \dot{p}_{cond_1} \left(\frac{\partial D_l(t, p)V_l(t)}{\partial p} + \frac{\partial D_{mx}(t, p)V_{mx}(t)}{\partial p} + \frac{\partial D_v(t, p)V_v(t)}{\partial p} \right) \\ + D_l(t, p)\dot{V}_l(t) + D_{mx}(t, p)\dot{V}_{mx}(t) + D_v(t, p)\dot{V}_v(t) \end{aligned} = \dot{m}_{in.c} - \dot{m}_{out.c} \quad (3.54)$$

In order to simplify the model, the volumes V_l , V_{mx} and V_v are held constant for the differential equation. Isolating \dot{p}_{cond_1} and renaming it to $\dot{p}_{cond_1,l}$ to indicate liquid output and substituting the partial derivatives for \mathcal{E}_c , \mathcal{F}_c and \mathcal{G}_c grants:

$$\dot{p}_{cond_1,l}(t) = \frac{\dot{m}_{in.c} - \dot{m}_{out.c}}{\mathcal{E}_c \cdot V_l + \mathcal{F}_c \cdot V_{mx} + \mathcal{G}_c \cdot V_v} \quad (3.55)$$

The partial derivatives are evaluated for constant enthalpy:

$$\mathcal{E}_c = \left. \frac{\partial D_l(p)}{\partial p_{cond}} \right|_{h_{out.c}} \quad (3.56)$$

$$\mathcal{F}_c = \left. \frac{\partial D_{mx}(p)}{\partial p_{cond}} \right|_{h_{mx}} \quad (3.57)$$

$$\mathcal{G}_c = \left. \frac{\partial D_v(p)}{\partial p_{cond}} \right|_{h_{in.c}} \quad (3.58)$$

The volumes V_v , V_{mx} and V_l will be found with the arithmetic mean of densities in the given phase region, the densities at a specific point with enthalpy h_k is found based on pressure and enthalpy

$$D = \Psi(h_k, p) \quad (3.59)$$

Errors resulting from the inaccurate relationships between masses and volumes, caused by the model simplifications, will be discussed in the Discussion Chapter 7.

While the pressure model above applies to a condenser with three regions, the dynamics change as soon as sub-cooling is omitted in favour of the mixed region and once more when the output is in the super-heated phase. The dynamics that take over in those cases are as follows:

$$\dot{p}_{cond1,mx}(t) = \frac{\dot{m}_{in.c} - \dot{m}_{out.c}}{\mathcal{F}_c \cdot V_{mx} + \mathcal{G}_c \cdot V_v} \quad (3.60)$$

Keeping in mind that for the mixed phase output, the density averaging range depends on the output quality of the mixed region.

$$\dot{p}_{cond1,v}(t) = \frac{\dot{m}_{in.c} - \dot{m}_{out.c}}{\mathcal{G}_c \cdot V_c} \quad (3.61)$$

For the vapour output, the volume term $V_v = V_c$, since the condenser is completely in vapour phase.

Constant Density Pressure Dynamics

The change of energy in the condenser causing a change in pressure can be described by the energy-flow balance which is the sum of the energy change in all the phase regions. Enthalpy is dependent on time and pressure $h = h(t, p)$ and while mass is time dependent $M = M(t)$:

$$\frac{dM_l(t)h_l(t, p)}{dt} + \frac{dM_{mx}(t)h_{mx}(t, p)}{dt} + \frac{dM_v(t)h_v(t, p)}{dt} = \dot{m}_{in.c}h_{in.c} - \dot{m}_{out.c}h_{out.c} - \dot{Q}_{r_{m.c}} \quad (3.62)$$

For the liquid enthalpy h_l , the output enthalpy $h_{out.c}$ is used, for the vapour region h_{in} , and h_{mx} is found as the arithmetic average from the dew to bubble-point:

$$\frac{dM_l(t)h_{out}(t, p)}{dt} + \frac{dM_{mx}(t)h_{mx}(t, p)}{dt} + \frac{dM_v(t)h_{in}(t, p)}{dt} = \dot{m}_{in.c}h_{in.c} - \dot{m}_{out.c}h_{out.c} - \dot{Q}_{r_{m.c}} \quad (3.63)$$

Using the product rule on Eq. 3.63 :

$$\begin{aligned} M_l \dot{h}_{out.c} + \dot{M}_l h_{out.c} + M_{mx} \dot{h}_{mx} + \dot{M}_{mx} h_{mx} + M_v \dot{h}_{in.c} + \dot{M}_v h_{in.c} \\ = \dot{m}_{in.c} h_{in.c} - \dot{m}_{out.c} h_{out.c} - \dot{Q}_{r_{m.c}} \end{aligned} \quad (3.64)$$

The chain rule is applied to the enthalpy time-derivatives resulting in:

$$\begin{aligned} M_l \frac{\partial h_{out.c}(p)}{\partial p} \dot{p}_{cond_2} + M_{mx} \frac{\partial h_{mx}(p)}{\partial p} \dot{p}_{cond_2} + M_v \frac{\partial h_{in.c}(p)}{\partial p} \dot{p}_{cond_2} \\ + \dot{M}_l h_{out.c} + \dot{M}_{mx} h_{mx} + \dot{M}_v h_{in.c} \\ = \dot{m}_{in.c} h_{in.c} - \dot{m}_{out.c} h_{out.c} - \dot{Q}_{r.m.c} \end{aligned} \quad (3.65)$$

By factorising Eq. 3.65 with respect to the pressure dynamics \dot{p}_{cond_2} and moving the remaining terms to the RHS:

$$\begin{aligned} \dot{p}_{cond_2} \left(M_l \frac{\partial h_{out.c}(p)}{\partial p} + M_{mx} \frac{\partial h_{mx}(p)}{\partial p} + M_v \frac{\partial h_{in.c}(p)}{\partial p} \right) \\ = \dot{m}_{in.c} h_{in.c} - \dot{m}_{out.c} h_{out.c} - \dot{Q}_{r.m.c} - \dot{M}_l h_{out.c} - \dot{M}_{mx} h_{mx} - \dot{M}_v h_{in.c} \end{aligned} \quad (3.66)$$

It is now possible to solve for the pressure dynamics \dot{p}_{cond_2} and rename it to $\dot{p}_{cond_2,l}$ to indicate liquid output:

$$\dot{p}_{cond_2,l}(t) = \frac{\dot{m}_{in.c} h_{in.c} - \dot{m}_{out.c} h_{out.c} - \dot{Q}_{r.m.c} - \dot{M}_l h_{out.c} - \dot{M}_{mx} h_{mx} - \dot{M}_v h_{in.c}}{M_l \mathcal{I}_c + M_{mx} \mathcal{J}_c + M_v \mathcal{K}_c} \quad (3.67)$$

The derivatives are evaluated for constant densities and the enthalpy of the different phase-regions.

$$\mathcal{I}_c = \left. \frac{\partial h_{out.c}(p)}{\partial p} \right|_{D_l} \quad (3.68)$$

$$\mathcal{J}_c = \left. \frac{\partial h_{mx}(p)}{\partial p} \right|_{D_{mx}} \quad (3.69)$$

$$\mathcal{K}_c = \left. \frac{\partial h_{in.c}(p)}{\partial p} \right|_{D_{in}} \quad (3.70)$$

It should be noted that $\mathcal{K}_c = 0$, when the input enthalpy $h_{in.c}$ is constant and $\dot{m}_{in.c} > 0$.

Once again, a sub-cooled liquid output is not guaranteed. In the case of other output phases, the masses and the products involving the output enthalpy $h_{out.c}$ are changed:

$$\dot{p}_{cond_2,mx}(t) = \frac{\dot{m}_{in.c} h_{in.c} - \dot{m}_{out.c} h_{out.c} - \dot{Q}_{r.m.c} - \dot{M}_{mx} h_{out.c} - \dot{M}_v h_{in.c}}{M_{mx} \mathcal{J}_c + M_v \mathcal{K}_c} \quad (3.71)$$

$$\dot{p}_{cond_2,v}(t) = \frac{\dot{m}_{in.c} h_{in.c} - \dot{m}_{out.c} h_{out.c} - \dot{Q}_{r.m.c} - \dot{M}_v h_{out.c}}{M_v \mathcal{K}_c} \quad (3.72)$$

Overall Pressure Dynamics

The overall pressure dynamics are the sums of the pressure pairs, dependent on the output enthalpy relative to the bubble and dew points:

$$\dot{p}_{cond_1} = \begin{cases} \dot{p}_{cond_1,l} & h_{out.c} < h_{bub.c} \\ \dot{p}_{cond_1,mx} & h_{dew.c} > h_{out.c} > h_{bub.c} \\ \dot{p}_{cond_1,v} & h_{out.c} > h_{dew.c} \end{cases} \quad (3.73)$$

$$\dot{p}_{cond_2} = \begin{cases} \dot{p}_{cond_2,l} & h_{out.c} < h_{bub.c} \\ \dot{p}_{cond_2,mx} & h_{dew.c} > h_{out.c} > h_{bub.c} \\ \dot{p}_{cond_2,v} & h_{out.c} > h_{dew.c} \end{cases} \quad (3.74)$$

The complete pressure state is the sum of 3.73 and 3.74, the first dependent on mass-flow and the second dependent on enthalpy.

$$\dot{p}_{cond}(t) = \dot{p}_{cond_1}(t) + \dot{p}_{cond_2}(t) \quad (3.75)$$

3.5 Flash-tank

The flash-tank is a cylinder shaped pressure-tank, designed such that it has a single input fed from the condenser through the input valve. There are two output flows, the first is the vapour output, where refrigerant flows through the compressor injection port. The second output is the liquid output that is fed to the evaporator through an expansion valve. A model of the flash-tank is shown in Fig. 3.5

Effectively the flash-tank works as an intermediate pressure buffer which reduces the flash-gas entering the evaporator, while reusing the intermediate pressure vapour directly in the compressor.

The available sensors in the flash-tank is a pressure sensor and a temperature sensor at the liquid outlet.

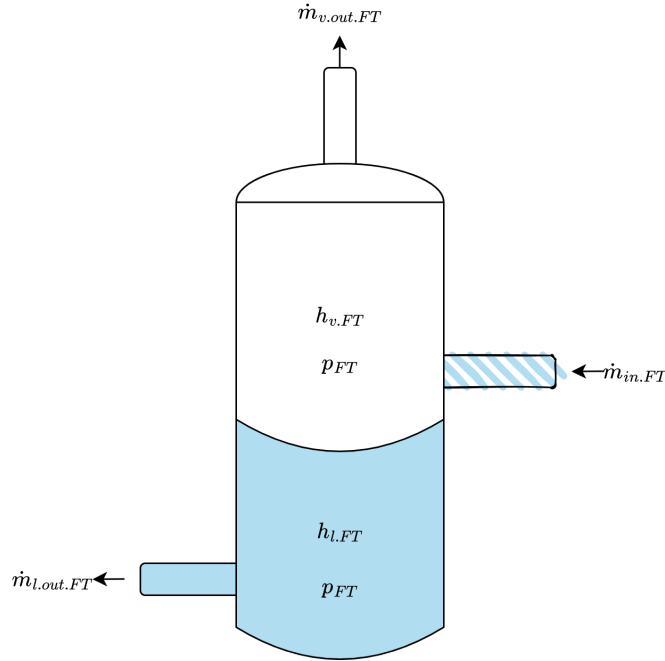


Figure 3.5: Model of flash-tank

Considering the pH characteristic of the refrigerant, seen in Section 2.1.3, it is evident that the pressure drop across the input valve can result in a relative phase change from liquid to a liquid-vapour mixture, given that the pressure drop is significant. This phenomenon is called flashing. The mass-flow into the flash-tank $\dot{m}_{in,FT}$, can be described as a sum of the mass-flow of the liquid $\dot{m}_{l,in,FT}$, and the vapour $\dot{m}_{v,in,FT}$, as:

$$\dot{m}_{in,FT} = \dot{m}_{l,in,FT}(p) + \dot{m}_{v,in,FT}(p) \quad (3.76)$$

Given that flashing has happened. The mass distribution can be described by the vapour-quality $\chi_{in} = \Psi(h_{in,FT}, p_{FT})$, the different phase mass-flows are calculated:

$$\dot{m}_{l,in,FT} = (1 - \chi_{in,FT}) \cdot \dot{m}_{in,FT} \quad (3.77)$$

$$\dot{m}_{v,in,FT} = \chi_{in,FT} \cdot \dot{m}_{in,FT} \quad (3.78)$$

Similar to the input flows, the output is described:

$$\dot{m}_{out,FT} = \dot{m}_{l,out,FT} + \dot{m}_{v,out,FT} \quad (3.79)$$

Differential equations for the control masses can be derived from the input and output flows:

$$\dot{M}_{l,FT} = \dot{m}_{l,in,FT} - \dot{m}_{l,out,FT} \quad (3.80)$$

$$\dot{M}_{v,FT} = \dot{m}_{v,in,FT} - \dot{m}_{v,out,FT} \quad (3.81)$$

$\dot{m}_{in,FT}$	Total input mass flow	$[kg \cdot s^{-1}]$
$\dot{m}_{v,in,FT}$	Vapour input mass flow	$[kg \cdot s^{-1}]$
$\dot{m}_{l,in,FT}$	Liquid input mass flow	$[kg \cdot s^{-1}]$
$\dot{m}_{out,FT}$	Total output mass flow	$[kg \cdot s^{-1}]$
$\dot{m}_{v,out,FT}$	Vapour output mass flow	$[kg \cdot s^{-1}]$
$\dot{m}_{l,out,FT}$	Liquid output mass flow	$[kg \cdot s^{-1}]$
$\chi_{in,FT}$	Vapour quality of input flow	$[\%]$
$\dot{M}_{l,FT}$	Change of liquid mass in flash-tank	$[kg \cdot s^{-1}]$
$\dot{M}_{v,FT}$	Change of vapour mass in flash-tank	$[kg \cdot s^{-1}]$

3.5.1 Pressure Dynamics in Flash-tank

The pressure dynamics in the flash-tank are derived similarly to the condenser in section 3.4.5 from the mass balance:

$$\frac{dM_{l,FT}(t,p)}{dt} + \frac{dM_{v,FT}(t,p)}{dt} = \dot{m}_{out,FT} - \dot{m}_{in,FT} \quad (3.82)$$

Assuming constant volumes $V_{v,FT}$, $V_{l,FT}$ the resulting pressure state equation is:

$$\dot{p}_{FT} = \frac{\dot{m}_{in,FT} - \dot{m}_{out,FT}}{\mathcal{F}_{FT} \cdot V_{l,FT} + \mathcal{G}_{FT} \cdot V_{v,FT}} \quad (3.83)$$

The derivatives are evaluated for constant enthalpy:

$$\mathcal{F}_{FT} = \left. \frac{\partial D_{l,FT}(p)}{\partial p} \right|_{h_{l,FT}} \quad (3.84)$$

$$\mathcal{G}_{FT} = \left. \frac{\partial D_{v,FT}(p)}{\partial p} \right|_{h_{v,FT}} \quad (3.85)$$

$V_{l,FT}$	Volume of liquid section	$[m^3]$
$V_{v,FT}$	Volume of vapour section	$[m^3]$

3.5.2 Enthalpy in Flash-tank

The enthalpy at the two flash-tank outputs are found via look-up table and are hence dependent on the dynamic pressure in the flash-tank and the qualities corresponding to the dew and bubble-points of the refrigerant:

$$h_{v,FT} = \Psi(p_{FT}, \chi_{FT} = 1) \quad (3.86)$$

$$h_{l,FT} = \Psi(p_{FT}, \chi_{FT} = 0) \quad (3.87)$$

Where:

$$\chi_{FT} \quad \text{Quality of the refrigerant} \quad [\%]$$

3.6 Evaporator

The Evaporator is the final stage in the refrigeration cycle. After the flash-tank's intermediate pressure drop and flashing, the refrigerant which is at bubble-point at flash-tank pressure, flashes slightly when being throttled through the evaporator expansion valve. It is known that the properties of liquid and vapour are different, concretely the heat transfer between the evaporator walls and the refrigerant is reduced once the refrigerant is in vapour form [11], yet it is detrimental if any liquid is allowed into the compressor resulting in compressor-slugging [16]. This stresses the importance of tracking the super-heat as it presents a tangible way of estimating how much energy has been absorbed since saturation, while it also indicates that vapour saturation has occurred. The evaporator model is a two-region moving boundary model, with a boundary placed between the mixed refrigerant region ($\chi < 1$) and the super-heated vapour region. The boundary also partitions the evaporator metal casing. The modelling approach mirrors that of the condenser in Modelling Section 3.4, with the main difference being that it includes a moving boundary and that it does not lump different refrigerant phases.

The available sensors is a pressure and a temperature sensor at the evaporator output.

3.6.1 Evaporator Boundary and Regions

The evaporator is modelled as shown in Fig. 3.6. The region containing mixed (mx) refrigerant is referred to as the mixed region and the region containing vapour is referred to as the super-heated region (sh).

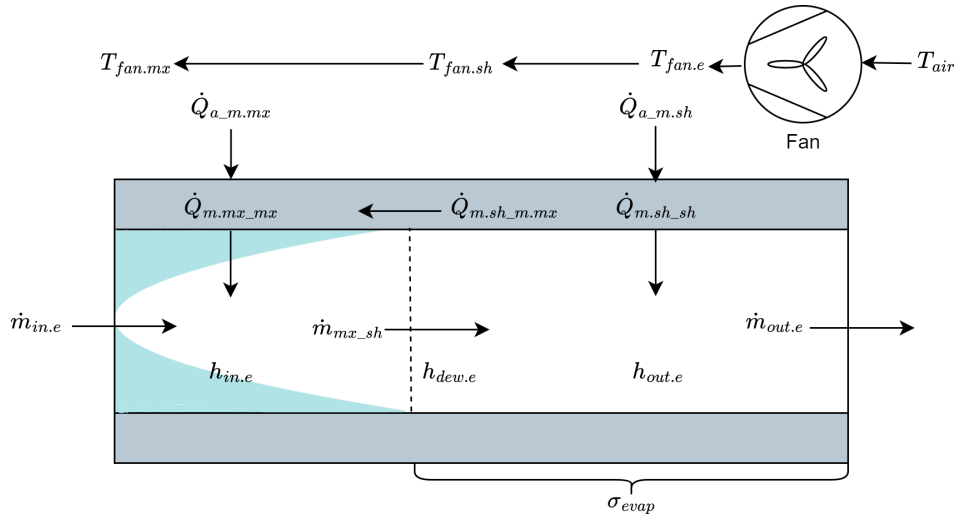


Figure 3.6: Model of Evaporator

The boundary location in the model is based on the total evaporator volume V_e , and the volume occupied by the super-heated region. The boundary location is estimated by using the mass of the super-heated region M_{sh} , and the average density across the super-heated region D_{sh} :

$$\sigma_{evap} = \frac{M_{sh}}{V_e \cdot D_{sh}} \quad (3.88)$$

σ_{evap}	Percentage of evaporator volume containing super-heated refrigerant	[%]
M_{sh}	Mass of super-heated region	[kg]
D_{sh}	Density of super-heated region	[kg · m ⁻³]
V_e	Evaporator total internal volume	[m ³]

As mentioned in the Discussion Chapter 7, the model does not take the void-fraction into consideration, but relies on averaging.

3.6.2 Fan Air Flow and Temperature

The air flow through the fan is calculated similarly to the way it was done for the condenser fan:

$$\dot{m}_{fan.e}(U_{f.e}) = \dot{V}_{air.e} \cdot D_{air.e} \quad (3.89)$$

The volume flow is supplied by BITZER:

$$\dot{V}_{air.e} = 0.7273 + 0.1202 \cdot U_{m.e} - 0.0044 \cdot U_{m.e}^2 \quad (3.90)$$

$U_{m.e}$ is the transformed fan speed given by:

$$U_{m.e} = (3060 \cdot U_{f.e} - 2270.4) \cdot 0.0017 \quad (3.91)$$

$D_{air.e}$	Density of air	$[kg \cdot m^{-3}]$
$U_{f.e}$	Control input of the evaporator fan	$[\%]$
$U_{m.e}$	transformed fan speed	$[s^{-1}]$
$\dot{V}_{air.e}$	Air volume flow through fan	$[m^3 \cdot s^{-1}]$

The heat transfer into the evaporator is dependent on the air flow and its temperature. The air from the fans decreases in temperature as it is blown across the evaporator from the super-heated to the mixed region. The first region of the evaporator that the air flows past is the super-heated vapour region:

$$T_{fan.sh} = T_{fan.in} - \frac{\dot{Q}_{a.m.sh}}{\dot{m}_{fan.e} \cdot C_{p.air}} \quad (3.92)$$

After transferring heat to the super-heated region, the air passes over the mixed region. This is the air that will be used to cool the reefer in Reefer Model Section 3.7:

$$T_{fan.mx} = T_{fan.sh} - \frac{\dot{Q}_{a.m.mx}}{\dot{m}_{fan.e} \cdot C_{p.air}} \quad (3.93)$$

Where

$T_{fan.in}$	Temperature of the air in reefer	$[K]$
$T_{fan.sh}$	Temperature of the air after blowing over the super-heated region	$[K]$
$T_{fan.mx}$	Temperature of the air after blowing over the mixed region	$[K]$
\dot{m}_{fan}	mass-flow of air from the fan	$[kg \cdot s^{-1}]$
$\dot{Q}_{a.m.sh}$	Energy flow from air to metal in super-heated region	$[W]$
$\dot{Q}_{a.m.mx}$	Energy flow from air to the metal in the mixed region	$[W]$
$C_{p.air}$	Heat capacity of air	$[J \cdot K^{-1}]$

3.6.3 Dynamics of Evaporator Metal

From Air to Metal

As seen above there is a heat flow from the reefer air to the metal. In the super-heated region the heat energy flow from air to metal $\dot{Q}_{a.m.sh}$, can be written as:

$$\dot{Q}_{a.m.sh} = (T_{fan.in} - T_{m.sh}) \cdot \dot{m}_{fan} \cdot C_{p.air} \quad (3.94)$$

For the mixed region the heat energy flow from air to metal is:

$$\dot{Q}_{a_m.mx} = (T_{fan.sh} - T_{m.mx}) \cdot \dot{m}_{fan} \cdot Cp_{air} \quad (3.95)$$

Where

$T_{m.sh}$	Temperature of metal in super-heated region	[K]
$T_{m.mx}$	Temperature of metal in mixed region	[K]

From Metal to Refrigerant

The heat energy flow from the metal to the refrigerant in the super-heated region is modelled with heat-transfer coefficient UA_{sh} and the factor σ_{evap} adjusting to the current super-heat volume:

$$\dot{Q}_{m.sh_sh} = UA_{sh} \cdot (T_{m.sh} - T_{out.e}) \cdot (\sigma_{evap}) \quad (3.96)$$

In the mixed region, the heat-transfer coefficient UA_{mx} is used in a similar manner with $(1 - \sigma_{evap})$ as the correcting factor:

$$\dot{Q}_{m.mx_mx} = UA_{mx} \cdot (T_{m.mx} - T_{in.e}) \cdot (1 - \sigma_{evap}) \quad (3.97)$$

$T_{in.e}$ is not measured and is found via a lookup table:

$$T_{in.e} = \Psi(p_{evap}, h_{in.e}) \quad (3.98)$$

UA_{sh}	Heat transfer coefficient for super-heated region	$[J \cdot K^{-1} \cdot s^{-1}]$
UA_{mx}	Heat transfer coefficient for mixed region	$[J \cdot K^{-1} \cdot s^{-1}]$
UA_m	Heat transfer coefficient for metal	$[J \cdot K^{-1} \cdot s^{-1}]$
$T_{in.e}$	Temperature refrigerant at input of evaporator	[K]
$T_{out.e}$	Temperature refrigerant at output of evaporator	[K]

Transfer Across Metal Boundary

There is also a flow of heat between the metal in the two regions, it is described by the equation:

$$\dot{Q}_{m.sh_m.mx} = UA_m \cdot (T_{m.sh} - T_{m.mx}) \quad (3.99)$$

The heat transfer coefficients for UA_{sh} , UA_{mx} , UA_m must be found empirically based on tests, and are in this project estimated by Kresten Sørensen in [15].

Temperature of Metal

The temperature dynamics of the metal in both regions is derived as the sum of all heat-energy flows affecting the metal bodies, divided by the metal region mass $M_{m.e}$ and the metal heat capacity $C_{p.m}$:

$$\dot{T}_{m.mx} = \frac{\dot{Q}_{a_m.mx} - \dot{Q}_{m.mx_mx} + \dot{Q}_{m.sh_m.mx}}{(1 - \sigma_{evap}) \cdot M_{m.e} \cdot C_{p.m}} \quad (3.100)$$

$$\dot{T}_{m.sh} = \frac{\dot{Q}_{a_m.sh} - \dot{Q}_{m.sh_sh} - \dot{Q}_{m.sh_m.mx}}{\sigma_{evap} \cdot M_{m.e} \cdot C_{p.m}} \quad (3.101)$$

Where

$M_{m.e}$	Mass of metal	[kg]
$C_{p.m}$	Heat capacity of the metal	[J · K ⁻¹]

3.6.4 Mass Balances

The dynamics of the masses are needed in order to estimate the output temperature and pressure. First the mass-flow from the mixed to the super-heated region is found as:

$$\dot{m}_{mx_sh} = \frac{\dot{Q}_{m.mx_mx}}{h_{dew} - h_{in.e}} \quad (3.102)$$

Where $h_{in.e}$ is the enthalpy of the refrigerant at the input of the evaporator and h_{dew} is the enthalpy at the dew-point of the refrigerant. The mass-flow between the mixed phase and liquid phase is found as the heat-energy flow from the mixed region to the metal, divided by the difference of enthalpy between the input and dew-point. The change in mass of the mixed-phase region is then derived:

$$\dot{M}_{mx} = \dot{m}_{in.e} - \dot{m}_{mx_sh} \quad (3.103)$$

And for the super-heated region:

$$\dot{M}_{sh} = \dot{m}_{mx_sh} - \dot{m}_{out.e} \quad (3.104)$$

Where $\dot{m}_{in.e}$ is determined by the valve model in section 3.2. $\dot{m}_{out.e}$ is determined by the compressor model in section 3.3.

3.6.5 Output Enthalpy Dynamics

The temperature at the output of the evaporator is found with the look-up table:

$$T_{out.e} = \Phi(h_{out.e}, p_{evap}) \quad (3.105)$$

The dynamics of the enthalpy are found in a similar way to how it was done for the condenser in Modelling Section 3.4.4, a detailed description of the derivation will not be given here.

$$\dot{h}_{out.e} = \frac{\dot{m}_{mx_sh} \cdot h_{dew} - \dot{m}_{out.e} \cdot h_{out.e} + \dot{Q}_{m.sh_sh} - \dot{M}_{sh} \cdot h_{out.e}}{M_{sh}} \quad (3.106)$$

3.6.6 Pressure Dynamics

As for the condenser, the pressure of the evaporator is expected to rise with an increase of refrigerant inflow relative to the outflow. Since only one pressure sensor is available, it is assumed that the pressure is constant across the evaporator:

$$p_{evap} = p_{mx} = p_{sh} \quad (3.107)$$

Constant Enthalpy

The derivation was done in the condenser Model Section 3.4.5 it will therefore be left out here. The dynamics of the pressure in the evaporator is assuming constant volumes derived to be:

$$\dot{p}_{evap_1}(t) = \frac{\dot{m}_{in.e} - \dot{m}_{out.e}}{\mathcal{F}_e \cdot V_{mx} + \mathcal{G}_e \cdot V_{sh}} \quad (3.108)$$

Where the partial derivatives \mathcal{F}_e and \mathcal{G}_e are evaluated for constant enthalpy at the input and output respectively:

$$\mathcal{F}_e = \left. \frac{\partial D_{mx}(p)}{\partial p_{evap}} \right|_{h_{in.e}} \quad (3.109)$$

$$\mathcal{G}_e = \left. \frac{\partial D_{sh}(p)}{\partial p_{evap}} \right|_{h_{out.e}} \quad (3.110)$$

Constant Density Pressure Dynamics

Given constant input and output, an increase in the super-heated region will excite the refrigerant resulting in an expansion, since an expansion is not possible in the confined space the pressure increases. Again the derivation is quite similar to the one in the condenser and will not be done here. The pressure dynamic from a change in enthalpy is derived:

$$\dot{p}_{evap_2}(t) = \frac{\dot{Q}_{m.sh} \cdot h_{sh} - h_{out.e} \cdot \dot{m}_{out.e} + \dot{Q}_{m.mx} \cdot h_{in.e} - h_{out.e} \cdot \dot{M}_{sh} - \chi_e \cdot h_{dew.e} \cdot \dot{M}_{mx} - (1 - \chi_e) \cdot h_{bub.e} \cdot \dot{M}_{mx}}{M_{sh} \cdot \mathcal{H}_e + M_{mx} \cdot (\chi_e \cdot \mathcal{I}_e + (1 - \chi_e) \cdot \mathcal{J}_e)} \quad (3.111)$$

Where

$$\mathcal{H}_e = \left. \frac{\partial h_{out.e}(p)}{\partial p_{evap}} \right|_{D_{sh}} \quad (3.112)$$

$$\mathcal{I}_e = \left. \frac{\partial h_{dew.e}(p)}{\partial p_{evap}} \right|_{D_{dew}} \quad (3.113)$$

$$\mathcal{J}_e = \left. \frac{\partial h_{in.e}(p)}{\partial p_{evap}} \right|_{D_{bub}} \quad (3.114)$$

The dynamics of the pressure with respect to both a change in mass-flow and enthalpy is:

$$\dot{p}_{evap}(t) = \dot{p}_{evap_1}(t) + \dot{p}_{evap_2}(t) \quad (3.115)$$

3.7 Reefer

The dynamics of the reefer are determined by the energy flows between the reefer metal box, the cargo, the refrigerated air inside and the ambient air outside.

The sensors available are thermometers measuring the temperature of the air supplied by the fan $T_{fan.mx}$, and the temperature of the air in the reefer T_{air} .

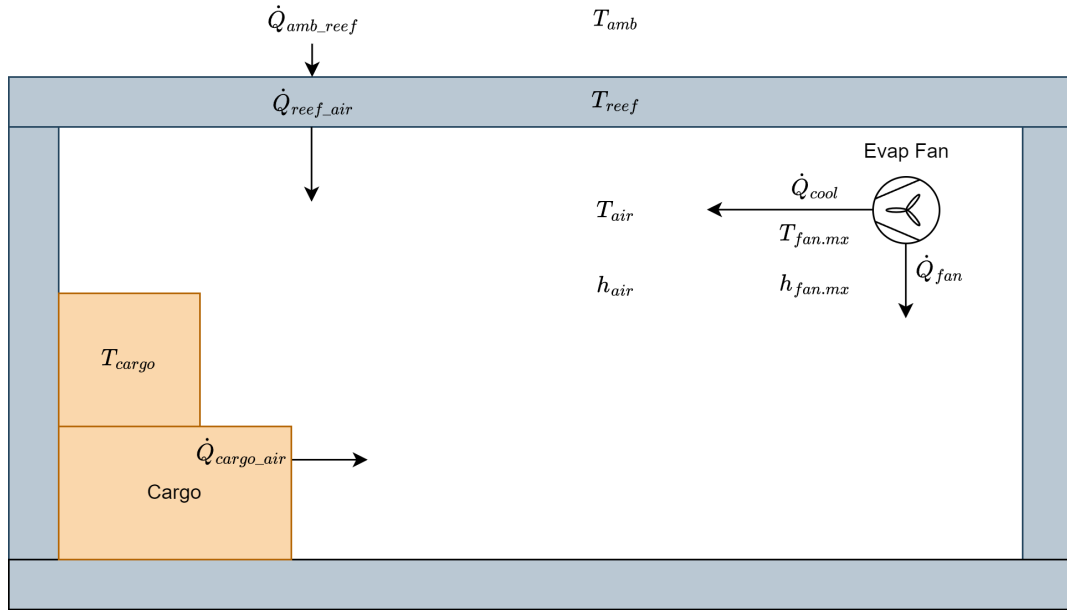


Figure 3.7: Model of Reefer

3.7.1 Energy Flows

The cooling effect on the air blown over the evaporator by the fans, can be described as the drop in temperature which the air is subject to when passing the evaporator with mass-flow $\dot{m}_{fan.e}$:

$$\dot{Q}_{cool} = (T_{air} - T_{fan.mx}) \cdot \dot{m}_{fan.e} (U_{f,e}) \cdot C_{p,air} \quad (3.116)$$

Where

$\dot{m}_{fan.e}$	Mass-flow of air through evaporator fan	$[kg \cdot s^{-1}]$
$T_{fan.mx}$	Temperature of the air that has blown over the evaporator	$[K]$
$U_{f,e}$	Evaporator fan control signal	$[\%]$

$T_{fan.mx}$ and $\dot{m}_{fan.e}$ are derived for the evaporator dynamics in Section 3.6.

The heat energy flow between the ambient air to the reefer:

$$\dot{Q}_{amb_reef} = UA_{reef} \cdot (T_{amb} - T_{reef}) \quad (3.117)$$

From the reefer to air in the reefer the heat energy flow is:

$$\dot{Q}_{reef_air} = UA_{reef} \cdot (T_{reef} - T_{air}) \quad (3.118)$$

From the cargo to the air in the reefer the heat energy flow is:

$$\dot{Q}_{cargo_air} = UA_{cargo} \cdot (T_{cargo} - T_{air}) \quad (3.119)$$

UA	Heat transfer coefficients	$[J \cdot K^{-1} \cdot s^{-1}]$
T_{amb}	Ambient temperature	$[K]$
T_{air}	Temperature inside reefer	$[K]$
T_{cargo}	Temperature of cargo	$[K]$
T_{reef}	Temperature of reefer	$[K]$

Fan Heat Contribution

The evaporator fan is placed inside the reefer container in order to circulate air, it is blown across the evaporator to increase the refrigeration effect. While this increases the cooling effect of the reefer air, the fan itself also results in a heat contribution, caused by the mechanical work and friction. This heat contribution is dependent on the fan control-signal $U_{f,e}$, it is modelled experimentally with a polynomial fitted by Kresten Sørensen in [15]:

$$\dot{Q}_{fan} = (155 \cdot U_{f,e}^2 + 40 \cdot U_{f,e}^3) \cdot 0.8 \quad (3.120)$$

\dot{Q}_{fan}	Heat-energy flow from fan	$[J \cdot K^{-1} \cdot s^{-1}]$
$U_{f,e}$	Evaporator fan control signal	$[\%]$

3.7.2 Temperature Dynamics

The differential equations of the reefer temperatures are derived by summing all the heat-flow contributions that affect the given body, and then dividing the result with the body's mass M_x and heat-capacity Cp_x :

$$\dot{T}_{air} = \frac{\dot{Q}_{cargo_air} + \dot{Q}_{reef_air} + \dot{Q}_{fan} - \dot{Q}_{cool}}{M_{air} \cdot Cp_{air}} \quad (3.121)$$

$$\dot{T}_{reef} = \frac{\dot{Q}_{amb_reef} - \dot{Q}_{reef_air}}{M_{reef} \cdot Cp_{reef}} \quad (3.122)$$

$$\dot{T}_{cargo} = \frac{-\dot{Q}_{cargo_air}}{M_{cargo} \cdot Cp_{cargo}} \quad (3.123)$$

Where

M_{air}	Mass of the air inside the reefer	[kg]
M_{reef}	Mass of the reefer	[kg]
M_{cargo}	Mass of the cargo	[kg]
Cp_{reef}	Heat capacity of the reefer	[J · K ⁻¹]
Cp_{cargo}	Heat capacity of the cargo	[J · K ⁻¹]

For control purposes, it is mainly the temperature of the reefer air T_{air} that is of interest, as it is measured directly with a thermometer and it is the body that the evaporator absorbs heat from.

3.8 Model Efficiency

The purpose of the refrigeration model is to simulate a complete refrigeration cycle, such that heat is moved from the refrigeration chamber to the ambient environment. Different set-points and system variables such as different degrees of sub-cooling, super-heating and flash-tank pressure are bound to result in different cooling efficiencies. One way to measure this is through the total power W_{tot} consumed by the system. In the current model, this is found by summing the power contribution of the compressor W_{cmpr} and the condenser and evaporator fans $W_{c.fan}$ $W_{e.fan}$ respectively:

$$W_{tot} = W_{cmpr} + W_{c.fan} + W_{e.fan} \quad (3.124)$$

Compressor power

For the compressor discussed in Section 3.3, the power draw W_{cmpr} is calculated based on the enthalpy changes across each of the two compression states h_{Δ_1} and h_{Δ_2} .

$$W_{cmpr_1} = \dot{m}_{suc} \cdot h_{\Delta_1} \quad (3.125)$$

$$W_{cmpr_2} = \dot{m}_{dis} \cdot h_{\Delta_2} \quad (3.126)$$

This can be written in the terms recognised from Section 3.3 where h_{suc} is the enthalpy at the output of the evaporator, h_{out_1} is the enthalpy after the first compression stage. Likewise, h_{in_2} is the enthalpy after injection and h_{dis} is the enthalpy at the compressor output:

$$W_{cmpr_1} = \dot{m}_{suc}(U_{\omega}) \cdot (h_{out_1} - h_{suc}) \quad (3.127)$$

$$W_{cmpr_2} = \dot{m}_{dis}(U_{\omega}) \cdot (h_{dis} - h_{in_2}) \quad (3.128)$$

From the two stages, the total power-draw is calculated:

$$W_{cmpr} = W_{cmpr_1} + W_{cmpr_2} \quad (3.129)$$

Fan Power

The Fans are modelled as a fitted polynomial. The characteristics are given by BITZER. The polynomials are already explained in Section 3.7 as \dot{Q}_{fan} and is taken from [15]:

$$\dot{Q}_{fan} = (155 \cdot U_f^2 + 40 \cdot U_f^3) \cdot 0.8 \quad (3.130)$$

For each individual fan, with their respective control signals $U_{f,c}$ and $U_{f,e}$, the power draw is found:

$$W_{c, fan} = \dot{Q}_{fan}(U_{f,c}) \quad (3.131)$$

$$W_{e, fan} = \dot{Q}_{fan}(U_{f,e}) \quad (3.132)$$

Coefficient Of Performance

From the total power, it is common practice in refrigeration to consider the Coefficient Of Performance COP. The COP is the cooling effect normalised to the total work. For the model at hand, the cooling effect is the sum of the energy flow in each of the two evaporator regions derived in Section 3.6:

$$\dot{Q}_e = \dot{Q}_{sh} + \dot{Q}_{mx} \quad (3.133)$$

From this the COP is derived:

$$COP = \frac{\dot{Q}_e}{W_{tot}} = \frac{\dot{Q}_{sh} + \dot{Q}_{mx}}{W_{cmpr} + W_{c, fan} + W_{e, fan}} \quad (3.134)$$

The COP presents a relative cooling-capacity. It should be noted that COP does not directly indicate model efficiency, but is a performance coefficient, thus a $COP > 1$ is possible. COP will henceforth be used as the performance coefficient that will be maximised during set-point optimisation.

3.9 eTRU State-space Model

In total 17 differential equations are modelled, including the compressor transient. The condenser has 4 modelled states, the flash-tank has 3 modelled states, the evaporator has 6 modelled states and finally the reefer has 3 modelled states. The equations are presented in the following format

$$\dot{x} = f(x, u) \quad (3.135)$$

$f(\mathbf{x}, \mathbf{u})$ is a non-linear function with states \mathbf{x} and inputs \mathbf{u} . All the inputs in the system are written below:

$$\mathbf{u} = [U_{\omega}, U_{f.c}, \phi_c, U_{f.e}, \phi_e, \phi_{vi}] \quad (3.136)$$

The inputs will only appear in the state-space equations in Eq. 3.139 if they appear directly in the associated terms in Section 3.9.2

The system states are the terms encapsulated in grey boxes in the prior modelling sections and are summarised as following, excluding the compressor transient:

$$\mathbf{x} = [T_{m.c}, M_c, h_{out.c}, p_{cond}, M_{l.FT}, M_{v.FT}, p_{FT}, T_{m.sh}] \quad (3.137)$$

$$T_{m.mx}, M_{mx}, M_{sh}, h_{out.e}, p_{evap}, T_{air}, T_{reef}, T_{cargo}] \quad (3.138)$$

Because of the condenser having different operation-modes dependent on the enthalpy output phase (vapour, mixed, liquid), the condenser states with sub-cooled output are used in the state-space model in Eq. 3.139.

3.9.1 States and Inputs

In Tab. 3.2 and Tab. 3.3 the input and state symbol meanings used in the state-space diagram are briefly explained.

Inputs:

U_{ω}	Control input for compressor speed	[%]
$U_{f.c}$	Control input for condenser fan speed	[%]
ϕ_c	Opening degree of the condenser expansion valve	[%]
$U_{f.e}$	Control input for evaporator fan speed	[%]
ϕ_e	Opening degree of the evaporator expansion valve	[%]
ϕ_{vi}	Vapour injection valve ON/OFF control signal	[·]

Table 3.2: State-space input signals

States:

$T_{m.c}$	Condenser metal temperature	[K]
M_c	Mass of refrigerant in condenser	[kg]
$h_{out.c}$	Enthalpy of refrigerant at the condenser output	[J · kg ⁻¹]
p_{cond}	Pressure in the condenser	[Pa]
$M_{l,FT}$	Mass of liquid refrigerant in flash-tank	[kg]
$M_{v,FT}$	Mass of vapour refrigerant in flash-tank	[kg]
p_{FT}	Pressure in the flash-tank	[Pa]
$T_{m.sh}$	Evaporator metal temperature in super-heated region	[K]
$T_{m.mx}$	Evaporator metal temperature in mixed-phase region	[K]
M_{mx}	Mass of refrigerant in mixed-phase region of evaporator	[kg]
M_{sh}	Mass of refrigerant in super-heated region of evaporator	[kg]
$h_{out.e}$	Enthalpy of refrigerant at output of evaporator	[J · kg ⁻¹]
p_{evap}	Pressure in the evaporator	[Pa]
T_{air}	Temperature of the air in the reefer	[K]
T_{reef}	Temperature of the reefer container	[K]
T_{cargo}	Temperature of the cargo in the reefer	[K]

Table 3.3: State-space states

Model diagram

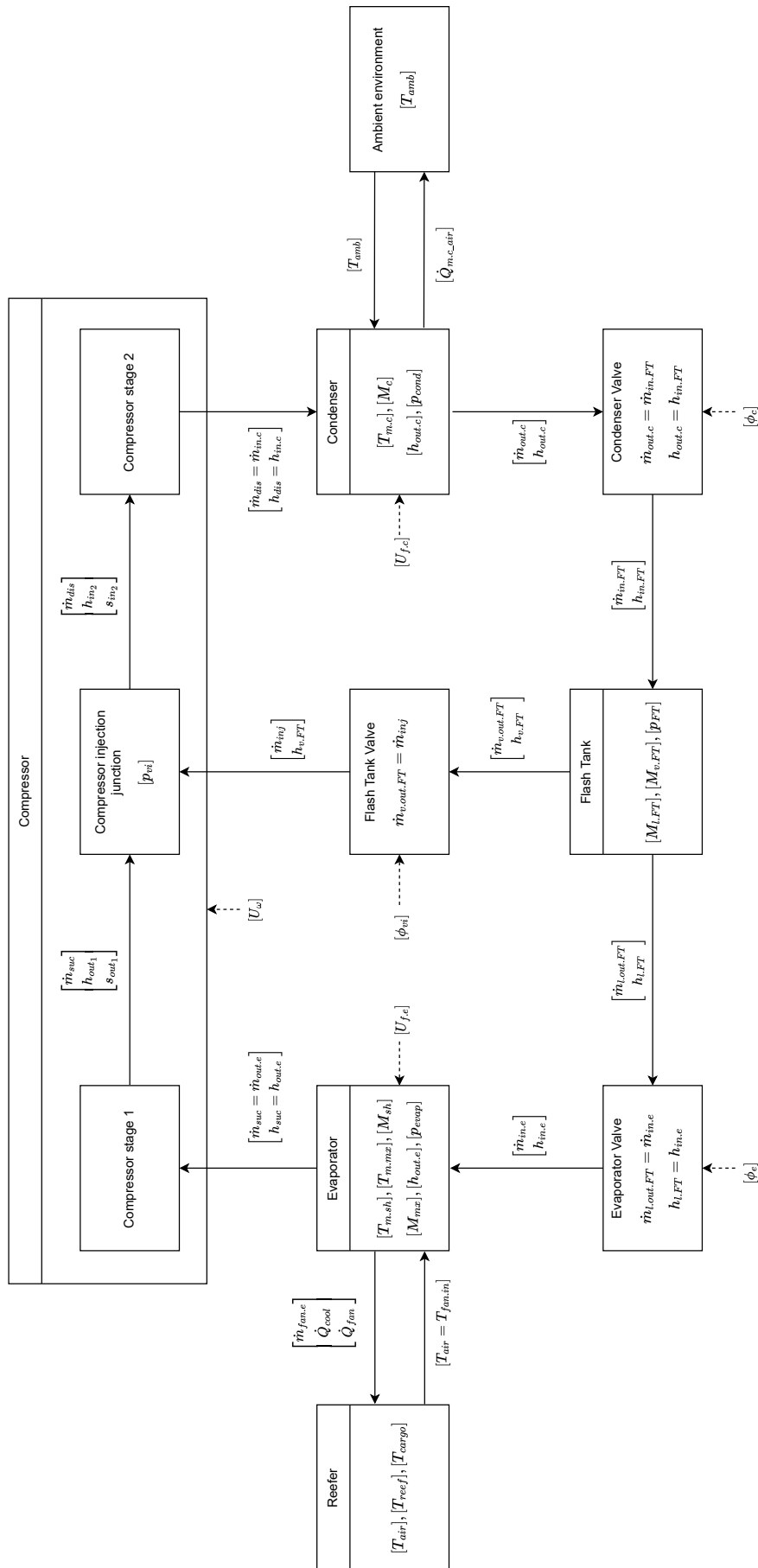


Figure 3.8: IBD diagram of eTRU model

3.9.2 State-space Model for Condenser Liquid Output

$$\begin{array}{c}
 \dot{T}_{m,c} \\
 \dot{M}_c \\
 \dot{h}_{out,c} \\
 \dot{p}_{cond} \\
 \dot{M}_{l,FT} \\
 \dot{M}_{v,FT} \\
 \dot{p}_{FT} \\
 \dot{T}_{m,sh} \\
 \dot{T}_{m,mx} \\
 \dot{M}_{mx} \\
 \dot{M}_{sh} \\
 \dot{h}_{out,e} \\
 \dot{p}_{evap} \\
 \dot{T}_{air} \\
 \dot{T}_{reef} \\
 \dot{T}_{cargo}
 \end{array}
 =
 \begin{array}{c}
 \frac{\dot{Q}_{r,c,m,c} - \dot{Q}_{m,c,air}}{M_{m,c} \cdot C_{p,m}} \\
 \dot{m}_{in,c}(U_\omega) - \dot{m}_{out,c}(\phi_c) \\
 \frac{\dot{m}_{in,c}(U_\omega)h_{in,c} - \dot{m}_{out,c}(\phi_c)h_{out,c} - \dot{Q}_{r,m,c} - \dot{M}_c h_{out,c}}{M_c} \\
 \frac{\dot{m}_{in,c}(U_\omega) - \dot{m}_{out,c}(\phi_c)}{\mathcal{E}_c \cdot V_l + \mathcal{F}_c \cdot V_{mx} + \mathcal{G}_c \cdot V_v} + \frac{\dot{m}_{in,c}(U_\omega)h_{in,c} - \dot{m}_{out,c}(\phi_c)h_{out,c} - \dot{Q}_{r,m,c} - \dot{M}_l h_{out,c} - \dot{M}_{mx} h_{mx} - \dot{M}_v h_{in,c}}{M_l \mathcal{L}_c + M_{mx} \mathcal{J}_c + M_v \mathcal{K}_c} \\
 \dot{m}_{l,in,FT}(\phi_c) - \dot{m}_{l,out,FT}(\phi_e) \\
 \dot{m}_{v,in,FT}(\phi_c) - \dot{m}_{v,out,FT}(\phi_{vi}) \\
 \frac{\dot{m}_{in,FT}(\phi_c) - \dot{m}_{out,FT}(\phi_e)}{\mathcal{F}_{FT} \cdot V_{l,FT} + \mathcal{G}_{FT} \cdot V_{v,FT}} \\
 \frac{\dot{Q}_{a,m,sh} - \dot{Q}_{m,sh,sh} - \dot{Q}_{m,sh,mx}}{\sigma_{evap} \cdot M_m \cdot C_{p,m}} \\
 \frac{\dot{Q}_{a,m,mx} - \dot{Q}_{m,mx,mx} + \dot{Q}_{m,sh,mx}}{(1 - \sigma_{evap}) \cdot M_m \cdot C_{p,m}} \\
 \dot{m}_{in,e}(\phi_e) - \dot{m}_{mx,sh} \\
 \dot{m}_{mx,sh} - \dot{m}_{out,e}(U_\omega) \\
 \frac{\dot{m}_{mx,sh} \cdot h_{dew} - \dot{m}_{out,e}(U_\omega) \cdot h_{out,e} + \dot{Q}_{m,sh,sh} - \dot{M}_{sh} \cdot h_{out,e}}{M_{sh}} \\
 \frac{\dot{m}_{in,e}(\phi_e) - \dot{m}_{out,e}(U_\omega)}{\mathcal{F}_e \cdot V_{mx} + \mathcal{G}_e \cdot V_{sh}} + \frac{\dot{Q}_{m,sh,sh} - h_{out,e} \cdot \dot{m}_{out,e}(U_\omega) + \dot{Q}_{m,mx,mx} + h_{in,e} \cdot \dot{m}_{in,e}(\phi_e) - h_{out,e} \cdot \dot{M}_{sh} - \chi_e \cdot h_{dew,e} \cdot \dot{M}_{mx} - (1 - \chi_e) \cdot h_{bub,e} \cdot \dot{M}_{mx}}{M_{sh} \cdot \mathcal{H}_e + M_{mx} \cdot (\chi_e \cdot \mathcal{L}_e + (1 - \chi_e) \cdot \mathcal{J}_e)} \\
 \frac{\dot{Q}_{cargo,air} + \dot{Q}_{reef,air} + \dot{Q}_{fan}(U_{f,e}) - \dot{Q}_{cool}}{M_{air} \cdot C_{p,air}} \\
 \frac{\dot{Q}_{amb,reef} - \dot{Q}_{reef,air}}{M_{reef} \cdot C_{p,reef}} \\
 \frac{-\dot{Q}_{cargo,air}}{M_{cargo} \cdot C_{p,cargo}}
 \end{array}
 \quad (3.139)$$

3.10 Module Test

Before discussing the control strategy, a few simulations will be made in order to discuss the effect of the actuators on the different system states. The condenser sub-cooling's and evaporator super-heating's dependence on output-flows will be controlled with a proportional-integral (PI) control strategy, in the case of the condenser, this is done for demonstrative purposes only. Similarly, the flash-tank's pressure is also controlled with a PI controller. The last section of this chapter demonstrates a steady state implementation of different flash-tank pressures and the effect on the evaporator and condenser heat transfer.

3.10.1 Evaporator

Input-flow and Super-heating

Super-heating is shown to be controllable through the evaporator mass-flows. The output flow is determined by the compressor, while the input flow is controlled by the evaporator-valve. Since the compressor will be reserved for controlling the reefer air temperature T_{air} the input-flow is left for controlling the super-heat. By setting a constant output-flow, Fig. 3.9 shows how the super-heat and pressure in the evaporator are dependent on the mass, which is controllable with the input flow.

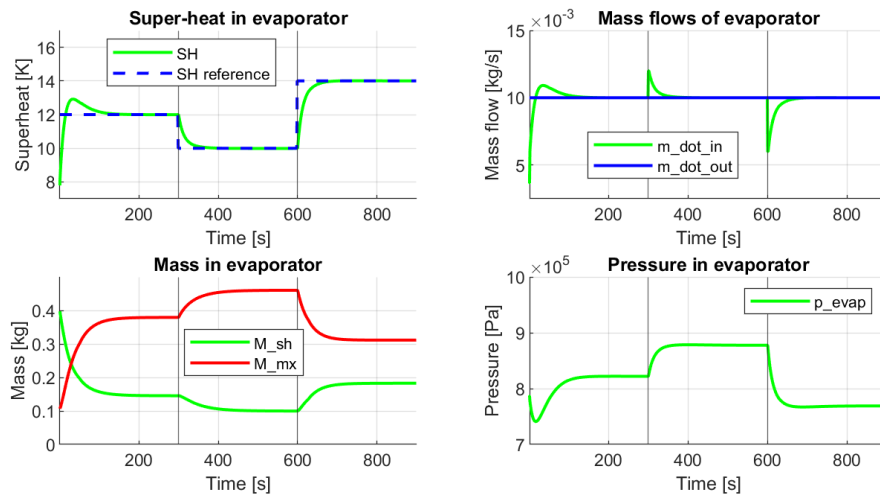


Figure 3.9: Super-heat control, with input flow

Evaporator Fan Effect

The evaporator fan has the effect of increasing the heat-flow from the evaporator metal to the reefer air. Fig. 3.10 shows two steps in fan intensity, first from 0% to 50%, followed by a step to 100%. The figure's third row clearly shows an effect on "Heat transfer to evaporator" $Q_{evap} = \dot{m}_{out.e} \cdot (h_{out.e} - h_{in.e})$ and super-heat. In addition the associated increase in heat-transfer increases the enthalpy, thus the pressure is seen to rise. The biggest change in Q_{evap} is seen during the first step in intensity. This is caused by evaporator output temperature $T_{out.e}$ approaching the boundary set by the air temperature T_{air} in the reefer, this is shown in the bottom row.

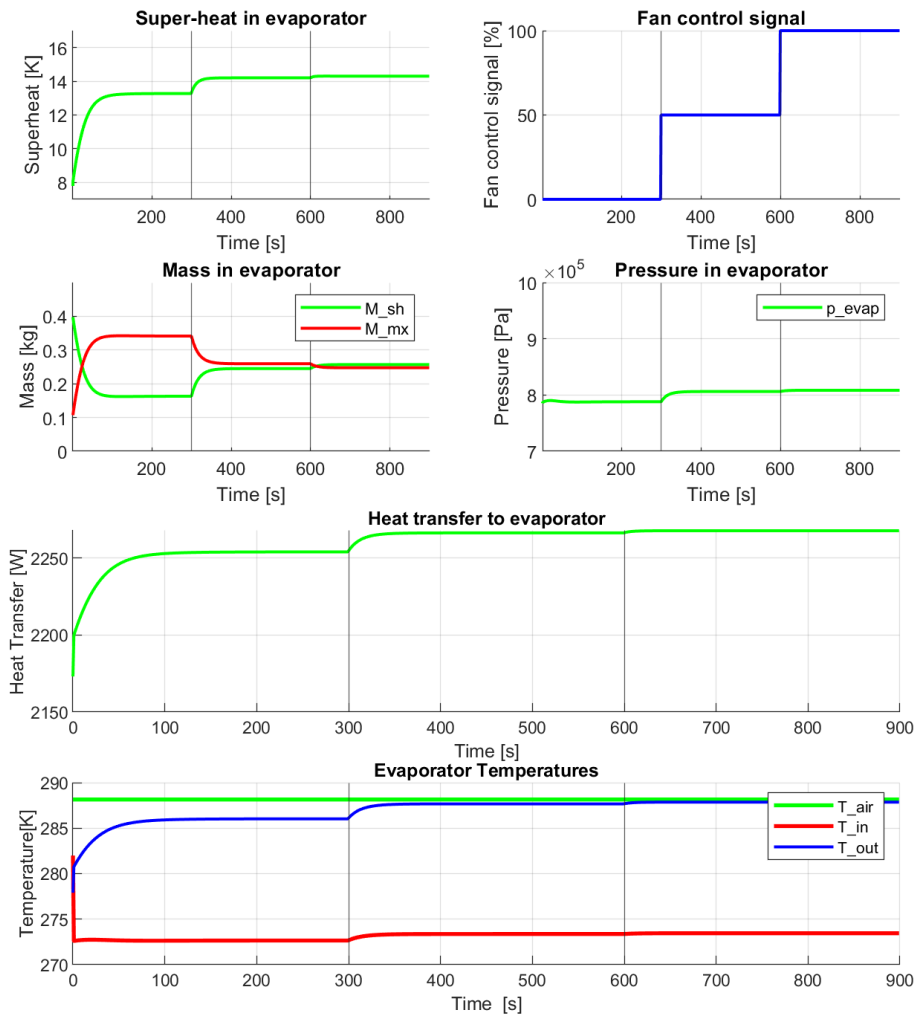


Figure 3.10: Effect of fan on evaporator states

Mass-flow and Heat-transfer

The temperature of the reefer is affected by the heat-transfer from reefer air to the evaporator metal. In Fig. 3.11 it is shown that increasing the mass-flow through the evaporator results in a significant increase in Q_{evap} , while decreasing the flow results in a decreased heat-transfer.

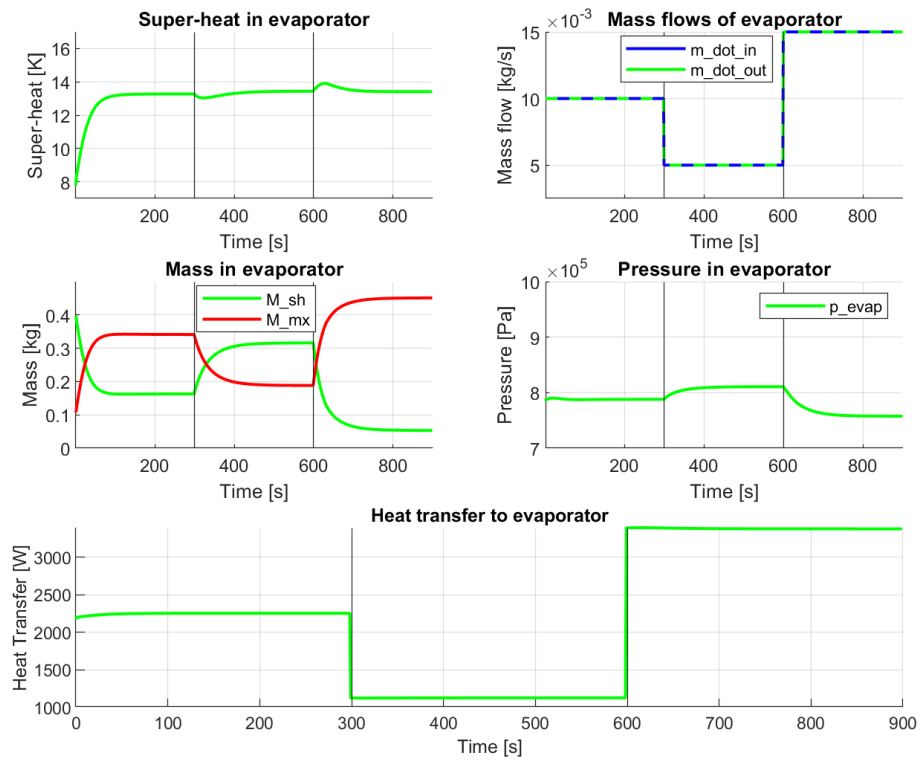


Figure 3.11: Heat transfer from condenser to constant temperature reefer air, with variable flow

3.10.2 Condenser

Output-flow and Sub-cooling

The sub-cooling in the condenser in Fig. 3.12 is seen to be controllable through the condenser output flow. The results are similar to those discussed for the evaporator.

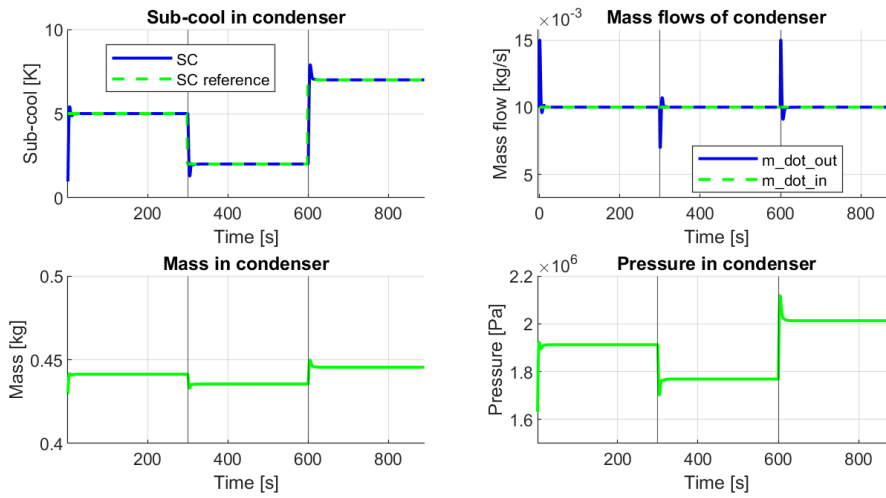


Figure 3.12: Sub-cool control, with condenser output flow

Condenser Fan Effect

Similarly to the evaporator, the fan intensity in Fig. 3.13 is applied in steps from 0% to 50%, followed by a step to 100%. In this case, sub-cooling increases significantly with intensity. Under the specific conditions simulated, the ambient temperature is far below the condenser output temperature $T_{out.e}$, thus unlike the evaporator, no boundary limitation is posed in the given example. The lack of significant pressure change indicates faulty enthalpy dependent pressure dynamics.

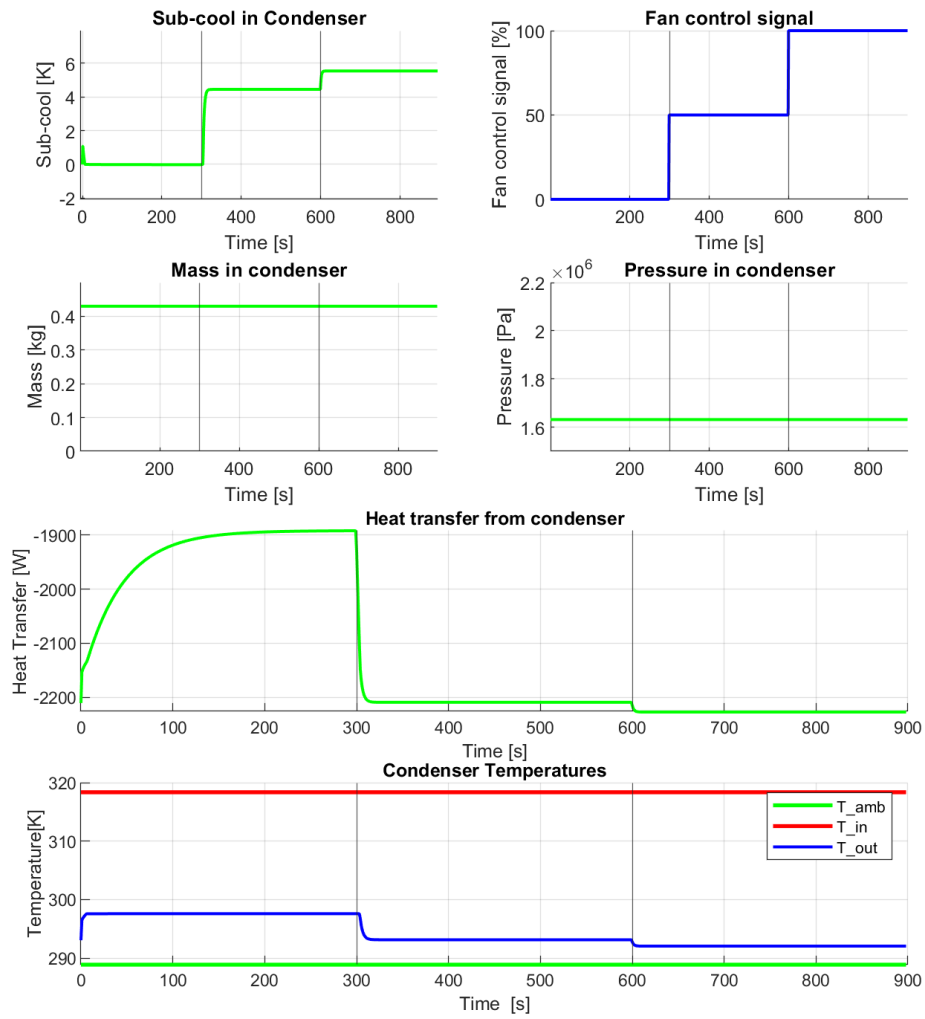


Figure 3.13: Effect of fan on condenser states

Mass-flow and Heat-transfer

The heat-transfer to the condenser in Fig. 3.14 is very similar to that of the evaporator. An increased mass-flow results in a greater heat transfer to the ambient environment. Again the pressure dynamics are considerably steady compared to what may be expected from a $\sim 4\text{K}$ change in sub-cooling

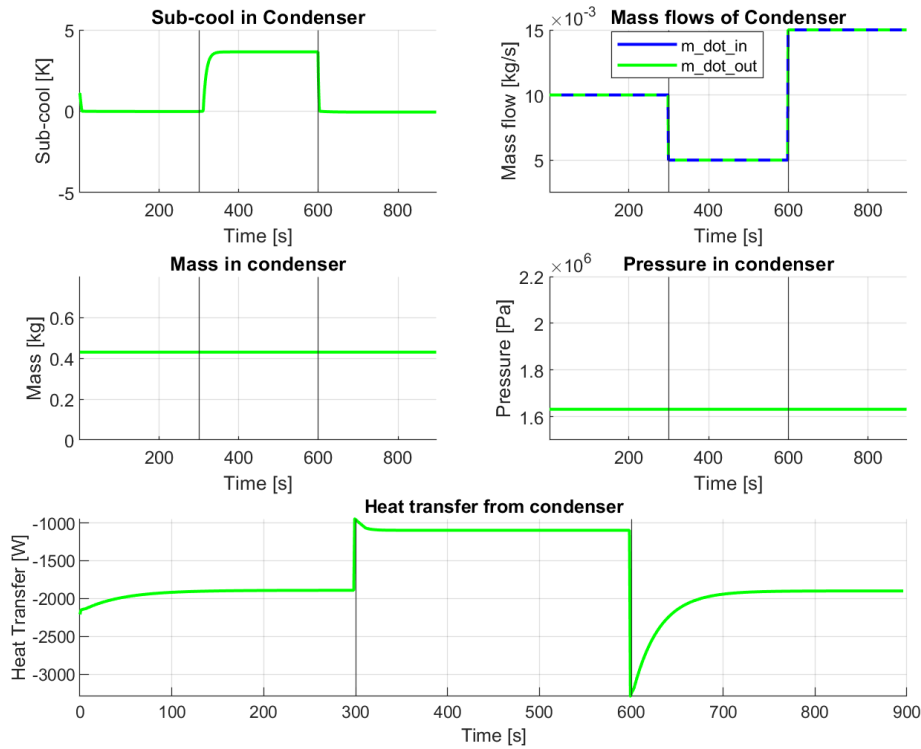


Figure 3.14: Heat transfer from condenser to constant temperature ambient air, with variable flow

3.10.3 Flash-tank

Pressure Control by Input Flow

The pressure ratio in the flash-tank seen in Eq. 3.140 is controlled by the input mass-flows.

$$r_{FT} = 1 - \frac{p_{cond} - p_{FT}}{p_{cond} - p_{evap}} \tag{3.140}$$

As expected the pressure increases when the input flow is greater than the output flow, while it decreases when the output flow is greater than the input flow.

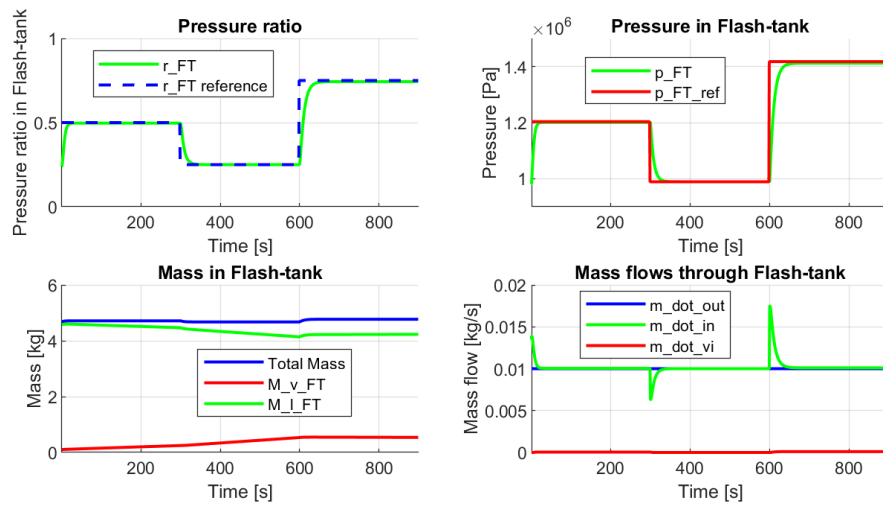


Figure 3.15: Flash-tank states during r_{FT} , reference tracking, with input flow control

Letting the simulation run for longer as in Fig. 3.16 shows that a set pressure ratio does not guarantee stability in the flash-tank as the mass starts drifting. The drift is caused by difference in input and output flows of the different phases. Looking at the first 900 samples of the second row in Fig. 3.16, a decrease in \dot{m}_{v_out} is seen when the pressure decreases in Fig. 3.15, while \dot{m}_{v_in} increases as pressure increases.

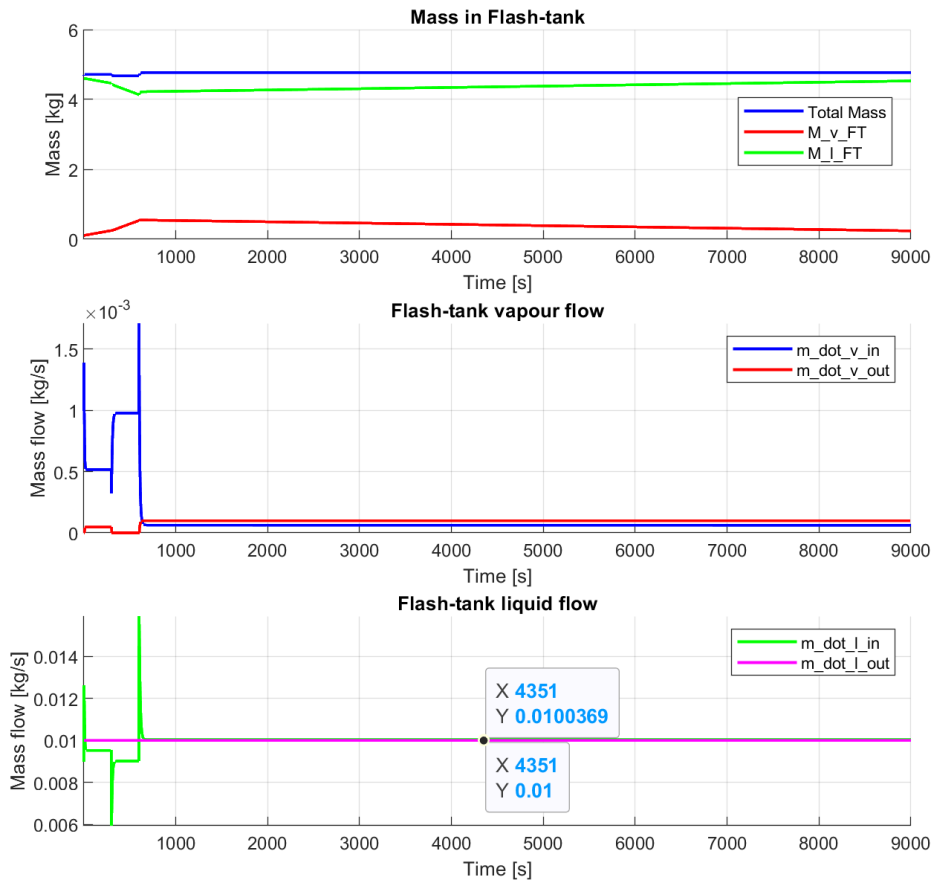


Figure 3.16: Mass drift in Flash-tank over time

A more general understanding of this is gained by considering the relationship between p_{vi} and the flash-tank pressure ratio r_{FT} . Fig. 3.17 shows on the X and Y axis different pressures in the condenser and evaporator, the vertical Z shows p_{vi} and the colouring expresses the corresponding flash-tank ratio.

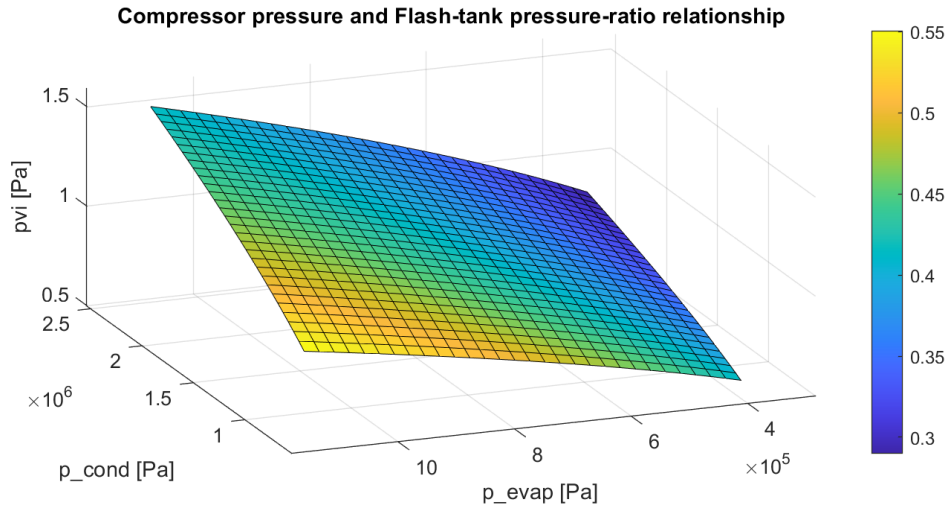


Figure 3.17: 4D plot of refrigeration pressures on the axis, with minimum flash-tank pressure ratio for vapour injection coloured

In-order to achieve vapour injection, r_{FT} must be set such that it corresponds to a warmer colour than the corresponding p_{vi} . The lowest plotted p_{evap} and highest plotted p_{cond} results in the lowest corresponding r_{FT} around 0.3, meaning that in the given case, any $r_{FT} > 0.3$ results in some degree of vapour injection, while $r_{FT} < 0.3$ results in no vapour injection at all. The highest required r_{FT} results from a high p_{evap} and low p_{cond} , where the corresponding r_{FT} must be greater than 0.55.

3.10.4 Steady-state Test

The flash-tank effect on the evaporator and condenser have been tested under steady-state conditions by varying the flash-tank pressure. The flash-tank pressure ratio has been changed in steps of 0.1 every 600th sample in the interval: $r_{FT} = [0.2; 0.9]$. The flash-tank pressure ratio and the dew/bubble-point enthalpy are shown in Fig. 3.18

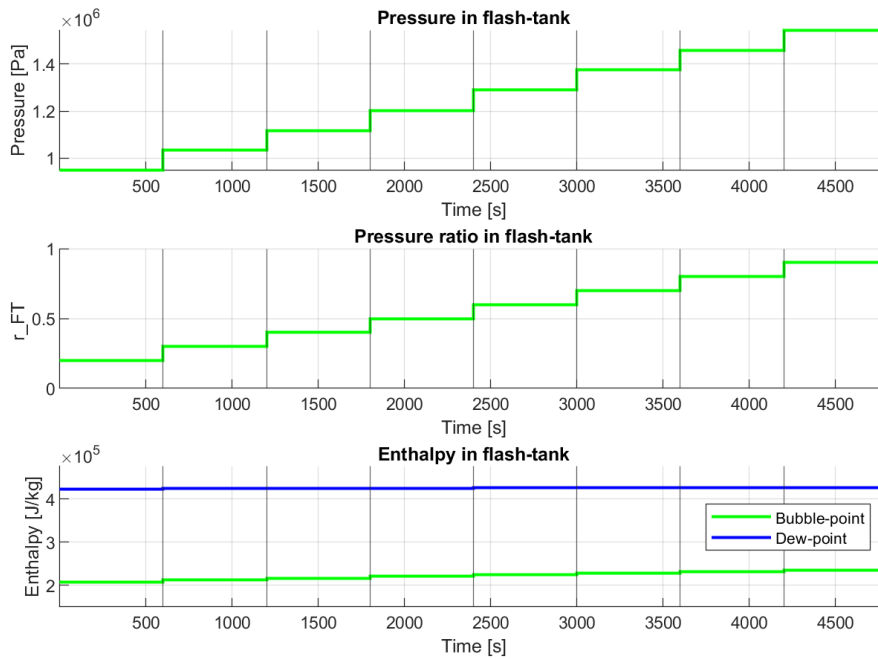


Figure 3.18: Flash-tank pressure and enthalpy

Varying r_{FT} in the flash-tank, changes the input enthalpy to evaporator, with a input/output mass-flow of 0.01kg/s , a higher heat transfer and lower input enthalpy is seen at a low r_{FT} . This is expected, as a lower pressure ratio results in less flashing within the evaporator and thus a lower input quality and higher cooling capacity of the refrigerant in the evaporator. Furthermore an increase in superheated mass is apparent, the expected pressure increase however does not happen, indicating inaccurate pressure dynamics in the evaporator.

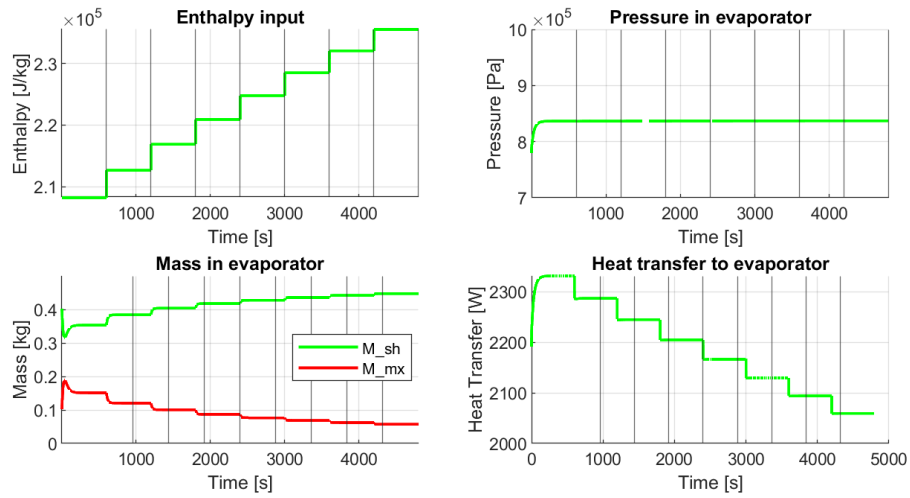


Figure 3.19: Changing input enthalpy resulting in changing heat transfer in the evaporator

Using the aforementioned evaporator enthalpy data from Fig. 3.19 and same flash-tank data from 3.18 as compressor inputs, the condenser is tested with varying degrees of forced vapour injection. This means that vapour injection in the following graph is independent of compressor and flash-tank pressure differences / compressor speed. The total mass-flow though the condenser is the sum of the suction-flow and vapour injection, as seen in the compressor model in Section 3.3.

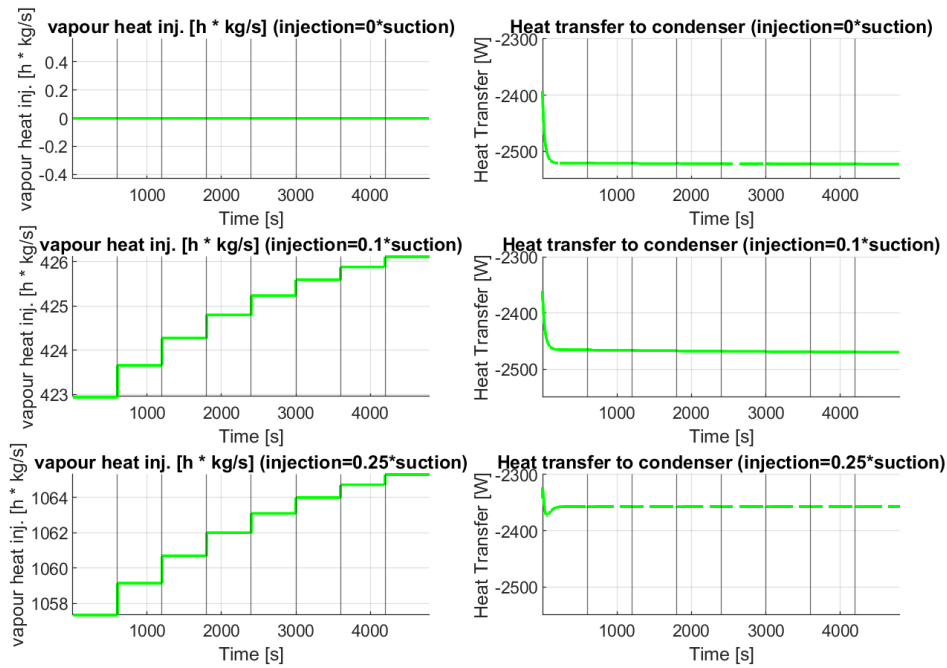


Figure 3.20: Condenser heat transfer, with varying degrees of vapour injection and flash-tank pressure ratio

Looking at the first row of Fig. 3.20, showing the condenser enthalpy given zero vapour injection, the quality/enthalpy of the evaporator input in Fig. 3.19 does not affect condenser heat transfer, as it remains constant. The bottom two rows of the figure, shows that an increase in vapour injection decreases the heat transfer from the condenser with slight variation dependent on flash-tank pressure.

3.11 Modelling Summary

In this chapter a 17 state model of the refrigeration system has been modelled and tested. Through testing of the different actuators and inputs and their effect on the system states, some issues with pressure dynamics are apparent. Nevertheless control-ability of heat transfer, flash-tank pressure and super-heating has been demonstrated.

Given the results found in Section 3.10 a control strategy for regulating the states in the model can be designed.

Chapter 4

Refrigeration Control

The control of the refrigeration system is relatively complex because of the high coupling between component states and the high non-linearity between states in the components themselves. The main control objectives are to:

- Control the super-heat in the evaporator
- Control the sub-cool in the condenser
- Control air temperature in the reefer
- Control flash-tank pressure

The super-heat of the refrigerant in the evaporator is significant because a low super-heat means more mixed refrigerant in the evaporator, ensuring a higher heat energy flow from the reefer air to the refrigerant as demonstrated in Section 3.10. Some degree of super-heat is however necessary in order to avoid liquid slugging in the compressor [16].

The sub-cool in the condenser is important because it relates to the energy transferred from the refrigerant to the ambient environment. A higher amount of sub-cooling is not always optimal as showcased in [13] and [26], where the COP was analysed for different operating conditions in heat pumps. As seen in Section 3.10 the enthalpy at the output of the condenser will also have an impact on the masses of liquid and vapour refrigerant in the flash-tank. Control of the reefer air temperature T_{air} is very important since the main purpose of the refrigeration system is to keep cargo at a certain temperature during transportation.

In addition, the control of the flash-tank pressure p_{FT} , is important because it affects the coefficient of performance (COP) of the system as shown in [28].

4.1 Control Method

The general control method used in this section, for stabilising and reaching specific temperature, super-heat, sub-cool and pressure set-points, is PI control. In some cases, these will be implemented in cascade, such that interconnected vari-

ables, such as flow and compressor-speed/valve opening degree can be controlled easier.

All gains, K_p and K_i , are tuned manually by testing the model in simulation and the values can be found in Appendix J. Furthermore, anti-windup has been implemented for the integrals while different saturation limits have been set on all outputs of the controllers. The integral limits here are set from $0 \rightarrow t$ where t is the current time.

4.1.1 Super-heat Control using Evaporator Input Flow

The super-heat is defined as the temperature at the output, $T_{out.e}$ minus the dew-point temperature, $T_{dew.e}$:

$$\Delta_{sh} = T_{out.e} - T_{dew.e} \quad (4.1)$$

The flow into the evaporator $\dot{m}_{in.e}$ is used to control the super-heat, this mass flow is determined with a PI controller using a reference point, Δ_{sh_ref} , proportional gain, $K_{p.sh}$, integral gain, $K_{i.sh}$, and the error between the actual super-heat and the reference. The mass flow into the evaporator $\dot{m}_{in.e}$ is found as:

$$\dot{m}_{in.e} = -(\Delta_{sh_ref} - \Delta_{sh}) \cdot K_{p.sh} - \int_0^t (\Delta_{sh_ref} - \Delta_{sh}) dt \cdot K_{i.sh} \quad (4.2)$$

When Δ_{sh} is above Δ_{sh_ref} , the mass flow is increased. In reality this controller should be used to control the opening degree of the evaporator expansion valve as the flow can not be directly controlled. The explanation for this is given in the Discussion Chapter 7. The cascaded PI controller for the valve is shown in Appendix I

4.1.2 Sub-cool Control using Fans

The sub-cooling was found to be difficult to control using only the condenser fan, it was therefore decided to use both fans. The fan speed control inputs for both the condenser and evaporator, $U_{f.c}$ and $U_{f.e}$, are determined by comparing the amount of sub-cooling in the condenser to a reference. The sub-cool in the condenser, Δ_{sc} is found by subtracting the output temperature of the condenser $T_{out.c}$ from the temperature of the refrigerant at bubble point, $T_{bub.c}$:

$$\Delta_{sc} = T_{bub.c} - T_{out.c} \quad (4.3)$$

The fan speed control inputs are then found as:

$$U_{f.e} = (\Delta_{sc_ref} - \Delta_{sc}) \cdot K_{p.U.e} + \int_0^t (\Delta_{sc_ref} - \Delta_{sc}) dt \cdot K_{i.U.e} \quad (4.4)$$

$$U_{f.c} = (\Delta_{sc_ref} - \Delta_{sc}) \cdot K_{p.U.c} + \int_0^t (\Delta_{sc_ref} - \Delta_{sc}) dt \cdot K_{i.U.c} \quad (4.5)$$

The fans' speed inputs are regulated with similar controllers because an increase in both fan speeds correspond to an increase in sub-cooling of the refrigerant.

4.1.3 Reefer Air Temperature Control using Compressor

In Section 3.10 it is found that the heat transfer from the reefer air to the refrigerant increases with an increase in mass-flow. Therefore the air temperature in the reefer T_{air} , is possible to regulate using the compressor. This is done using cascade control where one PI-controller is used to set a mass flow reference point while the other controls compressor speed

The first controller uses a reference point for the reefer air temperature T_{air_ref} , to set a mass-flow reference \dot{m}_{suc_ref} for the second controller, such that:

$$\dot{m}_{suc_ref} = -(T_{air_ref} - T_{air}) \cdot K_{p.T_{air}} - \int_0^t (T_{air_ref} - T_{air}) dt \cdot K_{i.T_{air}} \quad (4.6)$$

This reference is then used in the second controller to set the compressor speed control input U_ω :

$$U_\omega(\dot{m}_{suc_ref}) = (\dot{m}_{suc_ref} - \dot{m}_{suc}) \cdot K_{p.\dot{m}_{suc}} + \int_0^t (\dot{m}_{suc_ref} - \dot{m}_{suc}) dt \cdot K_{i.\dot{m}_{suc}} \quad (4.7)$$

The rate of mass flow into the compressor, \dot{m}_{suc} is dependent on several parameters such as the enthalpy and pressure in the evaporator, as well as the compressor speed. During simulation of the model, it was discovered that when the temperature of the reefer air was used as a control parameter to regulate the compressor speed directly, the compressor extracted excessive amounts of refrigerant from the evaporator. As a result, it was deemed more effective to regulate the compressor speed using a mass flow reference.

Compressor on/off-time

As was discussed during compressor modelling in Section 3.3, that the compressor has a minimum finite speed. Given that the desired reefer air temperature T_{air} in some instances may be achievable with a compressor speed state $\Omega_{state} < 900rpm$, fast switching in compressor control-input U_ω is expected. This results in the compressor speed transient oscillating around the correct state value. In a physical system this is not desirable, as it leads to unnecessary wear and tear on the compressor. To mitigate this, the compressor controller is designed such that once the control signal reaches 0, the compressor is forced to be turned off for some finite minimum time $\tau_{cpr.off}$. On the other hand, a compressor running for too long, can result in too much refrigerant escaping the evaporator, resulting in liquid-slugging. To mitigate this, a maximum allowed on time $\tau_{cpr.on}$ is implemented. These two parameters needs to be tuned, such that the necessary cooling capacity is achievable, without damaging the hardware, and risking slugging.

Limit on Compressor Control Input

In order to avoid refrigerant being sucked out of the evaporator too quickly causing immense pressure-drop in the evaporator and liquid slugging in the compressor, it was found necessary to set a maximal limit U_{ω_MAX} on the control input U_{ω} .

4.1.4 Flash-tank Pressure Control using Condenser Output Flow

To control the pressure in the flash-tank, p_{FT} a pressure ratio, r_{FT} is used. The ratio r_{FT} is defined such that the ratio stays within the range $[0;1]$ when the flash-tank has an intermediate pressure state between p_{cond} and p_{evap} :

$$r_{FT} = 1 - \frac{p_{cond} - p_{FT}}{p_{cond} - p_{evap}} \quad (4.8)$$

This ratio is compared to a reference, r_{FT_ref} . To reach this pressure ratio, the mass flow into the flash-tank is regulated with the following PI controller:

$$\dot{m}_{out.c} = (r_{FT_ref} - r_{FT}) \cdot K_{p,p_{FT}} + \int_0^t (r_{FT_ref} - r_{FT}) dt \cdot K_{i,p_{FT}} \quad (4.9)$$

The resulting control scheme works such that the input flow through the condenser valve increases when r_{FT} is below r_{FT_ref} . The pressure ratio reference ensures that the pressure in the flash-tank is always controlled to be somewhere between the condenser and evaporator pressure.

4.1.5 Flash-tank Mass Accumulation

The flash-tank liquid/vapour control volumes $V_{v,FT}$, $V_{l,FT}$ are prone to drifting, leading to the accumulation of either liquid or vapour refrigerant within the flash tank as seen in Section 3.10. A higher pressure within the flash-tank can result in liquid accumulation, while a lower pressure may induce more vapour accumulation. This behaviour can be attributed to the fact that the mass-flows of liquid and vapour into the flash-tank are reliant on the different pressures between the condenser and flash-tank and on the enthalpy at the outlet of the condenser. In order to control the volume drift, a vapour injection greater than the flash-vapour must exist, such that the relative vapour volume of the flash-tank can be decreased. Furthermore, the pressure ratio r_{FT} must be such that vapour injection is possible in the first place. Other factors of importance is the compressor speed and valve-model constant explained in the valve and compressor sections 3.2 and 3.3, which affects the mass-flow in addition to the pressure difference.

Having the aforementioned conditions met, vapour may be controlled using the vapour injection valve, as a on-off switch with status Vi_{on} for keeping the relative vapour-volume within a reference range, denoted $limit_{high}$ and $limit_{low}$ in the

conditional expression eq. 4.10.

$$V_{i_{on}} = \begin{cases} true & \frac{V_{v,FT}}{V_{FT}} > limit_{high} \\ false & \frac{V_{v,FT}}{V_{FT}} < limit_{low} \end{cases} \quad (4.10)$$

4.2 Refrigeration Control Summary

In this chapter the control strategy used to regulate the variables: Δ_{SH} , Δ_{SC} , T_{air} and r_{FT} , is described. All the variables are controlled with PI controllers, and in the case of T_{air} a cascade PI controller is used, combined with finite on-off times for compressor control. A control strategy for the relative liquid and vapour volumes in the flash-tank have also been designed. As will be discussed in the Sections 7.3 and 5.2, the valve cascade controls are not implemented, thus were not elaborated further.

Given the controller design in this chapter, the refrigeration model can now be simulated in order to verify and test its validity and realism.

Chapter 5

Simulation of model

In this chapter, the model presented in Chapter 3 will be tested and simulated. Because of stability issues, some simplifications are made and will be presented before the simulation tests commence. The coefficients and system constants can be found in Appendix B. The simulation is done in MATLAB R2022A, using python 3.8 for refrigerant table look-up.

5.1 General Considerations

5.1.1 ODE solving

Forward Euler Explicit Integration

Initially the method used for solving differential equations was Forward Euler integration, which generally for small sample frequencies is sufficient. The method is explicit meaning that the future sample $k + 1$ is predicted based on the current state at sample k .

$$\delta[k + 1] = \delta \cdot t_s + \delta[k] \quad (5.1)$$

This however lead to great difficulty and in an effort to prevent the overshooting that the system stiffness presents, more advanced solving algorithms are used.

ODE15s

The algorithm used for solving is the MATLAB solver ODE15s, which is designed for stiff problems using variable step-sizes and the variable order-method.

The ODE15s MATLAB solver makes it possible to define settings, using the function 'odeset()'. The settings include tolerances, number of steps, minimum step size and other useful parameters. In this case, the only setting used apart from the default settings is the 'NonNegative' keyword, this ensures that the states are positive at all times.

```
%N indicates the number of states  
options=odeset('NonNegative',[1:N]);
```

5.1.2 Look-up Table

The properties and relationships between the refrigerant pressure, enthalpy, density, temperatures and associated partial derivatives were not found algebraically, but using the python package "CoolProp -6.4.1". More information can be found at [5].

5.1.3 Architecture

Each system component modelled in the Modelling Chapter 3 is coded in their own module, the inputs of consecutive states are fed into the next component in the flow direction, starting with the compressor.

Each component module solves the ODEs internally, such that the ODE solver in practice is run for each of the dynamic components once every simulation loop. The control signals are then calculated after state estimation using the controllers from Chapter 4.

An alternative implementation using a single ODE-solver with all states, was tested with success. The upsides of the alternative approach is smaller steps between components, allowing for enthalpy and pressure differences between components to be smoother. In addition the control scheme can this way be easily implemented in the outer-loop independent of ODE step-size. The single ODE solver did however not perform better, thus the single solver is not prioritised and implemented in the simulation test section.

The time-period for each component is set to 0.5s, the ODE15s solver will divide this further to satisfy the perceived stiffness on a sample by sample basis.

5.2 Simplifications of Model and Numerical Issues

Because of difficulty during simulation, some shortcuts and simplifications needed to be made in-order to end up with a functional model. This was mainly done by implementing the compressor modelled in Section 3.3 with a minimum compressor-speed $\Omega_{min} = 1$. This means that the refrigeration system consistently has a finite mass-flow, this is also the case in OFF-MODE, which is when $MODE = 0$. Furthermore valves were omitted from the simulations.

In addition to the necessary simplifications, some numerical/simulation tricks are used, they will be explained below.

Even with the simplifications implemented, the simulation model is not completely stable. In most instances, simulation runs as expected, with the caveats mentioned in the test Section 5.3, but at times the pressure dynamics turn unstable, resulting in a system crash.

5.2.1 Compressor Simplification

Because of the condenser not having a dynamic enthalpy input-state, it was chosen to simulate the compressor with a minimum compressor speed $\Omega_{min} = 1$. This means that there at all times is a slight mass-flow into the condenser, resulting in a constant enthalpy input for each sample.

5.2.2 Valve Simplification

A lot of time was spent on simulation/model implementation, in some instances, functional valves were included, but in the current implementation they have been removed in favour of better mass-flow control, reducing the complexity and sources of error. An implementation using the valve model is included in Appendix E. The alternative implementation must still adhere to basic one-way valve dynamics, such that no upstream flow is possible. The simplified valve strictly blocks flow when the pressure difference becomes negative. The simplified valve model is shown in 5.2, where \dot{m}_{valve} denotes the valve mass flow, $\dot{m}_{v.ref}$ denotes the mass-flow reference and p_{in} and p_{out} denotes the pressures on the valve input and output side.

$$\dot{m}_{valve}(\dot{m}_{v.ref}) = \begin{cases} \dot{m}_{v.ref} & p_{in} - p_{out} > 0 \\ 0 & p_{in} - p_{out} \leq 0 \end{cases} \quad (5.2)$$

5.2.3 Evaporator Condenser Volume Boundary

When calculating the relative volumes of the two regions in the moving boundary evaporator model, the region mass states are divided by the average region densities. This means that the summed volumes may end up different from the volume boundary set by the physical constraints of the evaporator tubes. To correct for this the relative volumes of the two regions have been kept constant, while scaling the total volume to match the boundary volume. For the evaporator at sample k with volume constraint V_e and the average region densities $D_{sh}[k]$, $D_{mx}[k]$, the initial calculated volume estimates $V_{sh.est}[k]$ and $V_{mx.est}[k]$ are multiplied with a scaling ratio $r_{e.est}$ resulting in the corrected volumes $V_{mx}[k]$ and $V_{sh}[k]$:

$$\begin{aligned} V_{sh.est}[k] &= M_{sh}[k] \cdot D_{sh}[k]^{-1} \\ V_{mx.est}[k] &= M_{mx}[k] \cdot D_{mx}[k]^{-1} \\ r_{e.est}[k] &= \frac{V_e}{V_{sh.est}[k] + V_{mx.est}[k]} \\ V_{sh}[k] &= V_{sh.est}[k] \cdot r_{e.est}[k] \\ V_{mx}[k] &= V_{mx.est}[k] \cdot r_{e.est}[k] \end{aligned}$$

The mass regions in the condenser and flash-tank are also estimated in order to calculate the pressure dynamics, resulting in the need for a similar volume boundary solution.

While the scaling ensures that the physical volume boundaries are held, great scaling ratios indicate faulty mass and pressure relationships, and does not guarantee stability.

The scaling ratio will in Section 5.3.3 be used to evaluate the density estimations in the different system components.

5.2.4 Evaporator Mass Conservation

When solving the differential equations for the region masses in the evaporator in discrete time, there is a risk of undershooting region masses, such that the mass in the system turns negative. This is of course physically impossible. To workaround the possibility of this happening, the negative mass will be set to zero, while the absolute value of the negative mass is added to the non-negative mass. This is implemented in the evaporator for sample k with the following if statements:

```

if  $M_{mx}[k] < 0$  then
     $M_{sh}[k] = |M_{mx}[k]| + M_{sh}[k]$ 
     $M_{mx}[k] = 0$ 
end if
if  $M_{sh}[k] < 0$  then
     $M_{mx}[k] = |M_{sh}[k]| + M_{mx}[k]$ 
     $M_{sh}[k] = 0$ 
end if

```

Because of the ODE15s settings described in section 5.1.1 this should be redundant, the feature is however kept as a fail-safe.

5.3 Simulation Test

In this section the model described in Chapter 3 is simulated with the control strategy designed in Chapter 4 to test how well the model reaches the chosen reference points. Furthermore the model will be compared to real-life data from the BITZER eTRU plant to gain an insight into how a real refrigeration system behaves in comparison to the model. The purpose of this is not to discuss the accuracy of the simulation model, as estimation of parameters and constants have not been prioritised, rather the general characteristics are of interest. Finally the COP parameter will be evaluated for different system-states, in-order to see how flash-tank pressure, super-heat and fans affects the performance coefficient. Because of stability issues, it is chosen not to use vapour injection control during simulation, this is

elaborated in Section 5.3.2. The Model will only be tested for a 5 degrees Celsius ($278.15K$) reefer air T_{air} control temperature, with the average ambient temperature T_{amb} found in model initialisation Section 5.3.1.

5.3.1 Model Initiation

The initial conditions in the simulation are based on averaging of the data logged on the physical BITZER eTRU plant. Because of the relationship between the refrigerant mass and the component volumes with respect to the pressure states, realistic initial-conditions is of much importance for overall model accuracy and stability. In addition, badly chosen initial conditions may result in unstable startup transients. Since the BITZER eTRU data is subject to compressor switching, it is not possible to measure steady state values, in addition, the choice of some arbitrary sample set can lead to unstable startup transients caused by measurement noise and inaccuracies. The chosen approach is to take the mean of a relative steady sample-range from the BITZER data.

Fig. 5.1 shows the BITZER pressures and the associated means used for simulation initialisation. The selected sample range is $[1500;9000]s$. The samples before 1500s are seen to have a transient, while the samples after 9000s are invalid, indicated by the condenser pressure less than zero.

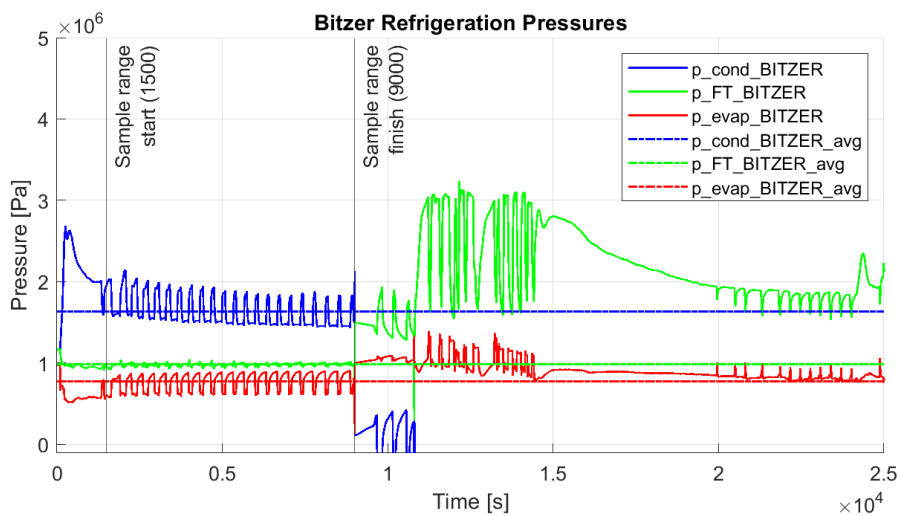


Figure 5.1: Bitzer pressure data

The system mass distribution and metal temperatures are not logged by BITZER, they must therefore be estimated. The metal temperatures for the evaporator are found as the average between the reefer air temperature T_{air} and the suction/out-

put temperature $T_{out.e}$ for the super-heated region. The mixed region metal temperature is the average between the reefer air temperature T_{air} and the input temperature $T_{in.e}$. The same is done for the condenser metal temperature $T_{m.c}$ using the ambient outside temperature T_{amb} and the condenser output temperature $T_{out.c}$. The refrigerant load (total refrigerant) is set to $5.6178kg$. The refrigerant is distributed around the system as shown in Tab. 5.1:

Component	Refrigerant mass	Phase volume
Condenser	$0.5043kg$	×
Evaporator	$0.4299kg$	98.75% mixed
Flash-tank	$4.6836kg$	64% liquid
Compressor	0	×
Total	$5.6178kg$	×

Table 5.1: Initial masses for simulation

In addition to the mass distribution, Tab. 5.1 shows the volume of mixed refrigerant in the evaporator and liquid volume in the flash-tank. The relative volumes and masses are chosen such that the total refrigerant load approaches $5.6kg$, taking the component pressures and associated densities into consideration.

5.3.2 Initial Simulation of Model

The first simulation that is shown has the reference-points listed in Tab. 5.2, the reference-points are chosen such that they result in a stable simulation start-transient given the aforementioned initial conditions. For now, the simulation purpose is not comparison to the logged BITZER data, but discussing the model dynamics.

Controlled State		Reference	State Average	250 sample Error
Reefer Air temperature	T_{air}	$278.15K$	$278.38K$	$0.23K$
Sub-cooling in condenser	Δ_{SC}	$5K$	$-0.0012K$	$-5.0012K$
Super-heating in evaporator	Δ_{SH}	$8K$	$8.019K$	$0.019K$
Flash-tank pressure ratio	r_{FT}	0.7	0.6989	0.0011

Table 5.2: Reference-points for simulation

In Tab. 5.2, the state references used for the following simulation are listed. In addition the 250 sample average (125s) and associated error is shown. The simulation implementation results in a temperature error of approximately $0.25K$, but demonstrates that the system-states overall are controllable. The sub-cooling is however not controlled to the desired reference point.

Reefer Air Temperature

Below in Fig. 5.2 the temperature of the air in the reefer, T_{air} can be seen to follow the reference, T_{ref} , set at 278.15K. A small steady-state error is observed, this should disappear with a higher maximum control compressor signal U_{ω_MAX} . The need for this is explained in control Chapter 4.

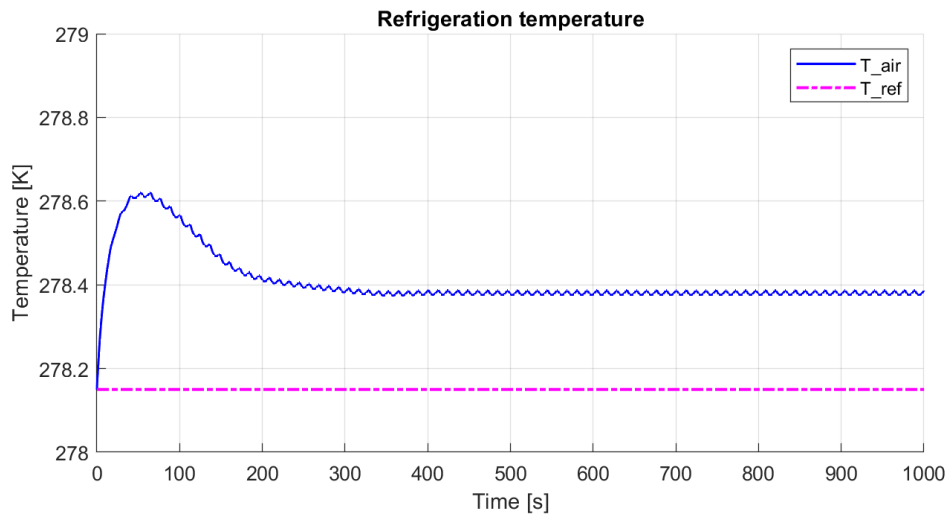


Figure 5.2: Plot of reefer air temperature compared to a reference

Sub-cooling and Super-heating

In Fig. 5.3 the super-heat in the evaporator and the sub-cool in the condenser can be seen. The super-heat, controlled with the flow into the evaporator, follows the reference with visible oscillations caused by the compressor ON/OFF characteristic, achieving a control-error of 0.019K, the associated mass-flows can be seen in Appendix D. The sub-cool was not possible to control in this simulation and goes to 0 quite rapidly. This means refrigerant at the output of the condenser is at bubble-point and not sub-cooled. At certain points slight sub-cooling is present. This overlaps with periodic switching of the compressor. Given the limit on the compressor control-signal, and the compressor off-time, visible sub-cooling is rare.

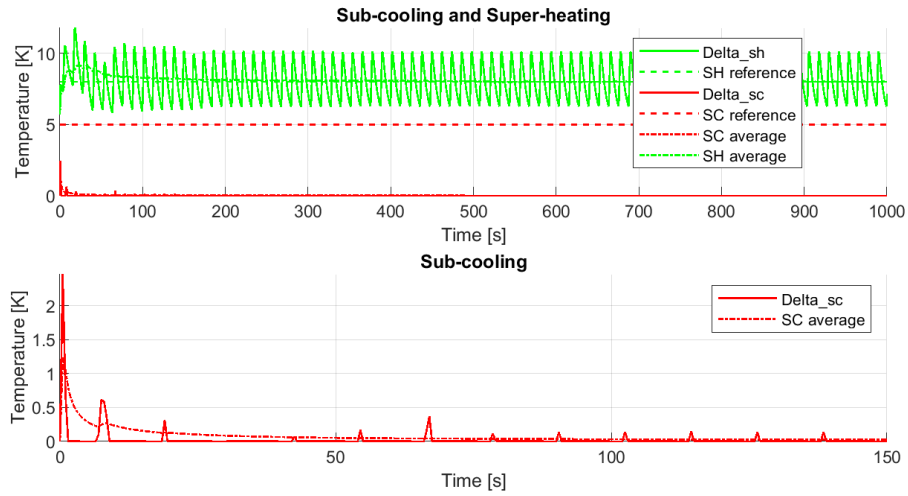


Figure 5.3: Plot of sub-cool and super-heat compared to references with averages

Pressure

The first plot in Fig. 5.4 shows the pressures in the various refrigeration components, the plot at the bottom shows the pressure ratio r_{FT} . The pressures in the components show an oscillating behaviour due to the compressor characteristics but they all exhibit steady state behaviour. The pressure ratio error is as noted in Tab. 5.2 at 0.0011 for a 125s average.

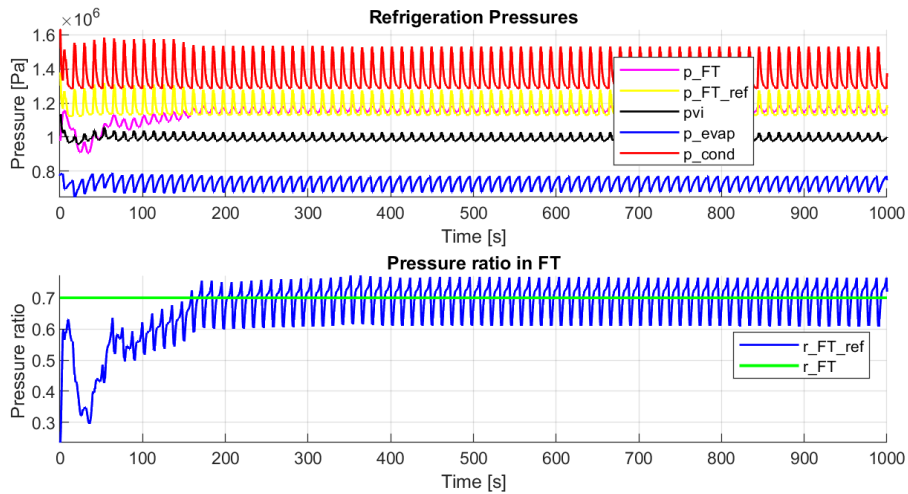


Figure 5.4: Plot of pressures in components

Masses in System

Without Vapour Injection Control

In Fig. 5.5 the masses in the individual components and total mass in the system can be seen. The total mass in the system stays relatively constant during simulation after a slight initial drop. The drop is expected to be caused by numeric difficulties during calculation of mass flows between the evaporator regions. The vapour injection mass flow also has an effect on the total mass in the system and seems to cause the oscillations as shown in Appendix G. The mass in the condenser accumulates slowly while the evaporator mass slowly lessens. It is notable that, as shown in the bottom graph in Fig. 5.5, the mass of vapour in the flash tank drifts and increases with time, this is caused by compressor speed, flash-tank pressure and the lack of sub-cooling resulting in a great degree of refrigerant flashing.

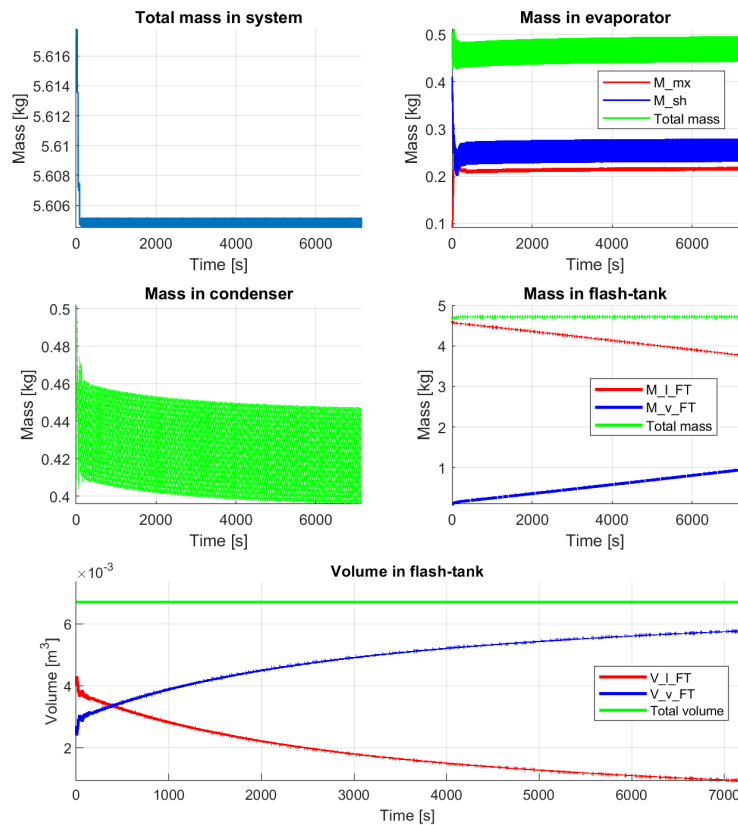


Figure 5.5: Plot of masses in system, no FT volume control

Changing the vapour injection valve constant only results in volume drift of different speed and direction, the system remains unstable.

With Vapour Injection Control

Implementing the vapour injection valve on/off control, it is possible given a sufficiently high flash tank ratio and injection valve constant, in this case 30 times greater than what is implemented in the controller-less solution, to keep the relative flash-tank volumes within specified bounds. Unfortunately this does not stabilise the system, as the mass-drift between the flash-tank masses migrates to the evaporator and condenser, resulting in an evaporator being depleted over time at a far greater degree than the condenser does without the on-off controller. This is shown in Fig. 5.6 .

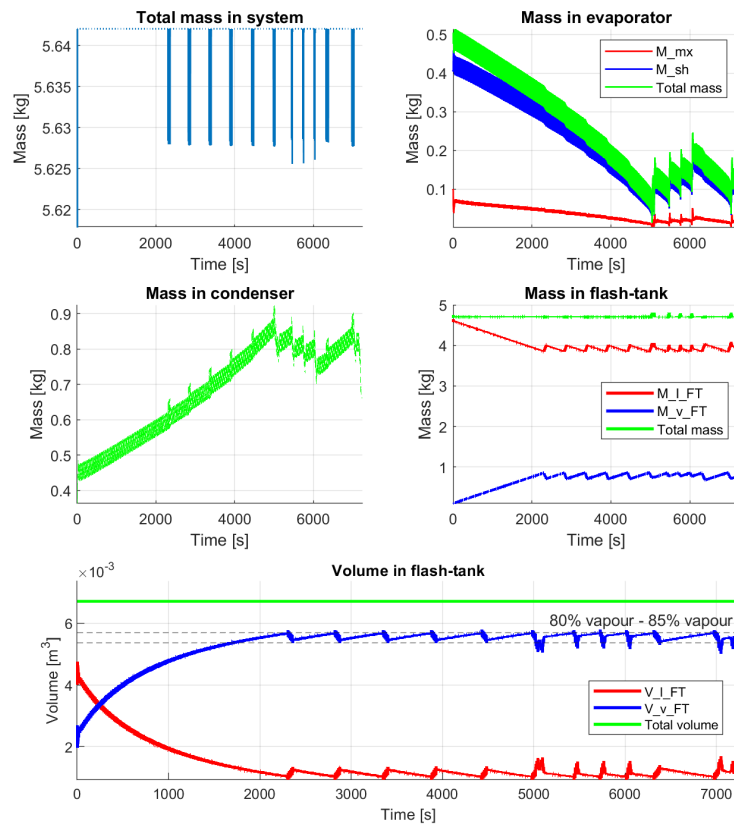


Figure 5.6: Plot of masses in system with on/off controller, for bounds 80% and 85% vapour volume

Because of this the rest of the tests of the system are done without flash-tank

vapour injection control, as the relative steady evaporator and condenser masses in Fig. 5.5 are deemed more important for later optimisation, than the volume and by extension mass control seen in Fig. 5.6

5.3.3 Volume Scaling Ratios

As mentioned in Section 5.2.3, the volume boundary may not correspond to the estimated masses and densities. In order to meet the volume constraints/boundaries, a scaling is done on the total estimated refrigeration mass. This ratio give some insight into the overall accuracy of the pressure and mass relationship of the components. A scaling ratio near 1 indicates accurate estimation, while scaling ratios above or below indicate density estimation errors. The definition is:

$$r_V = \frac{V_{boundary}}{V_{est}} \quad (5.3)$$

Such that a $r_V < 1$ indicates an average density greater than the true density or a pressure lacking behind the increase in refrigerant mass. Likewise a $r_V > 1$ stems from a low density estimation.

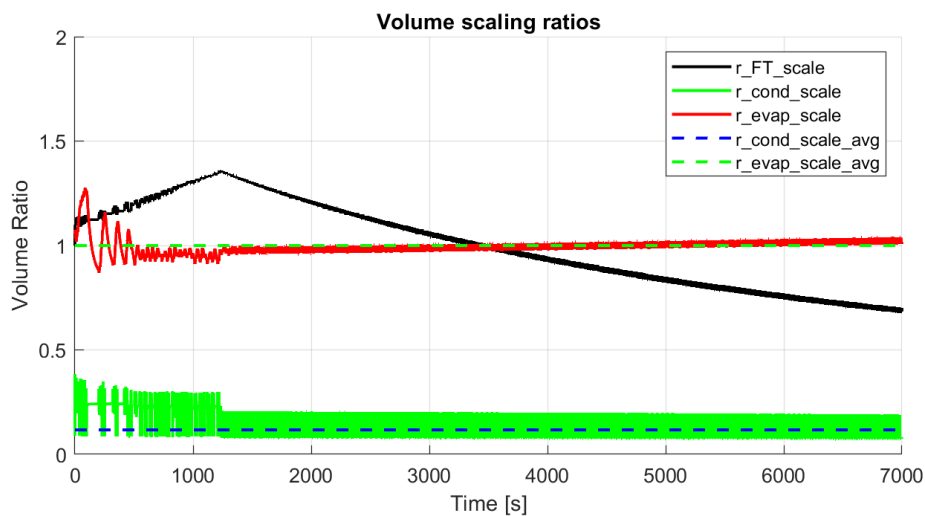


Figure 5.7: Volume Ratios in components

The evaporator volume estimation in Fig. 5.7 is seen to be relatively consistent with a scaling ratio 1 past the initial startup transient. The condenser scaling ratio is however averaging at 0.15 far below 1, indicating incompatible mass and pressure dynamics. Unexpectedly, the flash-tank ratio seems to drift with time, resulting in greater error over time.

5.3.4 Enthalpy Changes

Across the three active components: The compressor, condenser and evaporator a change in enthalpy occurs. In the condenser, energy is dissipated to the outside world through heat exchange. In the evaporator the opposite happens, as the enthalpy increases from input to output. Finally the compressor increases enthalpy through V-P work and vapour injection. The enthalpies seen in Fig. 5.8 are calculated for the respective components as the enthalpy at the input of the component subtracted from the enthalpy at the output of the component: $\Delta h = h_{out} - h_{in}$.

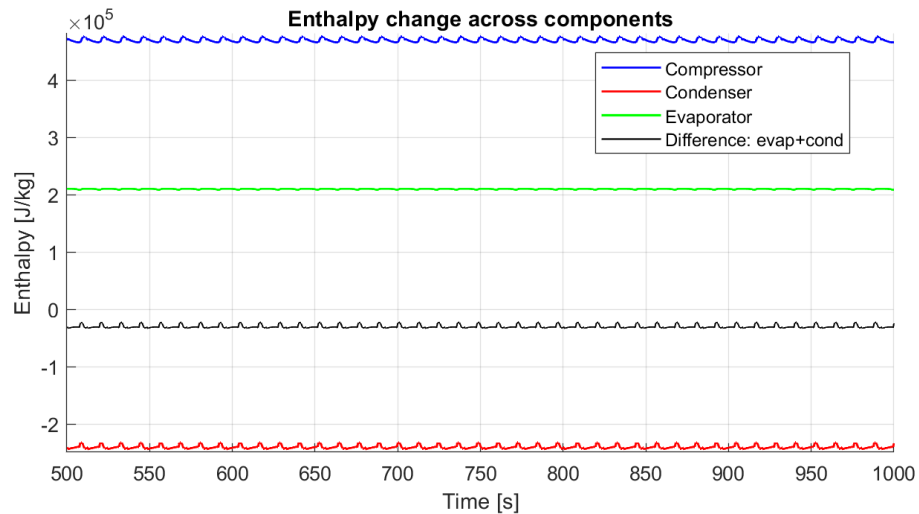


Figure 5.8: Plot of enthalpy changes in components

As can be seen in Fig. 5.8, the largest enthalpy change is through vapour compression. The graph also shows that more energy is expelled in the condenser than is gained in the evaporator.

5.4 Comparison with BITZER Test

A test was conducted at BITZER's test facilities in order to compare the general characteristics of the model developed in this project to the actual system. The references for super-heat, sub-cool and pressure ratio are set to the averages of the states found in BITZER's data, as seen in Tab. 5.3. It should be noted that the data in this section is taken from the same data-set as Fig. 5.1 but is limited to the sample range 2000s \rightarrow 3000s. The purpose is to compare the average model states to the average BITZER test states. Below in Tab. 5.3 the means of the various variables that are compared in this section are seen, where the means are taken over the sampled range. In Tab. 5.4 the difference between the equivalent BITZER

and modelled variables are seen.

Variable	Mean	Unit
p_{cond_BITZER}	$1.7711 \cdot 10^6$	[Pa]
p_{cond}	$2.5628 \cdot 10^6$	[Pa]
p_{FT_BITZER}	$9.7762 \cdot 10^5$	[Pa]
p_{FT}	$1.1511 \cdot 10^6$	[Pa]
p_{evap_BITZER}	$7.286 \cdot 10^5$	[Pa]
p_{evap}	$7.5206 \cdot 10^5$	[Pa]
p_{vi_BITZER}	$1.1263 \cdot 10^6$	[Pa]
p_{vi}	$1.3814 \cdot 10^6$	[Pa]
r_{FT_BITZER}	0.2305	[·]
r_{FT}	0.2254	[·]
Δ_{SC_BITZER}	5.6812	[K]
Δ_{SC}	23.9432	[K]
Δ_{SH_BITZER}	7.1517	[K]
Δ_{SH}	6.5408	[K]
T_{air_BITZER}	278.1925	[K]
T_{air}	278.1439	[K]

Table 5.3: Means of variables in BITZER test data and the model in this project

	Value	Unit
Condenser pressure difference	$7.917 \cdot 10^5$	[Pa]
Flash-tank pressure difference	$1.7347 \cdot 10^5$	[Pa]
Evaporator pressure difference	$2.3464 \cdot 10^4$	[Pa]
Vapour injection pressure difference	$2.5515 \cdot 10^5$	[Pa]
Pressure ratio difference	0.0051	[·]
Sub-cool temperature difference	18.2620	[K]
Super-heat temperature difference	0.6109	[K]
Reefer air temperature difference	0.0486	[K]

Table 5.4: Difference between BITZER variable means and model variable means

5.4.1 Compressor Discharge Mass-flow Comparison

The compressor dynamics modelled in Section 3.3 vary significantly from the BITZER compressor as can be seen in Fig. 5.9 below. This causes the higher frequency and the extra oscillations seen in the data from the simulated model throughout this section.

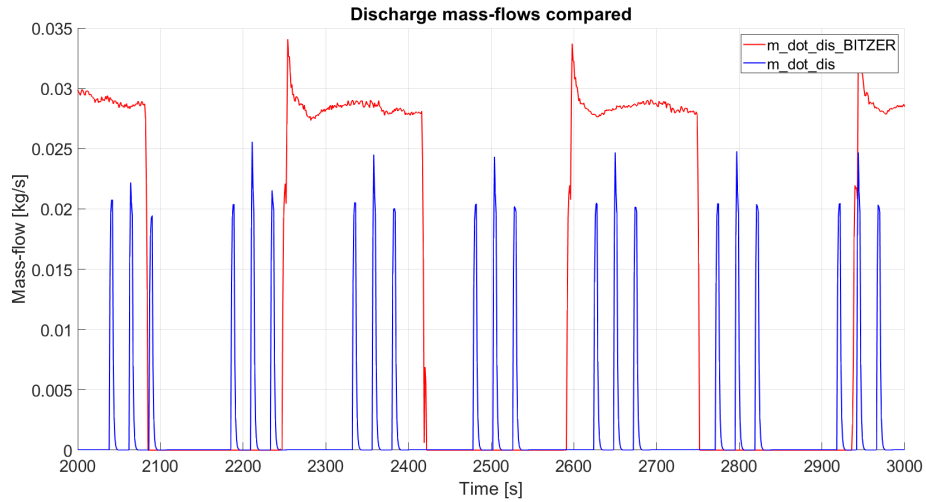


Figure 5.9: Comparison of compressor discharge mass-flows

5.4.2 Reefer Temperature

As seen in Fig. 5.10 the temperature of the air in the reefer reaches an average temperature of 278.1439K very close to the temperature reference. Fig. 5.10 shows that the reefer air temperature oscillates with lower amplitude and higher frequency in model simulation than in BITZER's test data. This is not surprising as the compressor modelled in this project does not reflect the real compressor dynamics fully as shown in Fig. 5.9.

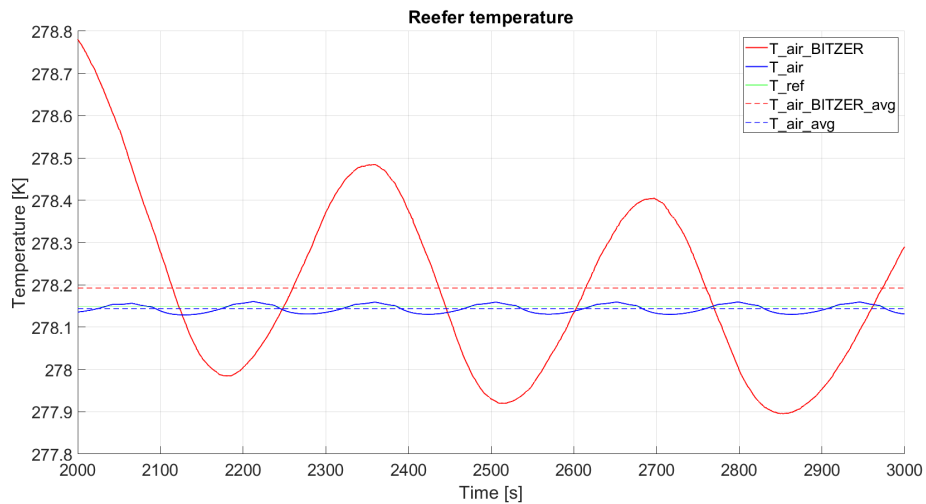


Figure 5.10: Comparison plot of reefer air temperature

5.4.3 Super-heat and Sub-cool

The super-heating and sub-cooling references are set to the averages of the BITZER data super-heating and sub-cooling. In Fig. 5.11 the resulting super-heat is controlled close to the 7.1517K reference whereas the sub-cool remains significantly above the 5.6812K reference.

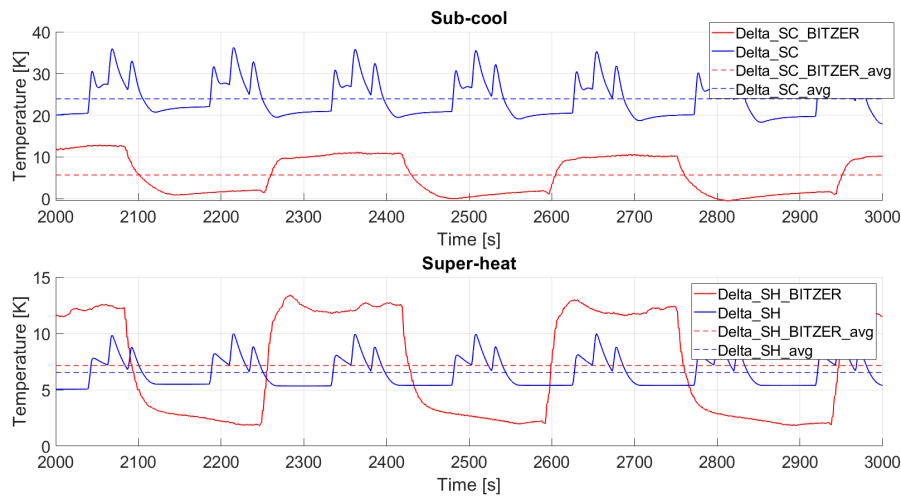


Figure 5.11: Comparison plot of super-heat and sub-cool

5.4.4 Pressure

Fig. 5.12 shows the pressure of the various model components, compared to the equivalent pressures found in the BITZER test data. The comparison shows that the condenser pressure and hence the vapour injection pressure, are above the equivalent BITZER test data pressures, with an average difference of $7.917 \cdot 10^5 Pa$ for the condenser and $2.5515 \cdot 10^5 Pa$ for the vapour injection pressure.

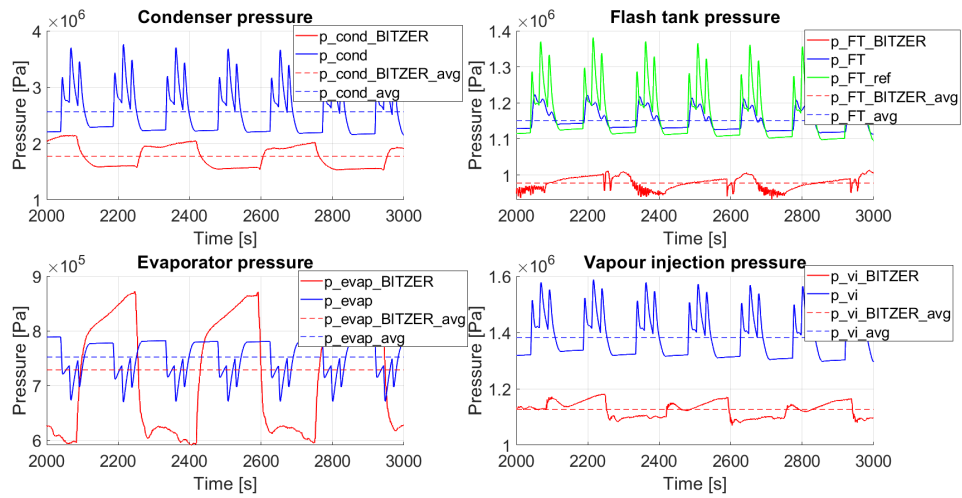


Figure 5.12: Comparison plot of component pressures

As seen in the top right corner of Fig. 5.12 the flash-tank pressure reference, which is derived from the pressure ratio reference in Fig. 5.13, is tracked quite accurately. Despite this, the BITZER flash-tank pressure is notably lower than the simulation model's, with an average difference of $1.7347 \cdot 10^5 Pa$, which indicates that the modelled condenser pressure is inaccurate. Despite this the evaporator pressure seems to be relatively realistic when compared to the BITZER test data, as the averaged difference is $2.3464 \cdot 10^4 Pa$, which is the most accurate of all the modelled pressure dynamics.

The pressure ratio which is dependent on the condenser pressure is, as mentioned in Section 4, used to control the flash tank pressure. Therefore a higher condenser pressure results in a higher flash tank pressure in order to follow the pressure ratio reference.

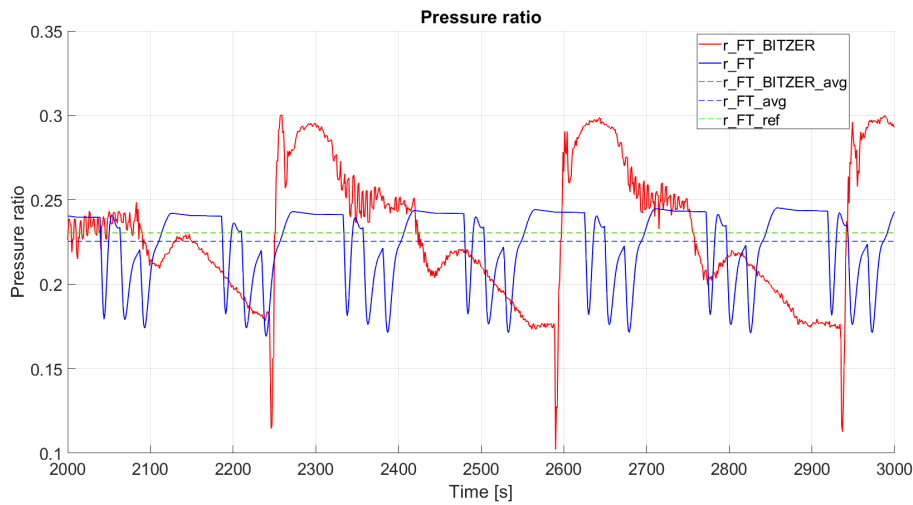


Figure 5.13: Comparison plot of pressure ratio

5.4.5 Enthalpy Change

The change in enthalpy across the components are plotted and compared in Fig. 5.14. It is important to note that the enthalpy at the output of the condenser and input of the evaporator is not readily available from the BITZER data. The enthalpies are found with look-up tables using quality, $\chi = 0$ and temperature of the liquid leaving the flash-tank to get the evaporator input enthalpy, and pressure at discharge and temperature at output of the condenser to get the condenser output enthalpy. It is assumed that there is no pressure difference across the condenser. The enthalpy differences shown in Fig. 5.14 are different, which is not surprising due to the pressure differences and heat transfer coefficient inaccuracies.

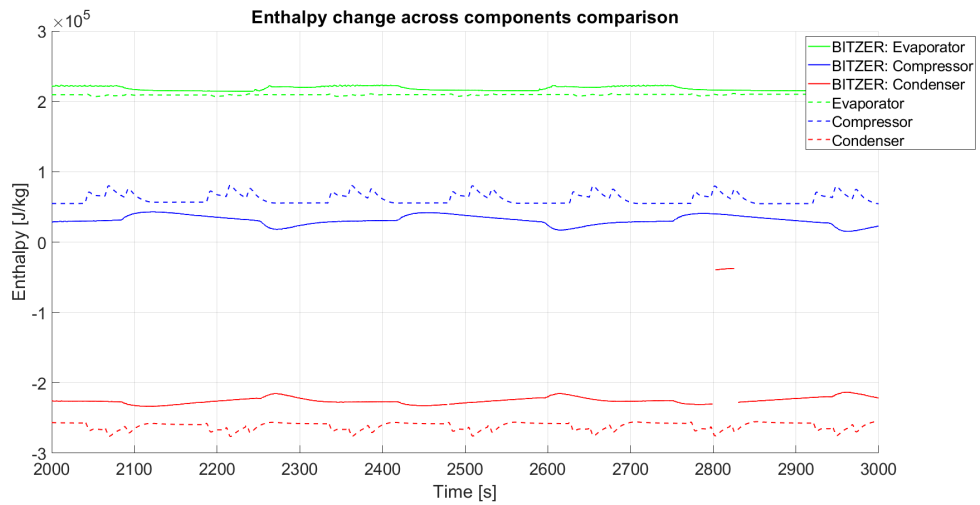


Figure 5.14: Comparison plot of enthalpy changes across components

5.5 System States and COP

The COP is calculated as shown in Section 3.8. In order to have a viable model for optimisation, it must be possible to measure a change in COP, with respect to the controller set-points. In order to show this, firstly a change in super-heat will be tested given a constant flash-tank pressure ratio r_{FT} . This will be followed by a test with constant super-heating and variable r_{FT} . As shown in the previous simulation Fig. 5.3, sub-cooling is not guaranteed with the current control strategy, yet increasing the fan-speeds will still have an effect on COP and is therefore tested for constant super-heating and pressure ratio.

The COP will, if averaged, be small. This is because of the oscillating compressor dynamics resulting in low cooling capacity, when the compressor speed is slow and approaching zero. As more efficient set-points will allow for longer compressor off-time, higher performance may be obscured through averaging. In order to get more meaningful results, the average will only be taken for samples with a compressor speed $\Omega_{state} \geq 200rpm$, across 1000 samples. The different averaging methods are plotted in Fig. 5.15

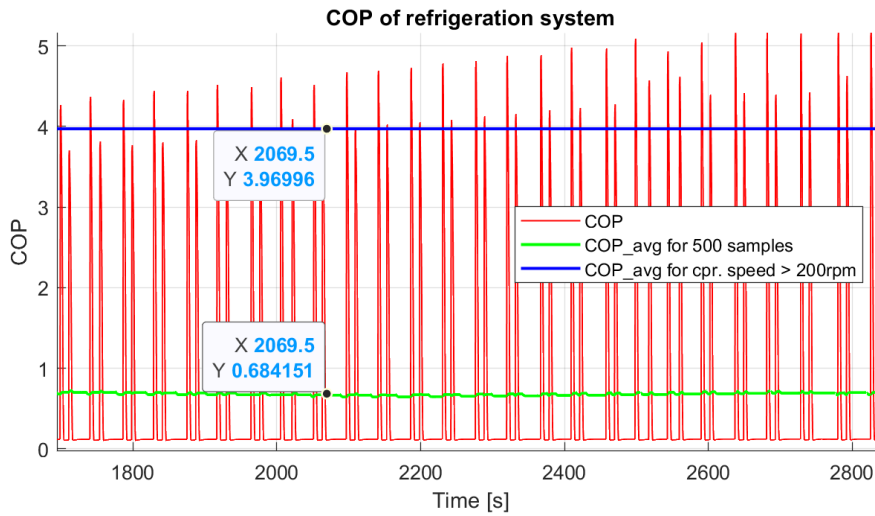


Figure 5.15: Plot of COP comparison between raw COP data, 500 sample mean and the means with minimum compressor speed of 200 rpm

For the following experiments, the initial conditions will be similar to that of the initial simulation in Section 5.3.2. The fans will however be turned off, until the experiments require them. The COP will be sampled between sample 4500 and 5500, such that most of the reference change associated transient will be gone. The test data can be found in Appendix F.

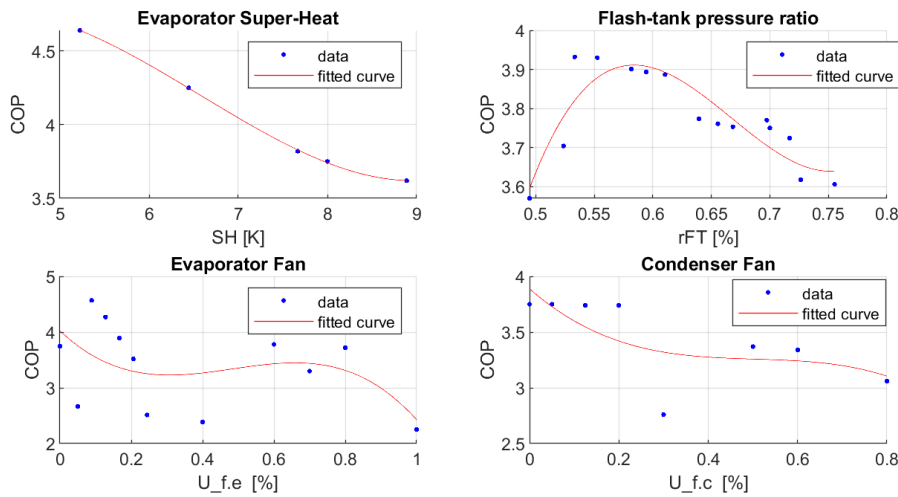


Figure 5.16: Plot of COP experiments, fitted with 3rd degree polynomial

Fig. 5.16 fits the 4 different experiments to third degree polynomials, in order to

show the existence of maximums. An increase in super-heat, reduces the COP monotonically. The flash-tank pressure ratio on the other hand has a maximum around $r_{FT} = 0.57$. It is difficult to conclude any trend for the fan control signals $U_{f,e}$ and $U_{f,c}$. For the condenser the general trend indicates a reduction in COP as fan speed/ control signal $U_{f,c}$ is increased. The evaporator data is generally inconsistent although it also indicates that the maximal fan control signal $U_{f,e}$ results in the smallest COP.

In common, the power-draw of a high fan control signal reduces COP significantly. An important thing to note in the fan experiments is that the COP is only considered above the compressor speed threshold of $200rpm$. The fans are therefore switched off as soon as the compressor speed $\Omega_{state} < 200rpm$.

5.6 Simulation Summary

The first simulation test is run with set-points, that result in a stable transient. While the evaporator super-heating Δ_{SH} and pressure ratio r_{FT} are sufficiently controlled, the simulation did not reach the desired steady-state reefer air-temperature T_{air} . This is likely due to the maximum compressor control signal being set too low. In the first experiment the sub-cooling Δ_{SC} is more or less non-existent. By changing the set-points to match the average BITZER test data, a correlation between pressure ratio, sub-cooling and general cooling ability is demonstrated. By lowering the pressure ratio r_{FT} significant sub-cooling appears, also an increase in reefer cooling is shown as T_{air} oscillates closely around the temperature reference of $278.15K$. In comparison to BITZER's test data the condenser, flash-tank and vapour injection pressures differ significantly, with respective average differences of $7.917 \cdot 10^5 Pa$, $1.7347 \cdot 10^5 Pa$ and $2.5515 \cdot 10^5 Pa$. The evaporator pressure is however quite similar when looking at the averaged difference which is $2.3464 \cdot 10^4 Pa$, which indicates that the evaporator pressure dynamics are relatively accurate compared to the rest. Even if assuming correct pressure-dynamics, the cause for the large differences in pressure is a combination of different compressor dynamics and inaccurate heat-transfer constants UA 's in the condenser and evaporator. Alternatively, the modelled pressure in mainly the condenser is at fault. The pressure ratio r_{FT} reference, being a ratio between the evaporator and condenser is accurately tracked in simulation, so are the references for T_{air} and Δ_{SH} . The results in Section 5.5 indicate that system variable set-points have an effect on the COP. Given the mass-drift seen in the flash-tank in Section 5.3.2, the estimated set-points may be biased. An increase in super-heat results in a decrease of COP. The pressure ratio tests indicate a maximum at $r_{FT} = 0.57$. The evaporator and condenser fans are shown to have a great effect on COP, however the testing gave inconclusive results. The reason for this, may be a result of the frequent on/off fan switching.

Chapter 6

Set Point Optimisation

As was demonstrated in simulation, the super-heat in the evaporator and flash-tank pressure have an effect on the COP. The flash-tank pressure ratio was shown to have an maximum COP, while an increasing super-heat monotonically decreased COP. With this in mind, it should be possible to find a set of set-points that maximise the COP, such that the system is as efficient as possible, while having a stable super-heat.

6.1 Optimisation Methods

The system model derived in Chapter 3 is not only nonlinear it is also not differentiable due to the use of look-up tables for calculating system states. Because of this the optimisation algorithms used in this section will be gradient-free. A gradient-free optimisation algorithm is defined such that an extremum is found through evaluating a cost function for discrete points. Dependent on the inner-workings of the algorithm at hand, these discrete points are iteratively updated and improved until an extremum is found within some tolerance, or a predefined N number of iterations have taken place. By request of BITZER, the two algorithms that have been considered is firstly the genetic algorithm and secondly the swarm algorithm.

6.1.1 Cost-function

The cost-function used for evaluating the efficiency of the set points is the COP discussed in Section 3.8:

$$COP = \frac{\dot{Q}_e}{W_{tot}}$$

Since the objective is to maximise the COP, the objective will be a maximisation problem. Evaluating the cost-function, introduces some challenges as it is the steady-state performance that is of interest. This means that the system needs to reach the set-points, and run for a while before the average COP can be evaluated. Given that a lot of set-points must be evaluated before reaching a maximum, the optimisation process will be computationally demanding.

6.1.2 Algorithm Choice

The two contesting gradient-free optimisation methods recommended by BITZER is the genetic algorithm and the particle swarm algorithm. The swarm optimisation algorithm tends to emphasise exploration where the swarm particles interact and share information, enabling them to collectively explore different regions of the solution space. The genetic algorithm, in contrast, updates pairwise and explores the solution by passing down genetic information and mutating. [23].

Due to the interaction between the particles in a swarm algorithm, the computational time tends to be higher for swarm algorithms when compared to the genetic algorithms [24]. Because of this, the genetic algorithm has been prioritised.

6.1.3 Genetic Algorithm

The genetic algorithm iterates through a specified number of generations and mutates set-points between generations in order to search the solution space and find an optimal set of set-points the maximises the cost-function.

How it Works

The genetic algorithm works in the following way [19]:

1. **Select initial population:**

The initial population of N pairs of set-points are generated, these initial set-points are uniformly chosen at random within the specified bounds.

2. **Select parents for next generation:**

The generated set-points are then used to evaluate the cost-function, and an output of the cost-function is found for each set of set-points in the population. The costs are then used to determine which set of set-points should be used as parents for the next generation of set-points.

3. **Select population in new generation**

The next generation of set-points are found by creating 3 types of offspring:

- (a) **Elite offspring**

The set of set-points associated with the best cost-function outputs in the previous generation. These offspring remain unchanged through the next generation. The amount of elite offspring E_o is determined manually.

- (b) **Crossover offspring**

Crossover offspring are found by selecting parents and combining their

attributes. To choose the number of crossover offspring in the new generation a crossover fraction C_f is specified.

(c) **Mutation offspring**

The last type of offspring is the mutated offspring. To create this type of offspring the algorithm randomly adds or subtracts from a randomly selected parent. The number of mutated offspring M_o is determined by: $M_o = N - (C_f \cdot (N - E_o))$, where N is the full population size.

4. **Algorithm termination:**

If termination criteria such as the number of generations, or a tolerance on convergence has been met, the algorithm halts.

In Appendix H a flow chart of a simplified genetic algorithm can be found.

Parameters

The following table shows some of the parameters that affect the genetic algorithm performance [18].

Parameter	Description
Population Size	The number of set of set-points in each generation. A larger population allows for more exploration of the solution space, increasing the likelihood of finding the global maximum while also increasing computational time since each set of set-points must be simulated.
Generation	A simulation cycle where a population size of N is run. The number of generations has an effect on the convergence of the set-points, the algorithm is more likely to converge if more generations are chosen.
Elite Count	The number of the best performing set-points that are preserved in each generation. Keeping the best performing individuals from the previous generation ensures that information is not lost and can lead to faster convergence.
Crossover Fraction	Fraction of the population used to generate crossover offspring. A higher crossover fraction can lead to more diverse set-points since a larger portion of the population is used.
Mutation Rate	Rate at which certain individuals in the population are mutated. A higher mutation rate ensures a wider search but may slow down convergence.
Fitness Scaling	The fitness scaling function converts cost-function outputs into values in a range that is suitable for the selection function. The default MATLAB fitness scaling function ranks sets of set-points in the population by evaluating their corresponding cost-function output. The cost-function outputs are then scaled by $\frac{1}{\sqrt{r}}$ where r is the rank of the individuals.

Selection Function	The selection function chooses the sets of set-points in each generation that are used for reproduction. The default selection function in MATLAB works by arranging a line where each parent represents a section of the line, with the length of the section proportional to the scaled value from the fitness scaling function. The algorithm moves along the line in uniform steps and for each step it selects a parent from the section it lands on.
Crossover Function	The function that determines how the crossover offspring are generated. The default crossover function for problems with integer constraints is either: $C_o = X_1 + b(X_1 - X_2)$ or $C_o = X_2 + b(X_1 - X_2)$ chosen at random. C_o is the crossover offspring, X_1, X_2 are the parents of the offspring and b is a random number drawn from a Laplace distribution.
Mutation Function	The function that determines how an individual is mutated for the next generation. The default mutation function in MATLAB when integer constraints are present works in the following way: $M_o = \begin{cases} X + s(ub - X) & t \geq r \\ X - s(X - lb) & t < r \end{cases}$ M_o is the mutated offspring, X is the parent, s is a random variable drawn from a power distribution, r is a random number drawn from a uniform distribution, t is the scaled difference between X and lb , lb is the lower bound and ub is the upper bound.

6.1.4 Swarm Algorithm

The inner workings of the swarm algorithm will not be dealt with in depth. It is sufficient to say that it is a gradient-free optimisation algorithm, that converges towards extremums through inter-particle communication combined with local

search by the individual particles. An explanation of the swarm algorithm can be found in Appendix H

6.2 Optimisation Implementation

In this section the genetic optimisation algorithm is implemented to find the optimal set-points: Δ_{SH_ref} and r_{FT_ref} . To implement this algorithm the built-in MATLAB function $ga()$ is used. The parameters for $ga()$ is a cost-function, which here is the averaged COP, along with different options such as upper and lower bounds, constraints, step resolution and number of generations. The non-default variables are specified below in Tab. 6.1.

Set-point	Lower bound	Upper bound	Res.	Gen.	Pop. size	Elite count
Δ_{SH_ref}	5	11	0.1	5	10	10%
r_{FT_ref}	0.3	0.9	0.01			

Table 6.1: Options for ga

Since simulation of the model takes a significant amount of time, the number of generations and population size is kept quite low. The upper and lower bounds are set such that there are 60 possible values for each set-point, and are kept in a range that is thought to be realistic. The elite count is set such that the best set of set-points make it through to the next generation.

6.2.1 Results

Here the results of the implemented genetic optimisation algorithm will be presented. The algorithm is tested without fans included due to the findings in Section 5.5.

Without Fans

Without fans means that the fan speed of the condenser and evaporator fans are set to zero: $U_{f,c} = U_{f,e} = 0$. Below in Fig. 6.1 the best average COP can be seen for each generation as well as the initial run. The best average COP is already reached in the second generation and never improves beyond that.

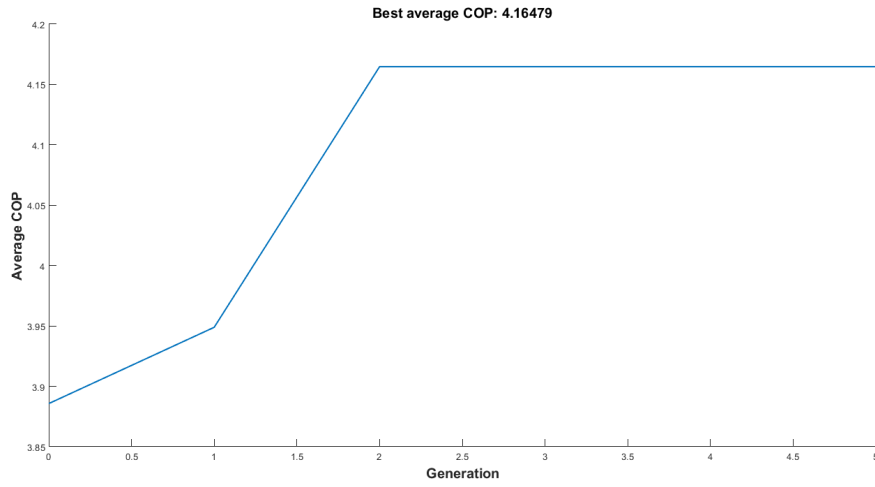


Figure 6.1: Best average COP each generation without fans

In Fig. 6.2 the average COP after each generation can be seen.

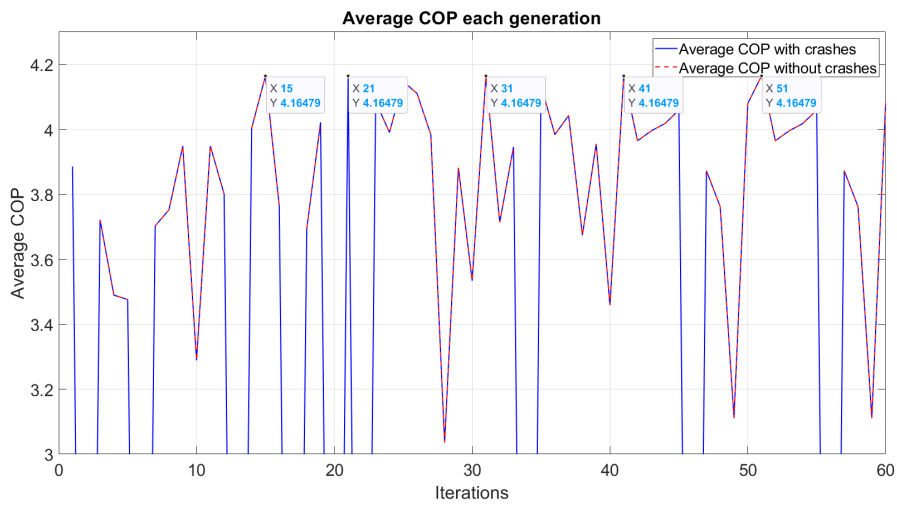


Figure 6.2: Average COP each iteration without fans

Fig. 6.3 shows the set-points Δ_{SH_ref} and r_{FT_ref} evaluated at each iteration.

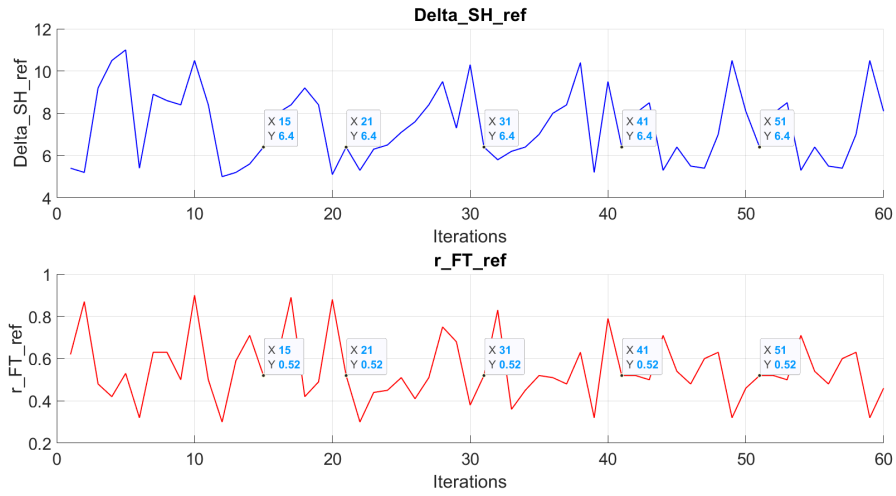


Figure 6.3: Set-points at each iteration without fans

In Tab. 6.2 the values for the best average COP and the corresponding set-points that were used to achieve it are shown.

Best average COP	r_{FT_ref}	Δ_{SH_ref}
4.16479	0.52	6.4

Table 6.2

In Fig. 6.4 system states: temperature, pressure, sub-cool, super-heat and pressure ratio can be seen.. The pressure ratio r_{FT} and the super-heat Δ_{SH} oscillate around their respective set-points of 0.52 and 6.4.

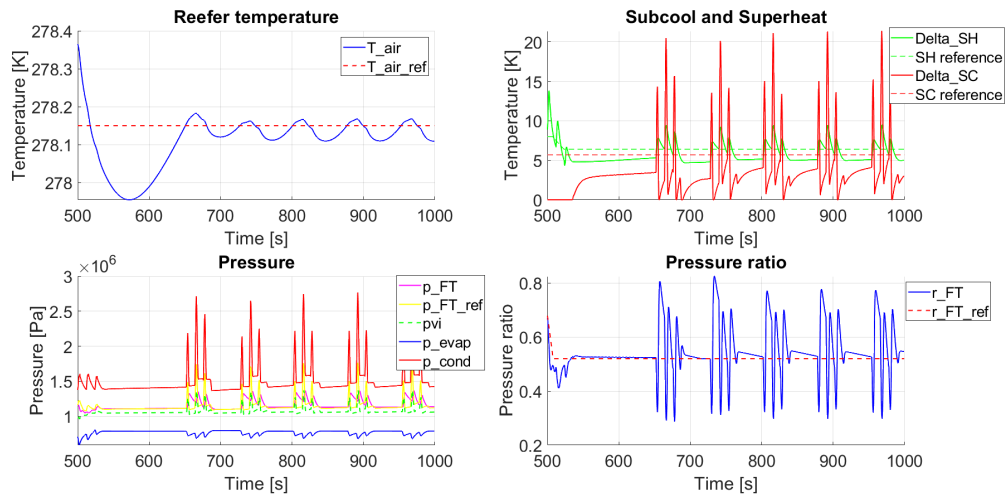


Figure 6.4: System states with best set-points without fans

With Fans

The genetic algorithm is also implemented with fans, the results can be found in Appendix H.

6.3 Optimisation Summary

The genetic algorithm is chosen over the swarm algorithm due to the lower computational time and its relative simplicity to implement. It is found that through the genetic algorithm it is possible to maximise COP for super-heat and pressure ratio. The parameters of the genetic algorithm were tuned manually but because of the long simulation times a limited combination of parameters were tried. The genetic algorithm converges to the optimal set-points in the second generation. This is likely due to a relatively large population size considering that only two set-points are being varied and their bounds are fairly tight.

Chapter 7

Discussion

The purpose of this section is to highlight the most significant observations and challenges from the different sections. The point of this is to point out possible future improvements and work that can be done, and what readers should be aware of when applying the discussed model and theory.

7.1 Compressor Dynamics

The compressor speed is in Section 3.3 modelled with an arbitrary first order characteristic, such that a step input as the control signal results in a speed increase with a given time-constant, this is done in order to avoid discontinuous and abrupt mass-flows. For a more accurate dynamic, the real scroll compressor should be measured, such that the model dynamics reflect reality. Furthermore, the compressor in a physical system has the ability to completely turn off. In order to avoid complications with the condenser input, the minimum speed is during simulation set to $\Omega = 1rpm$ such that the condenser and evaporator always have an active input/output, as mentioned in Section 5.2.

7.2 Zero-boundary Condenser Model

The condenser was initially modelled similarly to the evaporator with a moving boundary between a liquid phase and a combined vapour/mixed phase. Because of the possibility of a non sub-cooled output, this was changed to the zero-boundary-condenser model, with algebraically solved mass boundaries. The cost of this is less accurate pressure dynamics, as demonstrated in Section 5.3.3 and the model test Section 3.10.2. An improved condenser model will include all three control masses separately, resulting in a two-boundary-model, as seen in [33], with switching number of boundaries based on output phase.

7.3 Valve Simplification

As mentioned in Section 4.1.1, the valve model from Section 3.2 is not used to control the mass-flows through the condenser and evaporator valves. Instead the mass-flows are set directly by the controllers. This simplification was made due to difficulties encountered during simulation of the model. The simplification causes the valves to no longer be dependent on the pressure differences between the components they separate. Since the valves are modelled adiabatically and are not included in the COP calculations, this simplification is not significant for overall model accuracy. The interested reader is referred to the simulation in Appendix E, where the valves are fully implemented.

7.4 Vapour Injection Mass-flow

The vapour injection mass-flow is found with the valve function modelled in Section 3.2 multiplied with the compressor speed ratio between current and maximum compressor speed, as described in Section 3.3 with the equation:

$$\dot{m}_{inj} = A_{vx}C_{vx}\sqrt{D_{v_FT}(p_{FT} - p_{inj})} \cdot \frac{\Omega_{state}(t, U_\omega)}{\Omega(1)} \quad (7.1)$$

This assumes that the vapour injection mass-flow is linearly dependent on the compressor speed. In addition, the valve coefficient $K_{inj} = A_{vx}C_{vx} = \frac{K_{cond}}{4}$ is chosen to be a quarter of the condenser/evaporator valve constant. This might not be an entirely accurate description of the vapour injection mass-flow, since a real compressor's mass-flow intake is dependent on the refrigerant density and volume intake.

The vapour injection model causes slight oscillations in the total mass of the system. This is proved in Appendix G which shows that oscillations stop when $p_{FT} < p_{inj}$, meaning that no injection flow occurs.

7.5 Flash-tank Volume Drift

As mentioned in Chapter 4 and shown in Fig. 5.5, the flash-tank volumes tend to drift dependent on choice of reference points. This is briefly explained in Section 4.1.5 but will be further expanded on here. This drift is due to a number of factors. Firstly the pressure difference between condenser and flash-tank, secondly the enthalpy at the output of the condenser, both resulting in varying degrees of flashing. To keep the volume ratio between the two phases in steady-state, the amount of flashing must correspond to the vapour and liquid output-flows.

In the flash-tank model it is assumed that the mass-flow to the evaporator from the

flash-tank is in a liquid state while the mass-flow to the compressor is in vapour state. These assumptions do not hold when the flash-tank is entirely consumed with either liquid or vapour, thus the volume drift is a stability concern. In Section 5.3.3, the decrease in the scaling ratio r_V , indicates that the estimated volume not only drifts with respect to each other, but also with respect to the total allowed flash-tank volume, suggesting issues with pressure dynamics and density estimation.

The volumes of vapour and liquid refrigerant in the flash-tank are possible to control, this however requires that the flash-tank pressure is sufficiently above the pressure in the compressor injection port, as explained in Section 3.10.3 and that the compressor is running at a significant speed, and that the injection port valve model has a sufficiently high valve constant. Implementation of this did not result in stability overall, as a great mass drift appeared in condenser and evaporator.

In Appendix G the relationship between flash-tank pressure and volume can be seen.

7.6 Pressure and Mass Dynamics

The refrigerant mass stays relatively stable throughout the simulations, any small divergence is expected to be caused by numerical issues over time. On surface level this suggests reasonable mass dynamics. It has however become clear that the density relationships between different control volumes are non-ideal. While density and enthalpy averaging across single phase masses such as super-heated vapour and sub-cooled liquid is straight-forward, the mixed refrigerant phase density enthalpy are more difficult to estimate. In existing literature [33], it is common to take the refrigerant void-fraction [35] into consideration. The void fraction is the ratio of the cross-sectional area occupied by the vapour, relative to the entire cross-section. The void-fraction is not only dependent on refrigerant, but also the tube geometry and flow types. This theory should be applied for all equations involving enthalpy and density assumptions and estimations. A concurring problem in the model is the pressure dynamics, that seem to get unstable at times, resulting in huge pressure time derivatives. This may be caused by the inaccurate mass and volume estimations of the different refrigerant phases, demonstrated in the volume scaling ratio Section 5.3.3. A trick used to circumvent breaking the constant volume boundaries set by the physical attributes was explained in the simulation section 5.2.3, this method however presupposes that the relative volume ratio is correct in the first-place, as the regions are scaled with the same constant. Were the pressure states and mass states modelled correctly, there would be no need for the scaling ratio, as the masses would have the correct densities, this seemed to be the case in the evaporator, despite the void-fraction being replaced by simple

averaging across the mixed phase enthalpy. This issue mostly comes to light when the masses in the different phases are estimated for pressure dynamics in the zero-boundary condenser model. The issue also comes to light in the scaling ratio r_V flash-tank drift.

Considering the constant density mass-flow based pressure dynamics

$$\dot{p}_{cond_1,l}(t) = \frac{\dot{m}_{in.c} - \dot{m}_{out.c}}{\mathcal{E}_c \cdot V_l + \mathcal{F}_c \cdot V_{mx} + \mathcal{G}_c \cdot V_v} \quad (7.2)$$

With Density partials:

$$\mathcal{F}_c = \left. \frac{\partial D_{mx}(p)}{\partial p_{cond}} \right|_{h_{mx}} \quad (7.3)$$

The densities D (mass M , volume V relationship) are of big importance. Without proper density estimation, the density partials in the denominator may become small, although the mass-flow difference in the numerator is huge, resulting in unstable dynamics. Similarly, in the constant density enthalpy based pressure dynamics, the mass of the different phases is important.

$$\dot{p}_{cond_2,l}(t) = \frac{\dot{m}_{in.c}h_{in.c} - \dot{m}_{out.c}h_{out.c} - \dot{Q}_{r,m.c} - \dot{M}_l h_{out.c} - \dot{M}_{mx} h_{mx} - \dot{M}_v h_{in.c}}{M_l \mathcal{I}_c + M_{mx} \mathcal{J}_c + M_v \mathcal{K}_c} \quad (7.4)$$

With enthalpy partials:

$$\mathcal{J}_c = \left. \frac{\partial h_{mx}(p)}{\partial p} \right|_{D_{mx}} \quad (7.5)$$

The boundary-less model implemented for the condenser, estimates the different phase masses before finding the pressure dynamics. This is done by assuming the relative volume of each phase is linearly dependent on enthalpy, ignoring the differences in density. Another assumption made that should be revisited, after the enthalpy and density estimations, is the assumption of constant volume derivatives in the constant enthalpy pressure dynamics. As pressure increases, so does the density of refrigerant, with this in mind, it is possible that the inclusion of volume dynamics, would reduce the numerator, resulting in smaller and more stable pressure derivatives.

7.7 Model Realism

The comparison with the BITZER data in Section 5.4 sought out to prove the realism of the complete simulation model. Because of great differences in compressor model and compressor control, identical oscillation frequencies and amplitudes were not expected. However, based on the initial conditions, and system constants used for simulation, the average pressures in the system are expected to approximate the BITZER values. The moving-boundary evaporator, seemed reasonably

close to the BITZER test data. This is not the case for the other components, as especially the zero-boundary condenser pressure is far from the expected mean. With the overall pressure issues discussed earlier in mind, the deviation from the BITZER plant is in the case of the condenser unlikely related to inaccurate estimation of heat-transfer coefficients UA_x . In contrast, the evaporator performance seems to be correctable with tuning of the heat-transfer coefficients.

7.8 Optimisation

As mentioned earlier in Section 6.3 and 5.5, the fans seem to have a negative effect on the COP of the system. This indicates that they use significantly more energy than they produce in terms of cooling. This is not guaranteed in reality and is most likely due to modelling errors, since the fans are expected to have a positive effect on the COP [3]. However it is found that $r_{FT_{ref}}$ corresponds with the optimum found in the tests in Section 5.5, where Fig. 5.16 indicates that the optimisation is functioning as expected when fans are not included. In Fig. 5.16 some COP values are higher than the COP found in the optimisation Chapter 6. This is likely caused by shorter simulation times and part of the transient being averaged in the genetic-algorithm implementation, this was done to reduce the long optimisation times.

Ideally more set-points, such as the relative vapour-liquid volumes in the flash-tank, the fan speeds and the compressor on and off times would be interesting to consider for optimisation.

Chapter 8

Conclusion

The goal of this project was to model and optimise a vapour-compression refrigeration cycle with a flash-tank in order to maximise the COP of an eTRU refrigeration system. This has been demonstrated to be possible through the first principal modelling method. The resulting refrigeration system model is able to reach the required reefer air temperature T_{air} , reach the specified flash-tank pressure ratio r_{FT} and evaporator super-heat Δ_{SH} , using a dynamic scroll-compressor model with vapour injection an on-off switching.

The model is by large stable enough to perform gradient free optimisation of the COP of the system. Modelling of the refrigerant pressure dynamics has proven to be of great challenge and a source of stability issues, and improvements to the overall model would improve the results. Nevertheless, the COP of the model is shown to be dependent on the flash-tank pressure ratio, which forms the basis for a flash-tank dependent optimisation problem. This optimisation is done using the genetic algorithm with and without fans. It was found that the best results are obtained when fans are not included as they for the model at hand have a negative effect on the COP of the system. The effect of fans of the system, should however be reevaluated with a model that includes different pressure dynamics.

Due to the super-heat in the evaporator being optimal when as small as possible, only the flash tank pressure ratio is left to be optimised. Based on this assertion optimisation with genetic algorithm alone is not necessary. Ideally further states should be considered and included in the optimisation, this is hypothesised to be a good basis for future research on the subject. It is suggested that future research uses the genetic algorithm particularly with included compressor parameters such as on/off-time combined with the flash-tank volume-ratio, fan-speeds, super-heat and flash-tank pressure ratio. The resulting set-points used as initial control references for the industry tested and implemented extremum seeking controller [32], is hypothesised to be of value in future refrigeration control schemes and should therefore be researched further.

Bibliography

- [1] United States Environment Protection Agency. *Global Greenhouse Gas Emissions Data*. URL: <https://www.epa.gov/ghgemissions/global-greenhouse-gas-emissions-data>. (accessed: 16.09.2022).
- [2] H Ambarita and H V Sihombing. "The optimum intermediate pressure of two-stages vapor compression refrigeration cycle for Air-Conditioning unit". In: *Journal of Physics: Conference Series* (2018), p. 3. doi: 10.1088/1742-6596/978/1/012098. URL: <https://iopscience.iop.org/article/10.1088/1742-6596/978/1/012098>.
- [3] Sebastian Angermeier and Christian Karcher. "Model-Based Condenser Fan Speed Optimization of Vapor Compression Systems". In: *Energies* 13.22 (2020). ISSN: 1996-1073. URL: <https://www.mdpi.com/1996-1073/13/22/6012>.
- [4] Carel. *Scroll Compressors datasheet*. <https://www.carel.com/product/e2v-b-u-s-phase-out->. (accessed: 31.05.2023).
- [5] CoolProp. *CoolProp*. URL: <http://www.coolprop.org/index.html>. (accessed: 07.02.2023).
- [6] Sarah DeGuzman. *Flash Chamber*. URL: <https://www.punchlistzero.com/flash-chamber/>. (accessed: 19.09.2022).
- [7] Delta. *Fan datasheet*. Found in appendix Datasheet folder.
- [8] U.S DEPARTMENT OF ENERGY. *Biodiesel Blends*. URL: https://afdc.energy.gov/fuels/biodiesel_blends.html. (accessed: 16.09.2022).
- [9] Changqing Tian & Hongxing Yang Fei Qin Shuangquan Shao. "Model simplification of scroll compressor with vapor refrigerant injection". In: *International Journal of Green Energy* (2016), pp. 803–811. doi: 10.1080/15435075.2016.1161626. URL: <https://doi.org/10.1080/15435075.2016.1161626>.
- [10] Freon. *Freon™ 410A Refrigerant (R-410A) Thermodynamic Properties (SI Units)*. <https://www.freon.com/en/-/media/files/freon/freon-410a-si-thermodynamic-properties.pdf?rev=6b72bfaa299142d697540982b88a56eb>. (accessed: 27.09.2022).
- [11] A. Greco and G.P. Vanoli. "Flow-boiling of R22, R134a, R507, R404A and R410A inside a smooth horizontal tube". In: *International Journal of Refrigeration - revue Internationale Du Froid - INT J REFRIG* 28 (Sept. 2005), pp. 872–880. doi: 10.1016/j.ijrefrig.2005.01.008.

- [12] Bo Shen Haorong Li James E. Braun. "Modeling Adjustable Throat-Area Expansion Valves". In: *International Refrigeration and Air Conditioning Conference* (2004), pp. 1–10. URL: <https://docs.lib.purdue.edu/iracc/705/>.
- [13] Estefanía Hervas-Blasco et al. "Study of different subcooling control strategies in order to enhance the performance of a heat pump". In: *International Journal of Refrigeration* 88 (2018), pp. 324–336. ISSN: 0140-7007. DOI: <https://doi.org/10.1016/j.ijrefrig.2018.02.003>. URL: <https://www.sciencedirect.com/science/article/pii/S0140700718300343>.
- [14] HITACHI. *Expansion-valve datasheet*. https://www.google.com/url?sa=t&rct=j&q=&esrc=s&source=web&cd=&cad=rja&uact=8&ved=2ahUKEwjtp-zpnIP9AhVQRPEDHYbCCM8QFnoECA0QAQ&url=https%3A%2F%2Fwww.joap.dk%2Fdownload_file%2Fforce%2F274%2F384&usg=A0vVaw341zxngC0rBQbDfQZXLh9K. (accessed: 7.02.2023).
- [15] Kresten Kjær Sørensen. "Model Based Control of Reefer Container Systems". PhD thesis. Aalborg University, 2015. ISBN: 978-87-7152-063-7.
- [16] Z. Liu and W Soedel. *An Investigation of Compressor Slugging Problems*. <https://docs.lib.purdue.edu/cgi/viewcontent.cgi?article=2016&context=icec>. 1994.
- [17] Zhao Hiu-Xia Ma Guo-Yuan. "Experimental study of a heat pump system with flash-tank coupled with scroll compressor". In: *Energy and Buildings* 40.5 (2008), pp. 697–701. URL: <https://www.sciencedirect.com/science/article/pii/S0378778807001533>.
- [18] MATLAB. *Genetic Algorithm Options*. <https://se.mathworks.com/help/gads/genetic-algorithm-options.html>.
- [19] MATLAB. *How the Genetic Algorithm Works*. <https://se.mathworks.com/help/gads/how-the-genetic-algorithm-works.html>.
- [20] MATLAB. *Particle Swarm Optimization Algorithm*. <https://se.mathworks.com/help/gads/particle-swarm-optimization-algorithm.html>.
- [21] Jon Mosen. *Control Valve Gas Flow | Choked flow, Cavitation, Flashing*. <https://www.valin.com/resources/blog/gas-flow-control-valves>. (accessed: 07.03.2023).
- [22] Jon Mosen. *Control Valve Liquid Flow | Choked flow, Cavitation, Flashing*. <https://www.valin.com/resources/blog/control-valve-liquid-flow-choked-flow-cavitation-flashing>. (accessed: 02.03.2023).
- [23] B. Obayyanahatti and Yuhui Shi. "Comparison between Genetic Algorithms and Particle Swarm Optimization." In: *Lecture notes in computer science* 1447 (Mar. 1998), pp. 611–616. DOI: 10.1007/BFb0040812.

- [24] Sidhartha Panda and Narayana Prasad Padhy. "Comparison of particle swarm optimization and genetic algorithm for FACTS-based controller design". In: *Applied Soft Computing* 8.4 (2008). Soft Computing for Dynamic Data Mining, pp. 1418–1427. ISSN: 1568-4946. DOI: <https://doi.org/10.1016/j.asoc.2007.10.009>. URL: <https://www.sciencedirect.com/science/article/pii/S1568494607001330>.
- [25] EVfleet PG&E. *National Grocer Reduces Costs and Emissions with eTRUs*. <https://www.safeconnectsystems.com/wp-content/uploads/2021/07/albertsons-case-study.pdf>. (accessed: 16.09.2022).
- [26] Miquel Pitarch et al. "Evaluation of different heat pump systems for sanitary hot water production using natural refrigerants". In: *Applied Energy* 190 (2017), pp. 911–919. ISSN: 0306-2619. DOI: <https://doi.org/10.1016/j.apenergy.2016.12.166>. URL: <https://www.sciencedirect.com/science/article/pii/S030626191631947X>.
- [27] Hongjie Qi, Fuya Liu, and Jianlin Yu. "Performance analysis of a novel hybrid vapor injection cycle with subcooler and flash tank for air-source heat pumps". In: *International Journal of Refrigeration* 74 (2017), pp. 540–549. ISSN: 0140-7007. DOI: <https://doi.org/10.1016/j.ijrefrig.2016.11.024>. URL: <https://www.sciencedirect.com/science/article/pii/S0140700716304091>.
- [28] Ehsan Amiri Rad and Saeed Maddah. "Entropic optimization of the economizer's pressure in a heat pump cycle integrated with a flash-tank and vapor-injection system". In: *International Journal of Refrigeration* 97 (2019), pp. 56–66. ISSN: 0140-7007. DOI: <https://doi.org/10.1016/j.ijrefrig.2018.09.018>. URL: <https://www.sciencedirect.com/science/article/pii/S0140700718303499>.
- [29] *Refrigeration systems and applications*. eng. Third edition. Chichester, West Sussex, UK: John Wiley & Sons, Ltd., 2017. ISBN: 9781119230793.
- [30] SAFECONNECT. *WHAT IS ETRU AND WHY IS IT IMPORTANT?* URL: <https://www.safeconnectsystems.com/the-ultimate-user-guide-to-etr/what-is-etr-and-why-is-it-important/>. (accessed: 16.09.2022).
- [31] Thermoking. *TRAILER ELECTRIFICATION*. URL: <https://www.thermoking.com/content/dam/thermoking/documents/marketing/Trailer-electrification-position-paper-Thermo-King.pdf>. (accessed: 16.09.2022).
- [32] Wenyi Wang and Yaoyu Li. "Intermediate pressure optimization for two-stage air-source heat pump with flash tank cycle vapor injection via extremum seeking". In: *Applied Energy* 238 (2019), pp. 612–626. ISSN: 0306-2619. DOI: <https://doi.org/10.1016/j.apenergy.2019.01.083>. URL: <https://www.sciencedirect.com/science/article/pii/S0306261919300789>.

- [33] M. Willatzen, N.B.O.L. Pettit, and L. Ploug-Sørensen. "A general dynamic simulation model for evaporators and condensers in refrigeration. Part I: moving-boundary formulation of two-phase flows with heat exchange". In: *International Journal of Refrigeration* 21.5 (1998), pp. 398–403. ISSN: 0140-7007. DOI: [https://doi.org/10.1016/S0140-7007\(97\)00091-1](https://doi.org/10.1016/S0140-7007(97)00091-1). URL: <https://www.sciencedirect.com/science/article/pii/S0140700797000911>.
- [34] Reinhard Radermacher Xing Xu Yunho Hwang. "Performance comparison of R410A and R32 in vapor injection cycles". In: *International Journal of Refrigeration* 36 (2013), pp. 892–903. DOI: <https://doi.org/10.1016/j.ijrefrig.2012.12.010>. URL: <https://www.sciencedirect.com/science/article/pii/S0140700712003532?via%3Dihub>.
- [35] Yu Xu and Xiande Fang. "Correlations of void fraction for two-phase refrigerant flow in pipes". In: *Applied Thermal Engineering* 64.1 (2014), pp. 242–251. ISSN: 1359-4311. DOI: <https://doi.org/10.1016/j.applthermaleng.2013.12.032>. URL: <https://www.sciencedirect.com/science/article/pii/S1359431113009204>.
- [36] Ma Guoyuan Xu Shuxue. "Performance Evaluation of a Vapor Injection Refrigeration System Using Mixture Working Fluid R32/R1234ze". In: *IEA Heat Pump Conference* (2017), p. 2. URL: <https://heatpumpingtechnologies.org/publications/p-4-1-1-performance-evaluation-of-a-vapor-injection-refrigeration-system-using-mixture-working-fluid-r32-r1234ze/>.
- [37] Ti-Wei Xue and Zeng-Yuan Guo. "What Is the Real Clausius Statement of the Second Law of Thermodynamics?" In: *Entropy* 21.10 (2019). ISSN: 1099-4300. DOI: [10.3390/e21100926](https://doi.org/10.3390/e21100926). URL: <https://www.mdpi.com/1099-4300/21/10/926>.

Appendix A

Bitzer Data for Simulation Initials

The Bitzer data used for setting up the simulation initials is found attached in the appendix folder "BITZER_test_data"

Appendix B

Coefficients and System Constants

In this section the different constants used in the component models will be given
Valve:

Symbol	Meaning	Value	Unit
$O_{\%}$	Equal percentage constant	50	[.]
K_{vc}	Condenser valve coefficient	10^{-5}	[.]
K_{ve}	Evaporator valve coefficient	10^{-5}	[.]
$K_{v.vi}$	Vapour injection valve coefficient	25^{-6}	[.]

Compressor:

Symbol	Meaning	Value	Unit
V_{pr}	Volume of intake per revolution	50	$[cm^3]$
η_1	Isentropic efficiency through compressor before injection	98	[%]
η_2	Isentropic efficiency through compressor after injection	98	[%]
τ	Compressor time constant	0.5	[.]

Condenser:

Symbol	Meaning	Value	Unit
V_{cond}	Volume of the condenser	0.002	$[m^3]$
UA_l	Heat transfer coefficient of liquid section	3500	$[J \cdot K^{-1} \cdot s^{-1}]$
UA_m	Heat transfer coefficient across the metal boundary	50	$[J \cdot K^{-1} \cdot s^{-1}]$
UA_v	Heat transfer coefficient of vapour/mixed region	1700	$[J \cdot K^{-1} \cdot s^{-1}]$
$C_{p,m}$	Heat capacity of the metal	387	$[J \cdot K^{-1}]$
$M_{m.c}$	Mass of the condenser	3.0271	$[kg]$

Flash-tank:

Symbol	Meaning	Value	Unit
V_{FT}	Volume of the flash-tank	0.0067	$[m^3]$

Evaporator:

Symbol	Meaning	Value	Unit
V_e	Volume of the evaporator	0.0152	m^3
UA_{sh}	Heat transfer coefficient for super-heated region	2500	$[J \cdot K^{-1} \cdot s^{-1}]$
UA_{mx}	Heat transfer coefficient for mixed region	3510	$[J \cdot K^{-1} \cdot s^{-1}]$
$M_{m.e}$	Mass of the evaporator	22.976	$[kg]$

Reefer:

Symbol	Meaning	Value	Unit
M_{air}	Mass of air in the reefer	86.5	$[kg]$
M_{reef}	Mass of the reefer	2500	$[kg]$
M_{cargo}	Mass of the cargo	1	$[kg]$
$C_{p,air}$	Heat capacity of air	1003.5	$[J \cdot K^{-1}]$
$C_{p,reef}$	Heat capacity of the reefer	890	$[J \cdot K^{-1}]$
$C_{p,cargo}$	Heat capacity of the cargo	447	$[J \cdot K^{-1}]$

Appendix C

Model MATLAB Files

The Matlab Model is attached in the appendix folder "Git repository"

Appendix D

Flow-plot for Initial Simulation

Fig. D.1 shows the mass-flows through the evaporator and condenser in the initial simulation from Section 5.3.2

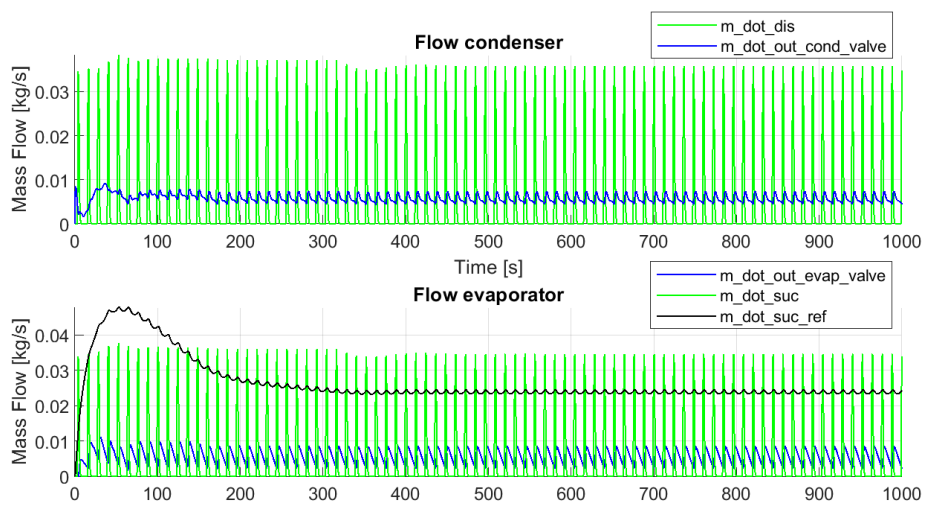


Figure D.1: Flows in condenser and evaporator

Appendix E

Model Comparison with Valve Models Implemented

The model used for simulation in Chapter 5 is implemented such that flows out of the condenser and flash tank are set directly with a controller. In reality this controller should be used to set a reference for a different controller that sets a opening degree for a valve, which with pressure difference and density sets a mass flow. Below such a control scheme is implemented and the valve model described in Section 3.2 is added to the simulated model. Below are comparisons of model states with and without valves to get an idea of the effect of adding valve models to the simulated system. In the data shown on the plots below the pressure ratio reference, r_{FT_ref} is changed at 1100 s from 0.7 -> 0.2304, besides this, the super-heat reference is changed at 1001 s from 8 -> 7.1517.

E.1 Reefer Temperature

In Figure E.1 it can be seen that the temperature of the air in the reefer box, T_{air} settles approximately 0.2K above the reference before the pressure ratio changes. With valves included T_{air} settles to a value close to the reference even before the pressure ratio change.

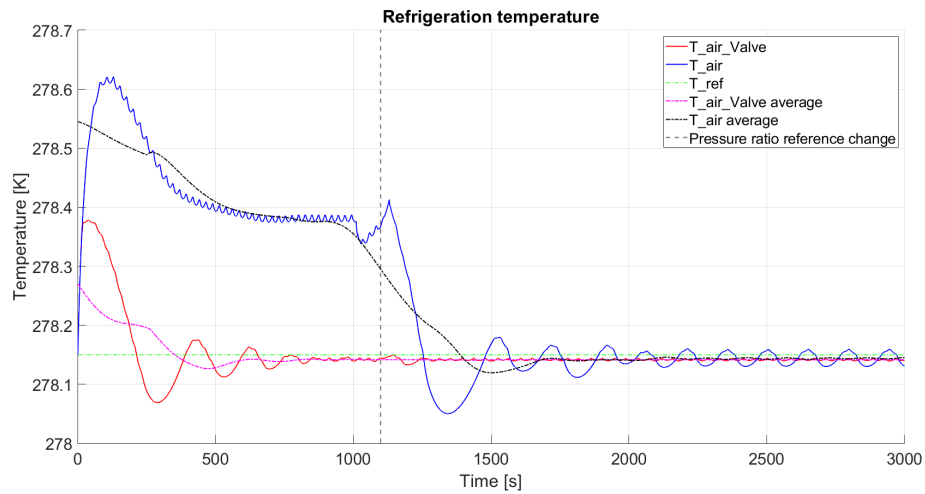


Figure E.1: Reefer air temperature

E.2 Pressure

In general the pressures in the components, as seen in Figure E.2, are significantly higher when the valve models are implemented than when they are not. The only exception to this is the evaporator where the pressures lay at similar levels. Another thing that becomes clear by analysing the pressures is that the offtime of the compressor is no longer as lengthy when the valves are implemented.

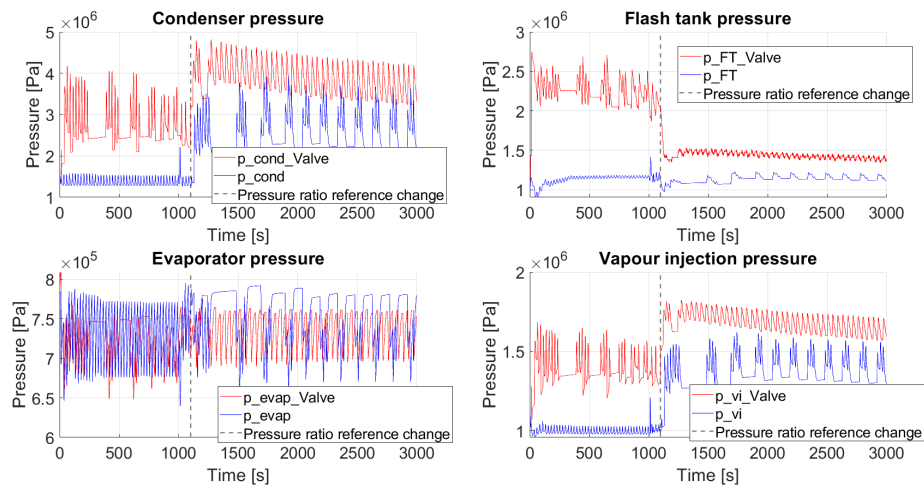


Figure E.2: Component pressures

The pressure ratio, r_{FT} as seen in Figure E.3, does not quite reach the reference be-

fore the change, when valves are implemented. After the reference change though, the pressure ratio reference is reached quickly.

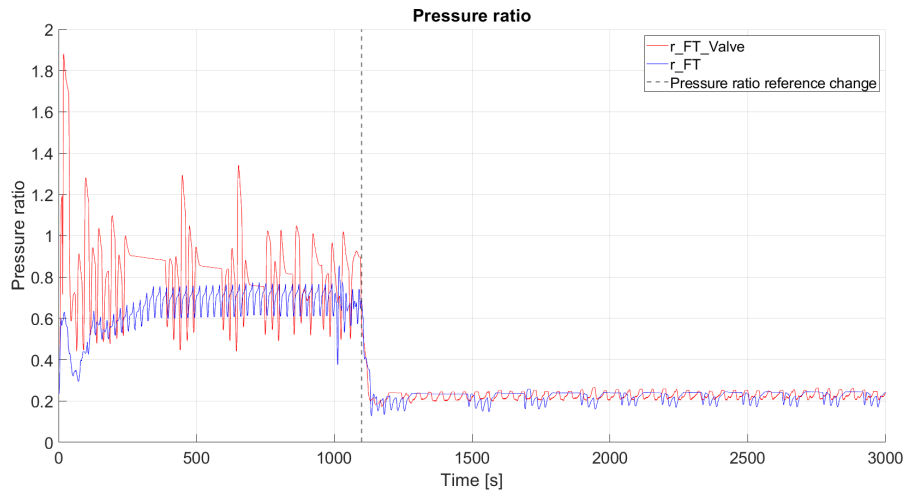


Figure E.3: Pressure ratio

E.3 Super-heat and Sub-cool

In Figure E.4 it can be seen that the super-heats when the valves are implemented and when they are not, act in an almost inverse manner to each other. The sub-cool is however significantly higher when the valve model is implemented. This is due to the pressure in the condenser being greater when the valves are implemented.

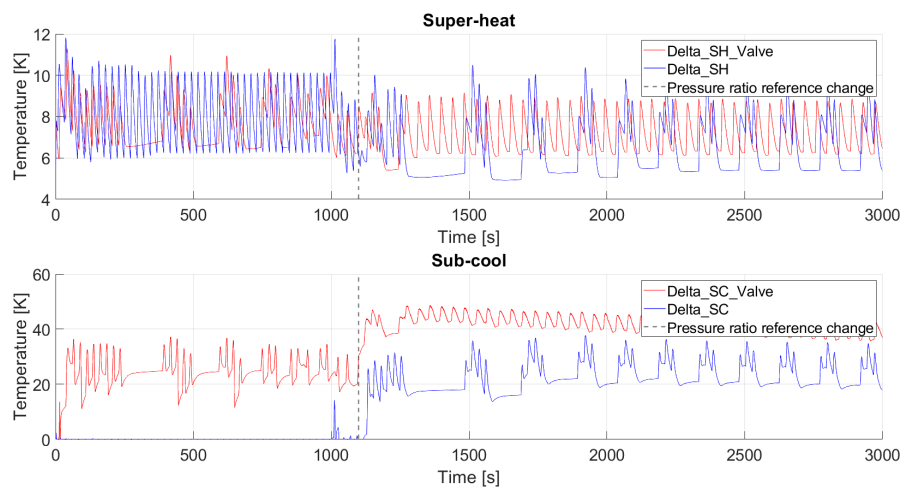


Figure E.4: Super-heat and sub-cool

E.4 Enthalpy

Below in Figure E.5 the enthalpy change across the various components can be seen. Here the enthalpy change is greater over the evaporator when valves are not implemented but lesser across the compressor and condenser.

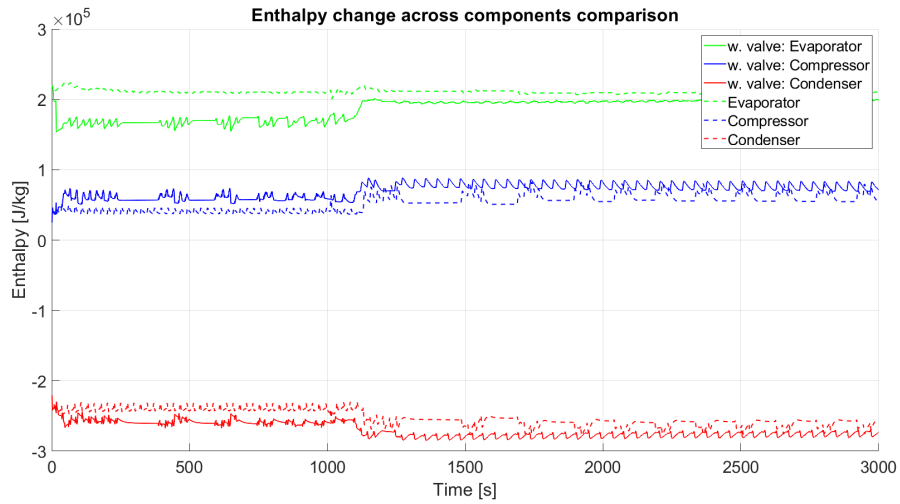


Figure E.5: Enthalpy change across components

Appendix F

COP Simulation Test

The system is simulated and COP is averaged for different states and fan control-signals when compressor speed has a greater speed than $200rpm$.

Δ_{SH} reference	r_{FT} reference	$U_{f,e}$	$U_{f,c}$	COP
8K	0.7	0	0	3.75

Table F.1: Table of initial COP test

F.0.1 Variable Super-heat

Δ_{SH} reference	r_{FT} reference	$U_{f,e}$	$U_{f,c}$	COP
8.9K	0.7	0	0	3.62
8K	0.7	0	0	3.75
7.7K	0.7	0	0	3.82
6.4K	0.7	0	0	4.25
5.2K	0.7	0	0	4.64

Table F.2: Table of variable Super-heating COP test

F.0.2 Variable Flash-tank Pressure Ratio

Δ_{SH} reference	r_{FT} reference	$U_{f,e}$	$U_{f,c}$	COP
8K	0.755	0	0	3.606
8K	0.726	0	0	3.618
8K	0.717	0	0	3.724
8K	0.697	0	0	3.77
8K	0.668	0	0	3.753
8K	0.656	0	0	3.761
8K	0.640	0	0	3.774
8K	0.611	0	0	3.887
8K	0.594	0	0	3.893
8K	0.582	0	0	3.901
8K	0.553	0	0	3.93
8K	0.533	0	0	3.932
8K	0.525	0	0	3.704
8K	0.495	0	0	3.570
8K	0.472	0	0	3.857

Table F.3: Table of variable Flash-tank pressure-ratio COP test

F.0.3 Variable Evaporator and Condenser Fans

Δ_{SH} reference	r_{FT} reference	$U_{f,e}$	$U_{f,c}$	COP
8K	0.7	0	1	2.46
8K	0.7	0	0.8	3.06
8K	0.7	0	0.6	3.34
8K	0.7	0	0.5	3.37
8K	0.7	0	0.3	2.76
8K	0.7	0	0.2	3.74
8K	0.7	0	0.125	3.74
8K	0.7	0	0.05	3.75

Table F.4: Table of variable condenser fan speed COP test

Δ_{SH} reference	r_{FT} reference	$U_{f,e}$	$U_{f,c}$	COP
8K	0.7	1	0	2.25
8K	0.7	0.8	0	3.72
8K	0.7	0.7	0	3.3
8K	0.7	0.6	0	3.78
8K	0.7	0.4	0	3.39
8K	0.7	0.24	0	3.514
8K	0.7	0.206	0	3.519
8K	0.7	0.167	0	3.885
8K	0.7	0.128	0	4.27
8K	0.7	0.089	0	4.569

Table E.5: Table of variable evaporator fan speed COP test

Appendix G

Vapour Injection Characteristic

It can be seen that the oscillation in the total mass, happens when the pressure ratio is such that vapour injection occurs.

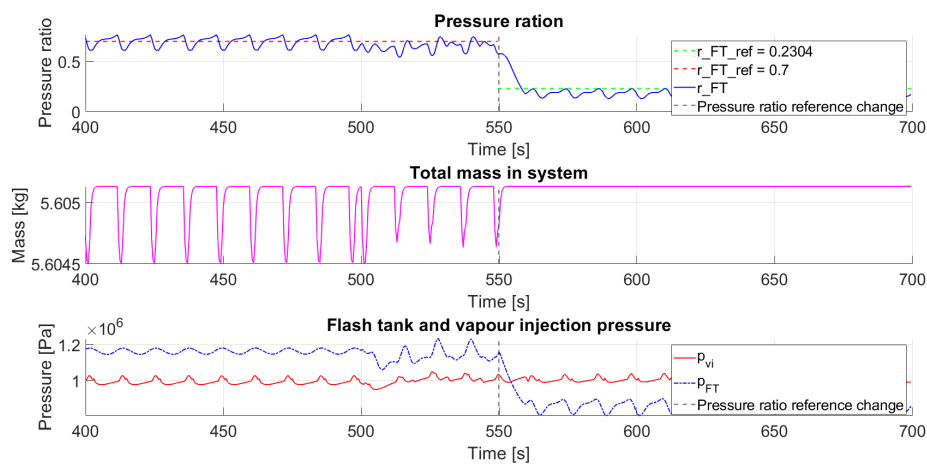


Figure G.1: Plot showing mass change with flash tank pressure

The vapour injections characteristics can be shown by observing the vapour-liquid volumes in the flash-tank and how they evolve over time. Below in Fig. G.2 the volume of vapour refrigerant in the flash tank can be seen to increase when the vapour injection pressure is above the flash tank pressure. The cause is that there is no mass flow of vapour refrigerant from the flash tank to the compressor once the pressure is reduced below the compressor pressure p_{vi} .

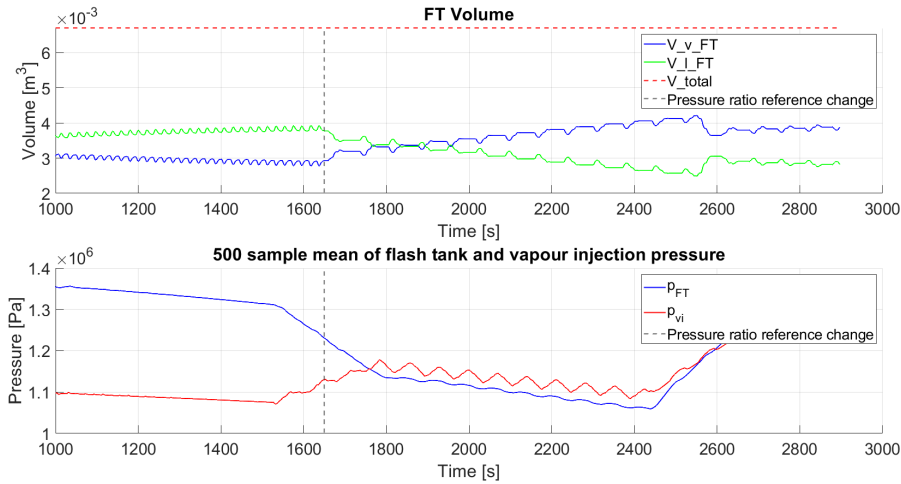


Figure G.2: Flash tank volume change with pressure change, using a 500order FIR filter

Appendix H

Optimization Appendix

Below in Figure H.1 a flow chart of the genetic algorithm can be seen.

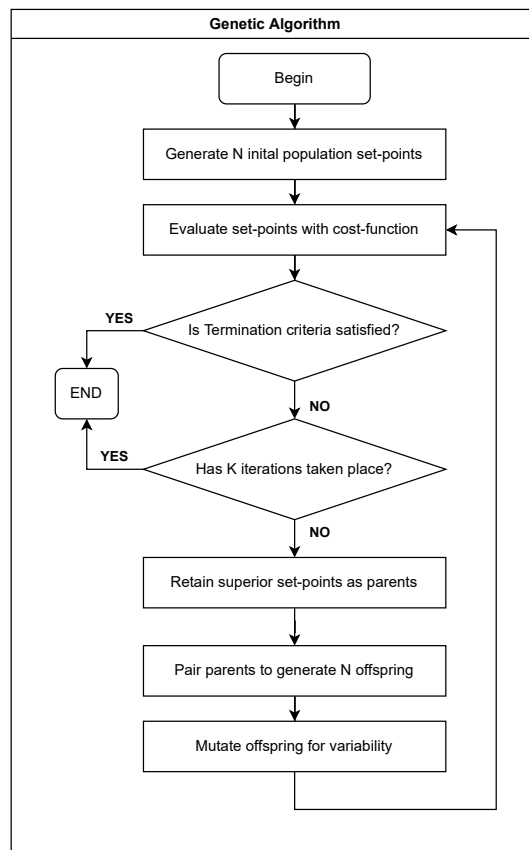


Figure H.1: Flow-chart of genetic algorithm

H.0.1 Swarm Algorithm

The swarm algorithm works in the following way [20]:

1. **Create initial particles:**

A population of particles, or set-points, are created with a random position

and velocity (moving direction) for each particle.

2. Iteration:

The algorithm iterates a particle through the following steps:

(a) **A neighbourhood is chosen**

A random subset, or neighbourhood, of particles is chosen.

(b) **The cost-function is evaluated**

For each particle in the neighbourhood, the cost-function output is found and the position of the best particle is determined.

(c) **Update velocities and position**

The velocities are updated using a weighted sum of the previous velocity, the difference between the current position and the best position. The position is then updated using the new velocity.

(d) **Reevaluate cost-function**

If the new position provides a better cost-function output, it stays as the new position. If not, the position is reset to the previous position.

3. Stop if criteria are met

If criteria such as the maximum number of generations or specified cost-function value has been reached within some tolerance the algorithm terminates.

Below in Figure H.2 a flow chart of the genetic algorithm can be seen.

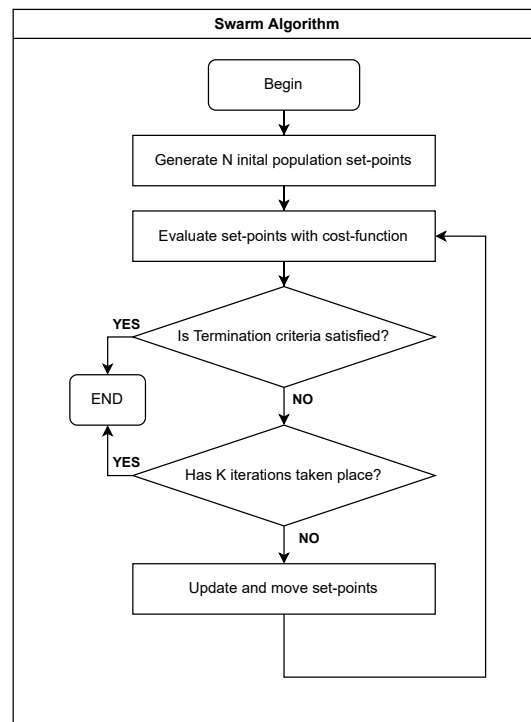


Figure H.2: Flow-chart for swarm algorithm

Implementation Results with Fans

Below in Fig. H.3 the best average COP can be seen for each generation as well as the initial run. The best average COP is already reached in the first generation and never improves beyond that.

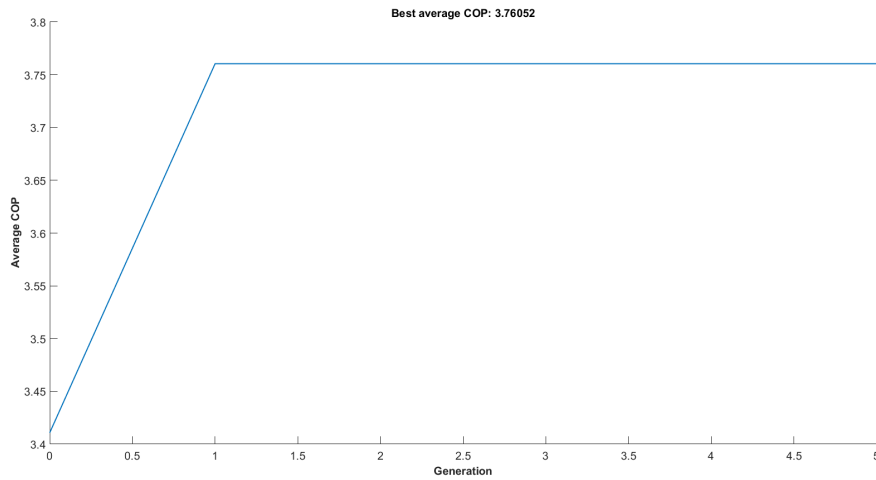


Figure H.3: Best average COP each generation with fans

In Fig. H.4 the average COP each iteration can be seen. When the blue line goes towards zero the system has become unstable either through a super-heat that is too low or unstable pressure dynamics. The dotted red line shows the average COP without the crash data to make it clearer where the crashes have happened.

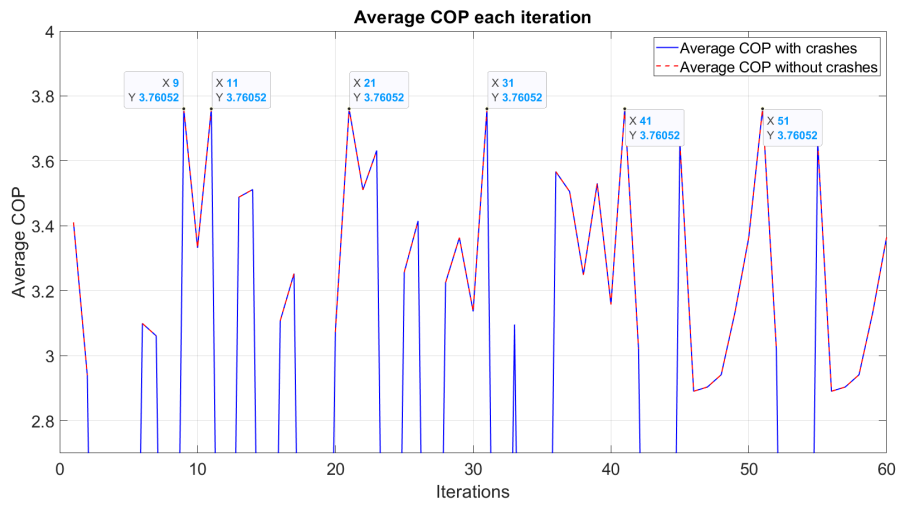


Figure H.4: Average COP each iteration with fans

In Fig. H.5 the set-points evaluated at each iteration can be seen.

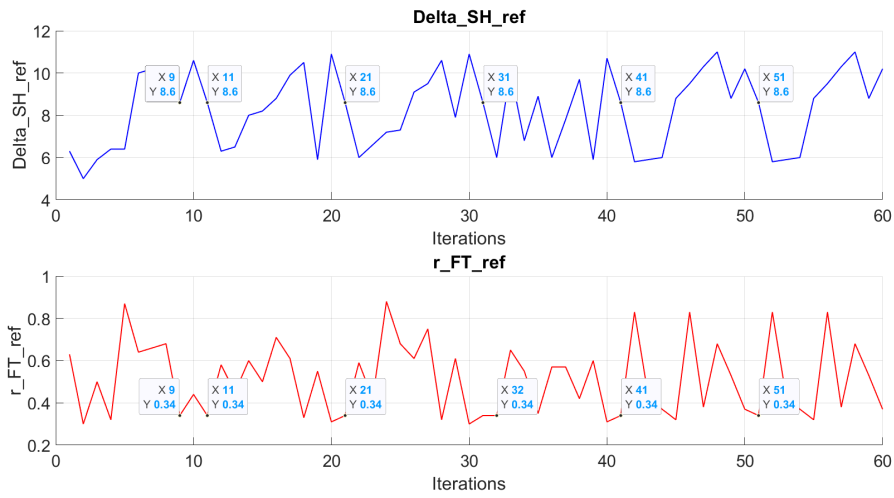


Figure H.5: Set-points at each iteration with fans

Tab. H.1 shows the best average COP and the corresponding optimal set-points when fans are included.

Best average COP	r_{FT_ref}	Δ_{SH_ref}
3.76052	0.34	8.6

Table H.1

Below in Fig. H.6 some system states can be seen. It seems that the set-points, Δ_{SH_ref} and r_{FT_ref} are followed by their respective corresponding states.

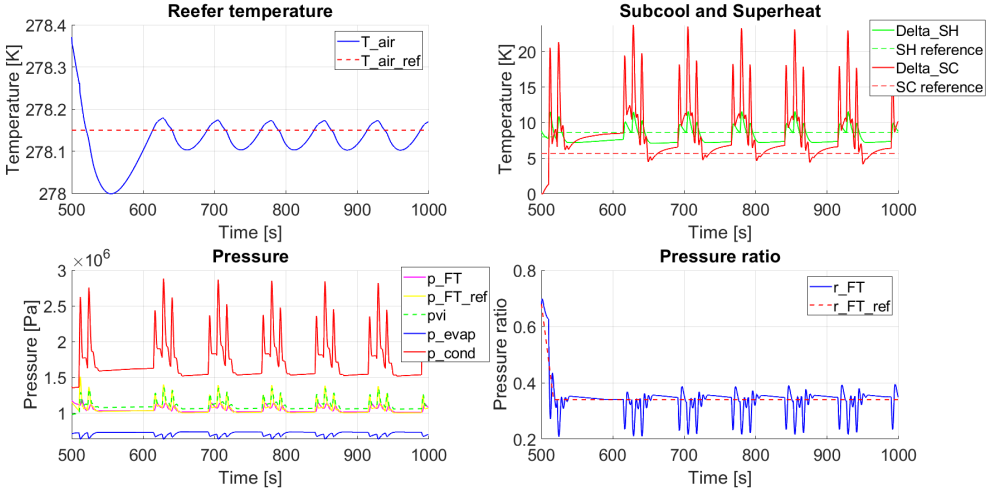


Figure H.6: System states with best set-points with fans

Appendix I

Cascade Control for Valves

The valves control signals are controlled similarly to the compressor control signals. The different valves and associated flows are denoted with x .

$$\phi_x = (\dot{m}_{x_ref} - \dot{m}_x) \cdot K_{p.v.x} + \int_0^t (\dot{m}_{x_ref} - \dot{m}_x) dt \cdot K_{i.v.x} \quad (\text{I.1})$$

Appendix J

Controller Gains and variables

Symbol	Meaning	Value
$K_{p.sh}$	Super-heat control proportional gain	0.0015
$K_{i.sh}$	Super-heat control integral gain	10^{-4}
$K_{p.U.e}$	Sub-cool evaporator fan control proportional gain	0.5
$K_{i.U.e}$	Sub-cool evaporator fan control integral gain	10^{-4}
$K_{p.U.c}$	Sub-cool condenser fan control proportional gain	0.5
$K_{i.U.c}$	Sub-cool condenser fan control integral gain	10^{-4}
$K_{p.\dot{m}_{suc}}$	\dot{m}_{suc} proportional gain	0.1
$K_{i.\dot{m}_{suc}}$	\dot{m}_{suc} integral gain	10^{-4}
$K_{p.T_{air}}$	Reefer air temperature proportional gain	50
$K_{i.T_{air}}$	Reefer air temperature integral gain	1
$K_{p.p_{FT}}$	Flash tank pressure ratio proportional gain	0.018
$K_{i.p_{FT}}$	Flash tank pressure ratio integral gain	10^{-4}
U_{Ω_Max}	Maximum compressor control signal value	0.1
\dot{m}_{suc_Max}	Maximum \dot{m}_{suc}	0.1
$\tau_{cpr.off}$	Minimum compressor off time	10s
$\tau_{cpr.on}$	Maximum compressor on time	1.5s

Table J.1: Controller gain values